Spring 2014

Dioxygen activation with Bis(arylimino)pyridine radical anion complexes of nickel

Antonio David Manuel
University of Iowa

DIOXYGEN ACTIVATION WITH BIS(ARYLIMINO)PYRIDINE RADICAL ANION COMPLEXES OF NICKEL

by

Antonio David Manuel

A thesis submitted in partial fulfillment
of the requirements for the Doctor of
Philosophy degree in Chemistry
in the Graduate College of
The University of Iowa

May 2014

Thesis Supervisor: Associate Professor Jan-Uwe Rohde

Graduate College
The University of Iowa
Iowa City, Iowa

CERTIFICATE OF APPROVAL

_____

PH.D. THESIS

_____

This is to certify that the Ph.D. thesis of

Antonio David Manuel

has been approved by the Examining Committee
for the thesis requirement for the Doctor of Philosophy
degree in Chemistry at the May 2014 graduation.

Thesis Committee: _____
Jan-Uwe Rohde, Thesis Supervisor

_____
Edward Gillan

_____
Gary Small

_____
Mishtu Dey

_____
Garry R. Buettner

ACKNOWLEDGMENTS

I would like to thank my advisor, Dr. Jan-Uwe Rohde, for all of his assistance and advice throughout my graduate studies. He was a great mentor and I learned a lot from him over the years.

I would like to thank all of the members of the Rohde group, especially Dr. Matthew Kelley, Dr. Travis Owen, Dr. Wei-Tsung Lee and Ricky Lange, for all of their support and assistance. It was a pleasure to work with all of them.

I would like to thank Dr. Dale Swenson for the collection of XRD data. I would also like to thank Dr. Lynn Teesch and Vic Parcell for their help in the mass spectrometry facility.

I would like to thank everyone that I have taught with over the years for making teaching during graduate school a great experience.

I would like to thank my entire family, especially my parents, for all of their encouragement and support over the years.

ABSTRACT

Complexes of redox-active ligands have received increasing attention, in part, because they have been shown to facilitate a variety of bond-forming and bond-breaking reactions, including the activation of small molecules. Unique attributes of redox-active ligands include that they influence the electronic properties of transition metal complexes and may participate in their multielectron redox chemistry. In this work, the utility of Ni complexes of redox-active bis(arylimino)pyridine ligands for the activation of dioxygen was explored. A series of bis(arylimino)pyridine complexes [Ni{2,6-(ArN=CMe)$_2$C$_5$H$_3$N}Cl$_2$] (where Ar = 4-X-2,6-^{i}Pr$_2$C$_6$H$_2$ and X = H, Cl, Br, NO$_2$, or N(CH$_3$)$_2$) were synthesized along with the deuterium-labeled complex [Ni{2,6-(ArN=CCD$_3$)$_2$C$_5$H$_3$N}Cl$_2$] (where Ar = 2,6-^{i}Pr$_2$C$_6$H$_3$). Characterization by X-ray crystallography of three complexes confirmed coordination of the Ni center by the three nitrogen donor atoms of the bis(arylimino)pyridine ligand and two chloro ligands. The structural analyses further revealed a distorted square pyramidal geometry of the Ni centers.

The reduced complexes [Ni{2,6-(ArN=CMe)$_2$C$_5$H$_3$N}Cl] (where Ar = 4-X-2,6-^{i}Pr$_2$C$_6$H$_2$ and X = H, Cl, or Br) and [Ni{2,6-(ArN=CCD$_3$)$_2$C$_5$H$_3$N}Cl] (where Ar = 2,6-^{i}Pr$_2$C$_6$H$_3$) were synthesized by reaction of the corresponding dichloride complexes with a sodium amalgam. These are four-coordinate complexes with distorted square planar geometry and are best characterized as ligand-radical complexes of Ni^{II} as opposed to Ni^{I} complexes on the basis of X-ray crystallography and electron paramagnetic resonance spectroscopy of [Ni{2,6-(2,6-^{i}Pr$_2$C$_6$H$_3$N=CMe)$_2$C$_5$H$_3$N}Cl].

Reactions of the ligand-radical Ni^{II} complexes with dioxygen were studied by UV-Vis spectroscopy, and the overall course of the reaction was similar for all four complexes. The half-life of the reaction was not affected by deuterium labeling of the acetimino methyl groups but was affected by different substituents in the 4-position of the phenyl groups of the ligand. The reactions caused intraligand C–C bond cleavage with formation of a new C=O double bond, resulting in the complexes [Ni{6-(ArN=CMe)C_5H_3N-2-C(O)NAr}Cl] (where Ar = 4-X-2,6-$^{i}Pr_2C_6H_2$ and X = H, Cl, or Br) and [Ni{6-(ArN=CCD_3)C_5H_3N-2-C(O)NAr}Cl] (where Ar = 2,6-$^{i}Pr_2C_6H_3$). The structures of the complexes [Ni{6-(ArN=CR)C_5H_3N-2-C(O)NAr}Cl] (where Ar = 2,6-$^{i}Pr_2C_6H_3$ and R = CH_3 or CD_3) were determined by X-ray crystallography. For all four complexes, the carboxamidato group was identified by a strong band in the infrared spectra assignable to the CO stretching vibration. Furthermore, the new carboxamidato ligands were removed from the metal center and isolated in their neutral form as 6-(ArN=CMe)C_5H_3N-2-C(O)NHAr (where Ar = 4-X-2,6-$^{i}Pr_2C_6H_2$ and X = H, Cl, or Br) and 6-(ArN=CCD_3)C_5H_3N-2-C(O)NHAr (where Ar = 2,6-$^{i}Pr_2C_6H_3$). Taken together, these results indicate that the activation of dioxygen occurs at the ligand and without an overall oxidation state change at the Ni center. The observed ligand-centered oxygenation in these reactions contrasts with the prevailing metal-centered chemistry of redox-active bis(arylimino)pyridine complexes and demonstrates that they can be directly involved in the activation and conversion of a small molecule.

TABLE OF CONTENTS

LIST OF TABLES

Table

LIST OF FIGURES

Figure

LIST OF SCHEMES

Scheme

CHAPTER 1

INTRODUCTION

This thesis covers the synthesis and characterization of bis(arylimino)pyridine nickel complexes and their reactivity with dioxygen. In the literature, it has been reported that complexes of transition metals with redox-active ligands can bind and activate small molecules. Transition metal complexes with bis(arylimino)pyridine ligands have been widely studied, however, the reactivity of these complexes with dioxygen has not been reported prior to this work. Results presented in this thesis show that reduction of nickel bis(arylimino)pyridine complexes occurs on the ligand and that the reduced complexes undergo a reaction with dioxygen leading to modification of the redox-active bis(arylimino)pyridine ligand.

A brief overview of redox-active ligands and their complexes will be presented in Chapter 2. A section will be devoted to bis(arylimino)pyridines and their transition metal complexes. The activation of small molecules with transition metal complexes of redox-active ligands typically entails overall electron transfer from the ligand to the small molecule, with reactivity occurring at the metal center. Examples of this type of small molecule activation with redox-active ligands will be discussed with bis(arylimino)pyridine supporting ligands as well as other supporting ligands. By contrast, in the transition-metal mediated oxidative cleavage of catechols, the catecholate ligand may be viewed as a redox-active substrate ligand that itself undergoes reaction. These examples will serve as a useful foundation for exploring the reactivity of O_2 with bis(arylimino)pyridine complexes of Ni.

The synthesis and characterization of bis(arylimino)pyridine complexes of Ni^{II} will be discussed in Chapter 3. The synthesis of 4-substitued-2,6-diisopropylanilines will be presented first, as they are important synthons for preparing the various Ni^{II} complexes to be studied. The preparation of the Ni^{II} complexes will then be discussed with characterization by infrared spectroscopy, X-ray crystallography, and electrochemistry. The infrared spectroscopy discussion will include a band that is consistent with an imino CN stretching vibration. The coordination geometry of the Ni center, along with relevant bond lengths and angles, will be discussed for each of the crystal structures. The electrochemical characterization will focus on the possibility of the reduction of the complexes.

The synthesis and characterization of bis(arylimino)pyridine radical anion complexes of Ni^{II} will be the focus of Chapter 4. The synthesis of these complexes is accomplished by a one electron reduction using a sodium amalgam under an inert atmosphere. An important question regarding the reduction is whether the reduction occurs at the metal center or on the redox-active ligand. A combination of electron paramagnetic resonance and X-ray crystallography can be used to elucidate the site of the reduction on the complexes. The discussion of the crystal structure data will include relevant bond lengths and angles, which will provide useful information pertaining to the location of the unpaired electron density in the complex.

Chapter 5 will focus on the reaction of the bis(arylimino)pyridine radical anion complexes of Ni^{II} with O_2. A combination of mass spectrometry, X-ray crystallography, and infrared spectroscopy reveals the imino C–C bond cleavage and formation of an amidato group on the ligand after the reaction. The C=O bond length will be highlighted

in the crystal structure discussion, along with other relevant bond lengths and angles. The ligand can be extracted from the complex and isolated. ^{1}H NMR spectroscopy of the extracted ligand confirms the formation of a ligand containing one imino group and one amidato group. The reactions were monitored by UV–Vis spectroscopy, which revealed a reaction course that does not change with respect to different substituents on the ligand. However, the half-life of the reaction was influenced by substitution of the bis(arylimino)pyridine ligand with halogens on the phenyl groups, but not influenced by deuterium labeling of the acetimino methyl group. The reaction of an analogous bis(arylimino)pyridine radical anion complex of Co^{II} with O_2, which led to an electron transfer with no observable bond cleavage or formation, will be discussed. Finally, the mechanistic implications from the reactivity data and product analysis suggesting direct attack of the ligand radical by O_2 will be examined.

CHAPTER 2

BACKGROUND

2.1 Introduction

The activation of cheap and abundant dioxygen is of interest due to the potential for a wide variety of organic transformations using O_2. However, reactions with O_2 are difficult to control due to a kinetic barrier arising from its triplet ground state, and a high activation energy that reduces selectivity.[1] As such, O_2 in its natural form is not useful for organic transformations on any scale. Activation of O_2 with transition metal complexes to control reactivity is one approach that has been extensively studied.

A method to enhance the ability of transition metal complexes to mediate multi-electron redox transformations, including the activation of small molecules, to form useful products is to use a redox-active ligand on the metal center. In transition metal complexes with redox-active ligands, the redox-active ligand can act as an electron reservoir for oxidation or reduction reactions. This allows for high-valent transition metals to participate in oxidative addition chemistry and the activation of O_2.[2-4]

The bis(arylimino)pyridine ligand forms complexes with a wide variety of transition metals, and has been shown to be a redox-active ligand that can accept up to 3 electrons.[5-8] The bis(arylimino)pyridine complexes have been studied extensively for small molecule activation and ethylene polymerization. However, research into O_2 activation using transition metal complexes of bis(arylimino)pyridines is lacking. At the start of this work there were no examples of O_2 activation with transition metal

complexes of bis(arylimino)pyridine. More recently, one example of an oxovanadium(V) complex with a bis(arylimino)pyridine ligand has been reported in the literature.[9]

This chapter begins with examples of redox-active ligands and their complexes. An overview of the bis(arylimino)pyridine ligand and complexes with the bis(arylimino)pyridine ligand will be presented, along with some examples of the reactivity of these complexes. The activation of small molecules using redox-active ligand complexes will then be reviewed. This discussion should serve to show that the bis(arylimino)pyridine ligand system is a good candidate for a supporting ligand for the activation of O_2.

2.2 Redox-Active Ligands and Their Complexes

There are a variety of redox-active ligand systems, and one thing they all have in common is that they may participate directly in the redox-reactivity of transition metal complexes.[10] This participation of the redox-active ligand results in electron transfer between the ligand and the reactant molecule. Three redox-active ligand systems will be highlighted here owing to previously researched chemistry that is of interest. These are the catecholate type ligands, ethenediamido ligands, and bis(arylimino)pyridine ligands. Catecholate ligands have been studied extensively. These ligands typically have either N or O donor atoms and can have a variety of substituents on the aromatic ring. These ligands can accept up to two electrons as highlighted in Scheme 1.[11,12]

A consequence of the ability of the redox-active ligand to have multiple redox states is that the ligand, in addition to the metal center, can act as the source of the

electrons in an oxidation reaction. An example of this type of reactivity is given in Scheme 2, where halogens undergo oxidative addition to a Zr^{IV} complex containing two *N,N'*-bis(*neo*-pentyl)-*ortho*-phenylenediamide ligands, which is the catecholate form of the ligand. The oxidation state of Zr remains +4 after the reaction is complete, but the ligands have each been oxidized by one electron to *N,N'*-bis(*neo*-pentyl)-*ortho*-diimino-semiquinonate, the semiquinonate analog of the ligand.[11]

Scheme 1. Redox States of Catecholate Type Ligands.

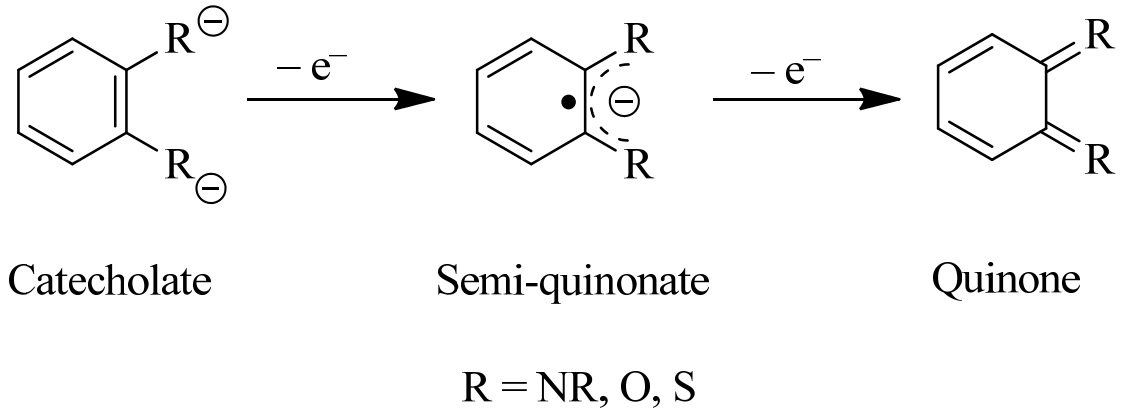

Scheme 2. Oxidative Addition of Halogens to a Zr^{IV} Complex.

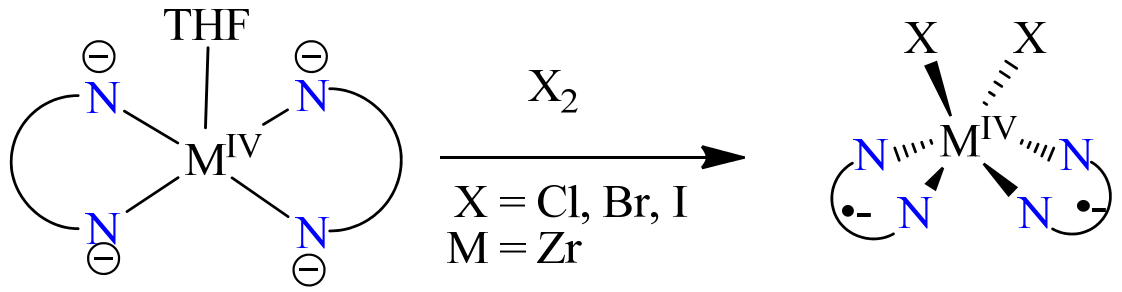

The second type of ligand system that is worth highlighting contains an ethenediamido group, which enables the ligand to participate in multi-electron redox

processes by conversion from an ethenediamido ligand to a diimino ligand. An example of this has been shown with a tetrahedral Zr^{IV} complex containing two ethenediamido ligands which can react with dioxygen to afford an octahedral Zr^{IV} complex containing two side-on peroxo ligands. Each ethenediamido ligand is oxidized by two electrons, and each O_2 molecule has been reduced by two electrons as shown in Scheme 3.[13]

Scheme 3. Activation of Dioxygen by a Redox-Active Ligand Complex of Zr^{IV}.

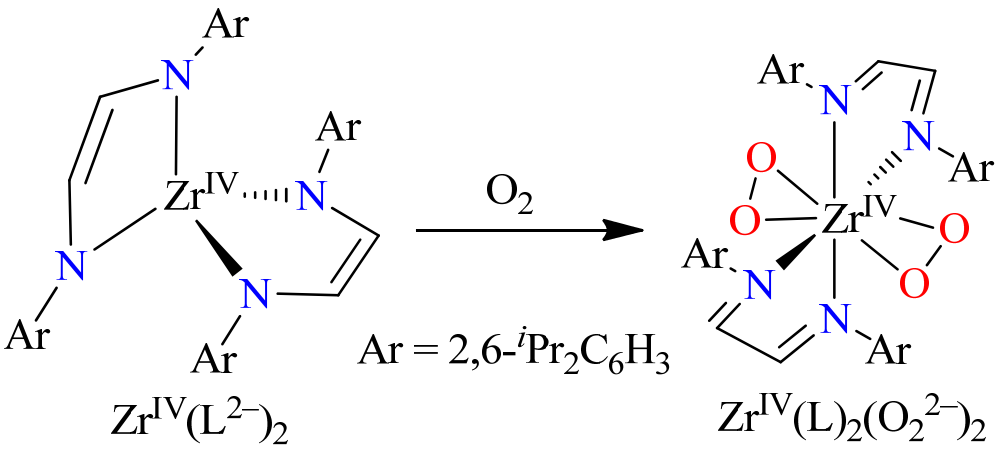

Scheme 4. Reduction of the Bis(arylimino)pyridine Ligand.

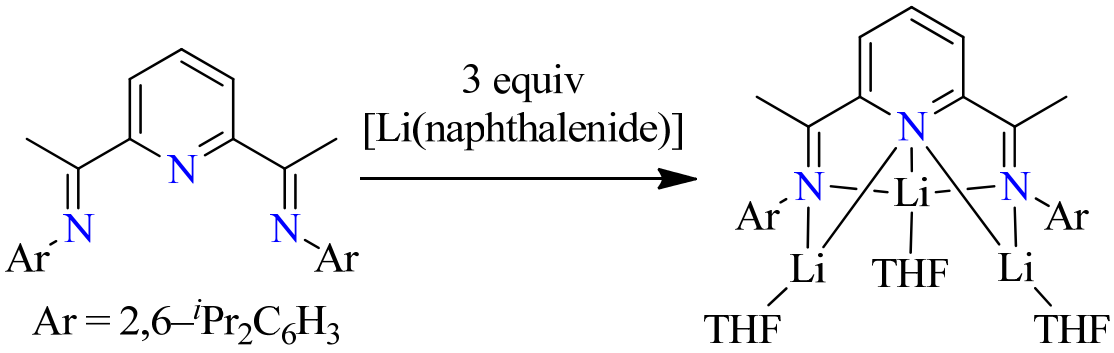

The final ligand system to be highlighted here is the bis(arylimino)pyridine system. This ligand system is of interest, because it is well known for ethylene polymerization and various types of small molecule activation. Prior to this work, there were no examples of O_2 activation using transition metal complexes of bis(arylimino)pyridine reported in the literature, and presently there is only one example reported in the literature.[5,9] The small molecule activation with bis(arylimino)pyridine complexes will be highlighted in Section 2.4. The ligand itself has been shown to accept up to three electrons upon reduction with [Li(naphthalenide)], a powerful reductant, as shown in Scheme 4.[6] Transition metal complexes with bis(arylimino)pyridines can also undergo one and two electron reductions which will be highlighted in the next section.

2.3 Bis(arylimino)pyridine Complexes

Transition metal complexes of bis(arylimino)pyridine ligands have been synthesized with a wide variety of substitution of the ligand backbone. The positions R_1 – R_4 in Scheme 5 are common positions to substitute, but many other derivatives with substitutions in other positions have been synthesized.[5] Fe and Co are the most common metal centers used to form complexes with the bis(arylimino)pyridine ligand, however, a wide variety of metal centers have also been used to synthesize bis(arylimino)pyridine complexes, including all of the first row transition metals.[5,14-22] Ni complexes have been synthesized with a wide variety of substitution on the bis(arylimino)pyridine (BIP) ligand in positions that include R_1 – R_4, and also in other positions. The first type of Ni complexes worth discussing are five coordinate complexes of the type [Ni(BIP)X_2],

which adopt a distorted square pyramidal geometry and have been crystallographically characterized with X = Cl, Br, SPh, and SePh.[20,21,23] A second type of complex, [Ni(BIP)X_2(solv)], occurs when a solvent molecule coordinates to the Ni center, resulting in an octahedral complexes which have been crystallographically characterized with X= Cl and H_2O or CH_3CN solvent molecules.[24,25] Octahedral complexes with 2 bis(arylimino)pyridine ligands of the type, [Ni(BIP_2], have been crystallographically characterized with R_3 = H, and R_1 = OMe or H. [26,27] Previously synthesized Ni^{II} complexes of relevance to this work due to the substitution pattern of R_1 = H, R_2 = Me, R_3 = ^{i}Pr, R_4 = H with X = Cl or Br have been reported and crystallographically characterized.[20-21] Ni complexes with $R_1 \neq$ H, R_2 = Me, R_3 = ^{i}Pr, and R_4 = H, have not been synthesized previously nor has a Ni complex with $R_2 = CD_3$, and this work will be the focus of Chapter 3. However, Fe and Co complexes with R_1 = Br or NO_2, R_2 = Me, R_3 = ^{i}Pr, and R_4 = H have been previously reported, as has the free ligand with R_1 = Cl, R_2 = Me, R_3 = ^{i}Pr, and R_4 = H.[28-30]

Scheme 5. Bis(arylimino)pyridine Transition Metal Complexes and Common Ligand Substitution Positions.

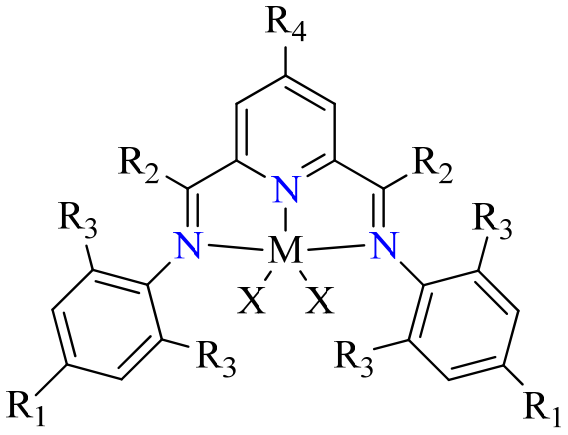

There have been three previously reported examples of bis(arylimino)pyridine complexes of Ni that have undergone a one electron reduction. The first two of these had the substitution R_1 = H, R_2 = Me, R_3 = H, and R_4 = H with X = SPh or SePh, and the second complex was an octahedral complex containing two bis(arylimino)pyridine ligands with the substitution R_1 = 4-MeOPh, R_2 = Me, R_3 = H, and R_4 = H.[23,26] More recently, after this work began, Ni complexes with R_1 = H, R_2 = Me, R_3 = ^{i}Pr, R_4 = H with X = CH_3 or N_2 have been synthesized and described as distorted square planar complexes that have been reduced by one (X = CH_3) or two electrons (X = N_2).[31] These reductions will be revisited in Chapter 4, as the metal-centered reduction found in the Ni complexes with X = SPh or SePh and the 2:1 complex contrasts with the results found from the reduced complexes characterized in this work, the Ni complexes with X = CH_3 or N_2, and also with previously reported reductions of Fe, Cr, and Co complexes of the bis(arylimino)pyridine ligand (R_3 = ^{i}Pr, R_1 = H). The Cr and Co complexes have also been shown previously to undergo chemical reduction by one electron, and the Fe complex by two electrons.[19,32-34] The location of the reduction is shown in Scheme 6. Using X-ray diffraction data, the length of the C_{imine}–$C_{pyridine}$ bond becomes significantly shorter upon reduction in these complexes, indicating increased electron density in a ligand-based orbital. The C_{imine}–N_{imine} bond also lengthens in these complexes. This location of the reduction on the ligand is further supported by DFT calculations and Mössbauer spectroscopy of the Fe complex, indicating that Fe remains in the +2 oxidation state.[34]

Scheme 6. One Electron Reduction of Bis(arylimino)pyridine Transition Metal Complexes.

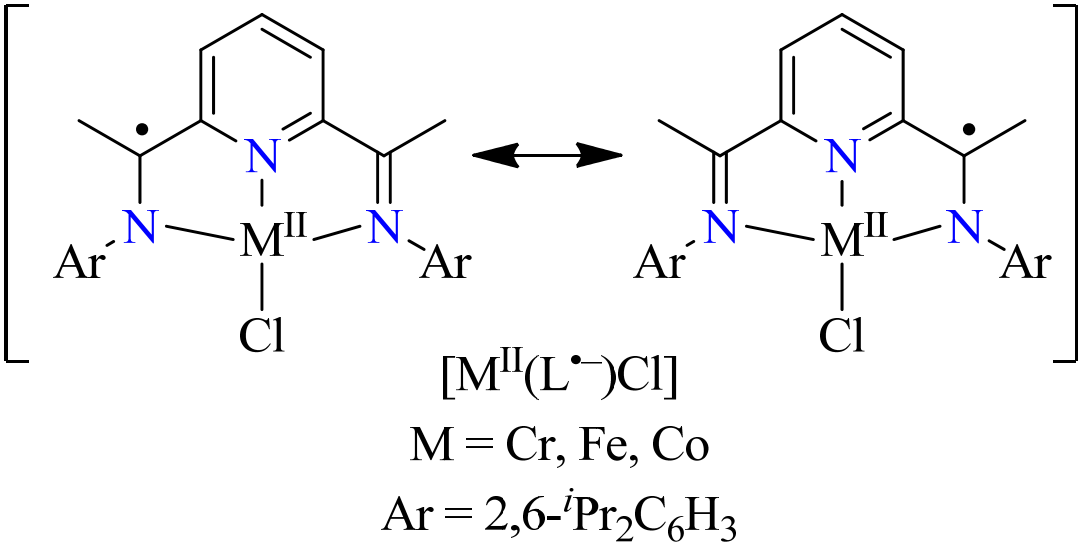

$[M^{II}(L^{\bullet -})Cl]$

M = Cr, Fe, Co

Ar = 2,6-$^{i}Pr_2C_6H_3$

2.4 Activation of Small Molecules with Redox-Active Ligand Complexes

The activation of small molecules typically, but not always, occurs at the metal center in transition metal complexes with redox-active ligands, even though electrons involved in the reaction come from the ligand and not necessarily the metal center. An example of this was presented in section 2.2 with Scheme 3, where O_2 is activated on the Zr center of a bis(ethenediamido) ligand complex. This type of small molecule activation is also observed with bis(arylimino)pyridine complexes.

When the bis(arylimino)pyridine Fe complex is reduced under an N_2 atmosphere by two electrons, two molecules of N_2 will coordinate. However, the activation of N_2 is minimal as the length of the N–N bond in the complex is statistically similar to that of

free dinitrogen.[15] This two electron reduced Fe complex is useful for activating other small molecules, however, as this complex has been shown to react with a series of diazoalkenes. This reactivity entails cleavage of the N–N diazoalkene bond, and formation of a mixture of Fe-nitrile and Fe-imino complexes as shown in Scheme 7. The Fe center remains in the +2 oxidation state throughout the reaction as the electrons necessary for the reaction are provided by the ligand and not the iron.[35]

Scheme 7. Activation of Diazoalkenes by a Bis(arylimino)pyridine Complex of Fe^{II}.

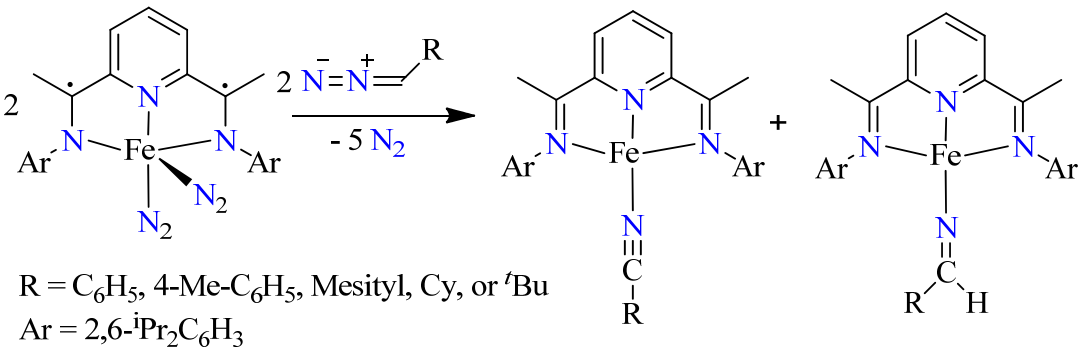

R = C_6H_5, 4-Me-C_6H_5, Mesityl, Cy, or ^{t}Bu
Ar = 2,6-^{i}Pr$_2$$C_6H_3$

Previous to this work, there were no examples of O_2 activation using a bis(arylimino)pyridine complex. Recently, on example of O_2 activation using a bis(arylimino)pyridine complex has been published.[9] This example also highlights that the metal center can work with a redox-active ligand with both sources contributing electrons for small molecule activation. A complex containing two V^{III} centers each with a two electron reduced bis(arylimino)pyridine ligand and connected via a bridging N_2^{2-} ligand was prepared.[9] In this case, electrons from the bis(arylimino)pyridine ligand, the bridging nitrogen ligand, and the metal center are involved in a 8 electron process converting two O_2 molecules into 4 oxo ligands, with two oxo ligands on each V center

(Scheme 8). Each V is now in the +5 oxidation state, each bis(arylimino)pyridine ligand has been oxidized by one electron, and the bridging nitrogen ligand has been oxidized to N_2. This process was also shown to work with elemental sulfur and an azo N=N bond.[9]

Scheme 8. Small Molecule Activation Using a Bis(arylimino)pyridine Complex of V^{III}.

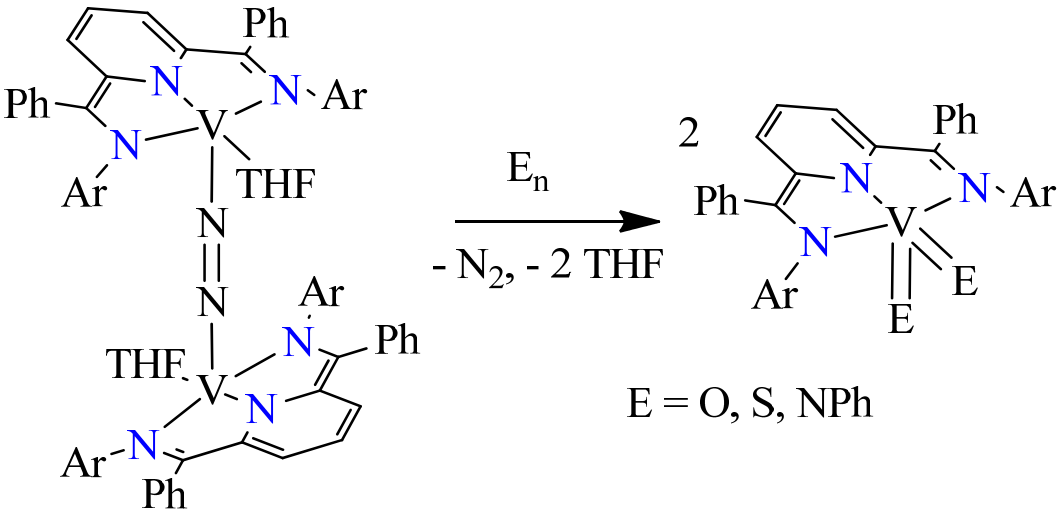

One final example is worth highlighting, as it is an example of ligand centered reactivity in small molecule activation. A V^{V} complex containing a 3,5-di-*tert*-butylcatecholate ligand and a 3,5-di-*tert*-butylsemiquinonate ligand radical has been proposed as the active species for the catalytic oxidation of 3,5-di-tert-butylcatechol into a mixture of intradiol, extradiol, and autoxidation products as shown in Scheme 9. It has been proposed that O_2 binds to the ligand radical in the first step of the catalytic cycle.[36,37] In this case, the ligand acts as the substrate which is released from the V center upon completion of the reaction while a new equivalent of catecholate comes in to regenerate the active species. There is another example of O_2 activation using a catecholate complex of Re that has been reported, however, the catecholate ligand remains unmodified and the

redox-state change occurs at the Re center as it is oxidized from +5 to +7 to form the Re-oxo complex.[38]

Scheme 9. Catechol Oxidation Using a Vanadium Catalyst.

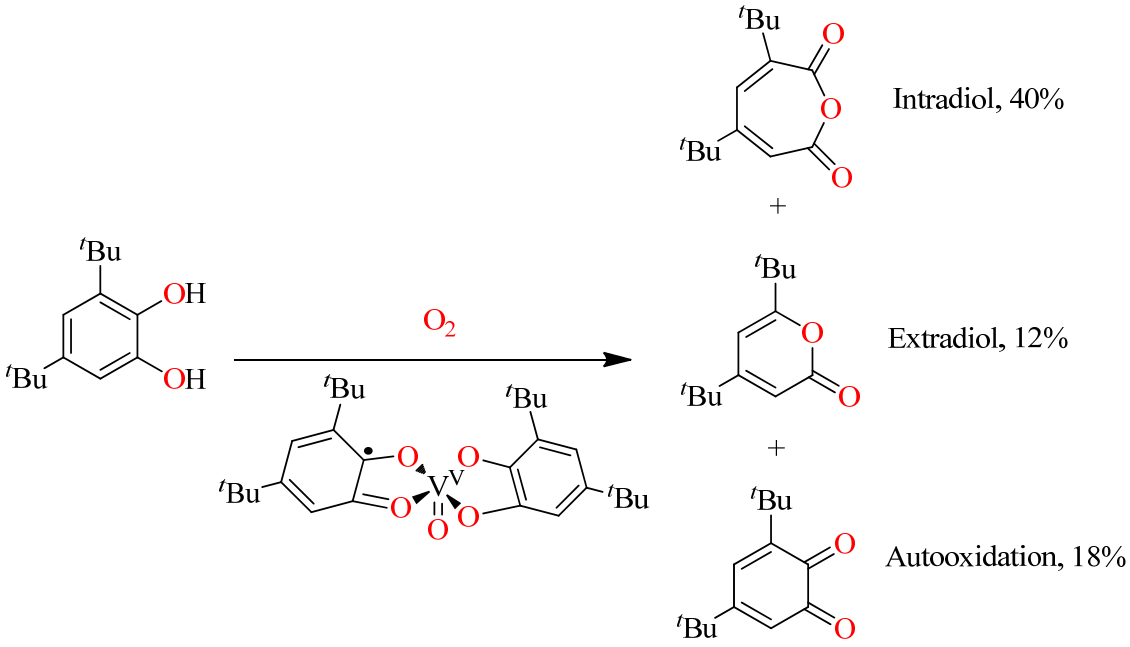

2.5 Conclusion

The ability of redox-active ligands to act as an electron reservoir has important implications in the search for new transition metal complexes capable of activating dioxygen and other small molecules. While the transition metal complexes of bis(arylimino)pyridine have been extensively studied, the potential for these complexes to activate O_2 has been mostly neglected. In this work, we have synthesized new Ni complexes of bis(arylimino)pyridine and reduced some of these complexes by one

electron. The ability of these reduced complexes to activate O_2 has been examined, along with a product of the reaction. This study should help to further the understanding of O_2 activation using redox-active ligand complexes.

CHAPTER 3

SYNTHESIS AND CHARACTERIZATION OF BIS(ARYLIMINO)PYRIDINE COMPLEXES OF NICKEL(II)

3.1 Introduction

The synthesis of Ni^{II} complexes supported by bis(arylimino)pyridine derivatives will be the focus of Chapter 3. The general method for synthesizing these complexes entails the template reaction of an aniline with diacetylpyridine and $NiCl_2$ in the appropriate molar ratio. The targeted derivatives in this work include substitution in the 4-position of the aniline rings and deuterium labeling of the methyl groups adjacent to the imine group on the ligand. The derivatives are prepared by synthesizing the appropriate aniline or diacetylpyridine derivative, which can then be used in the template reaction in order to synthesize the targeted complex. This work will be the focus of sections 3.1 and 3.2.

Characterization of the complexes by single crystal X-ray diffraction (XRD), infrared (IR) spectroscopy, and mass spectrometry (MS) was conducted in order to confirm the identity of the complexes synthesized. The single crystal X-ray diffraction will also provide a basis for comparison to the reduced complexes in Chapter 4 and the reaction product in Chapter 5. Cyclic voltammetry (CV) and differential pulse voltammetry (DPV) was done in order to asses the reducibility of the transition metal complexes. This work will be the focus of sections 3.3, 3.4, and 3.5.

3.2 Experimental Section

Materials. All reagents and solvents were purchased from commercial sources and were used as received, unless noted otherwise. Anhydrous $NiCl_2$, 98% was purchased from Sigma-Aldrich. Dichloromethane, acetonitrile, and diethyl ether were purged with N_2 and then purified by passage through two packed columns of molecular sieves under an N_2 pressure (MBraun solvent purification system). Elemental analysis was performed by Atlantic Microlab, Inc., Norcross, GA.

Physical Methods. NMR spectra were recorded on a Bruker Avance II 300 spectrometer at ambient temperature. ^1H chemical shifts are reported in parts per million (ppm) and were referenced to residual solvent peaks. Mass spectral data were acquired on a quadrupole ion trap ThermoFinnigan LCQ Deca mass spectrometer using an electrospray ionization source. IR spectra were recorded on a Bruker Vertex 70 Fourier-transform IR spectrometer using samples prepared by mixing the solid compound with KBr and pressing the mixture into a disk. Cyclic voltammetry and differential pulse voltammetry measurements were carried out with a CH Instruments potentiostat (Model 620C Electrochemical Analyzer) and a standard three-electrode configuration consisting of a Pt disc working electrode, a Pt wire counter electrode and an $Ag/AgNO_3$ reference electrode (0.01 M $AgNO_3$ in MeCN; supporting electrolyte, 0.1 M NBu_4ClO_4). The voltammograms were recorded on solutions of the analyte (1 mM) and the supporting electrolyte (0.1 M NBu_4ClO_4) in CH_2Cl_2 under an Ar atmosphere at 293 K with a scan rate of 0.1 $V \cdot s^{-1}$. *Caution*: Mixtures of perchlorate salts and metal complexes are potentially explosive, handle with care. Potentials are reported referenced to an external

$[FeCp_2]/[FeCp_2]^+$ redox system which can be converted to the SCE scale by adding 0.48 V (SCE, aqueous saturated calomel electrode).[39,40] Potentials relative to SCE can be converted to the NHE scale by adding 0.24 V (NHE, normal hydrogen electrode).[41]

Iodobenzene Dichloride, $PhICl_2$. This procedure was adapted from a previous report.[42] A total of 2.8 mL of iodobenzene (5 g, 0.0245 mol) was dissolved in 10 mL of dichloromethane in a 250 mL round bottom flask which was placed in an icebath. Chlorine gas was generated by dropwise addition of 15 mL of conc. HCl to 2.37 g of $KMnO_4$ (15 mmol). The outlet needle for the chlorine gas was kept above the iodobenzene solution (*Caution*: Chlorine is a toxic gas). The solution was stirred for 1 h at 0 °C. A yellow precipitate formed, which was filtered and washed once with 5 mL of −25 °C dichloromethane. The precipitate was dried in *vacuo*, and 5.23 g (78%) of a yellow crystalline material was obtained. ^{1}H NMR (300 MHz, $CDCl_3$, δ): 8.19 (d, J = 7.8 Hz, 2H, Ar H), 7.60 (t, J = 7.8 Hz, 1H, Ar H), 7.48 (t, J = 8.1 Hz, 2H, Ar H).

4-Chloro-2,6-diisopropylaniline, 4-Cl-2,6-^{i}Pr$_2$C$_6$H$_2$NH$_2$. This compound has been synthesized previously,[43] however a completely different procedure is used here. A total of 3.44 g of iodobenzene dichloride (0.0125 mol) was added to a solution of 2.57 mL of 2,6-diisopropylaniline (2.22 g, 0.0125 mol) in 70 mL dichloromethane. The solution heated to reflux with stirring for 4 h. After the solution was cooled, it was washed with 70 mL of 1 M NaOH, and the organic phase was separated after extraction. The aqueous phase was washed with another 70 mL of dichloromethane. The organic phases were combined, dried over $MgSO_4$, filtered, and the solvent was removed under reduced pressure to give 3.76 g of an oil. The oil was dissolved in ca. 6 mL of 2:1 hexanes-dichloromethane and purified in 1 mL fractions (6 columns total) by column

chromatography using a silica gel stationary phase and 2:1 hexanes-dichloromethane as the mobile phase. After the product fractions from all six separations were combined and evaporated to dryness, 1.38 g (52%) of a dark oil was obtained. ^{1}H NMR (300 MHz, $CDCl_3$, δ): 6.98 (s, 2H, Ar H), 3.70 (s, 2H, NH_2), 2.89 (sept, J = 6.9 Hz, 2H, Ar C*H*(CH_3)$_2$), 1.25 (d, J = 6.9 Hz, 12H, Ar CH(C*H*$_3$)$_2$).

4-Bromo-2,6-diisopropylaniline hydrobromide, 4-Br-2,6-^{i}Pr$_2$C$_6$H$_2$NH$_2$·HBr. This procedure was adapted from a previous report.[44] A total of 2.5 mL of bromine (7.80 g, 0.0488 mol) was added dropwise to a solution of 5 mL (4.33 g, 0.0244 mol) of 2,6-diisopropylaniline in 25 mL of 95:5 nitromethane-water. A brown precipitate immediately formed. The mixture was stirred for 24 h at 20 °C. The precipitate was filtered, dissolved in 90 °C ethanol, and placed immediately at –25 °C for crystallization, yielding 3.90 g (47%) of an offwhite light pink microcrystalline product. ^{1}H NMR (300 MHz, $CDCl_3$, δ): 10.03 (s, 2H, NH_2), 7.36 (s, 2H, Ar H), 3.67 (sept, J = 6.6 Hz, 2H, Ar C*H*(CH_3)$_2$), 1.30 (d, J = 6.9 Hz, 12H, Ar CH(*CH*$_3$)$_2$).

4-Bromo-2,6-diisopropylaniline, 4-Br-2,6-^{i}Pr$_2$C$_6$H$_2$NH$_2$. This procedure was adapted from a previous report.[44] 15 mL of 1 M NaOH was added to a solution of 1.50 g (0.0044 mol) of 4-Br-2,6-diisopropylaniline hydrobromide in 15 mL dichloromethane, and the resulting mixture was stirred for 15 min at 20 °C. The organic phase was removed, and the aqueous phase was washed twice with 15 mL of dichloromethane. The organic fractions were pooled, dried over $MgSO_4$, filtered, and then evaporated to dryness, yielding 0.88 g (78%) of a brown oil. ^{1}H NMR (300 MHz, $CDCl_3$, δ): 7.11 (s, 2H, Ar H), 3.72 (s, 2H, NH_2), 2.88 (sept, J = 6.9 Hz, 2H, Ar C*H*(CH_3)$_2$), 1.25 (d, J = 6.9 Hz, 12H, Ar CH(C*H*$_3$)$_2$).

***N*-(4-Toluenesulfonyl)-2,6-diisopropylaniline, 2,6-^{i}Pr$_2$C$_6$H$_3$NHSO$_2$C$_6$H$_4$Me.** This procedure was adapted from a previous report.[45] A total of 10.28 g (0.054 mol) of 4-toluenesulfonyl chloride was added to a solution of 10 mL (8.65 g, 0.0488 mol) 2,6-diisopropylaniline in 20 mL of pyridine. The resulting solution was heated under reflux for 4 h, then cooled to 20 °C, and poured into 64 mL of 2 M HCl under stirring. A solid precipitate formed, which was separated by filtration, dissolved in 90 °C ethanol and placed at –25 °C for crystallization. A yellow precipitate formed within 24 h, which was washed with ice-cold ethanol and dried in *vacuo*. Yield: 13.59 g (84%). ^{1}H NMR (300 MHz, dmso-d$_6$, δ): 9.36 (s, 1H, NH), 7.56 (d, J = 8.1 Hz, 2H, Ar H), 7.35 (d, J = 7.8 Hz, 2H, Ar H), 7.20 (t, J = 7.2 Hz, 1H, Ar H), 7.07 (d, J = 7.5 Hz, 2H, Ar H), 3.07 (sept, J = 6.6 Hz, 2H, Ar C*H*(CH$_3$)$_2$), 2.35 (s, 3H, ArCH$_3$), 0.89 (d, J = 6.3 Hz, 12H, Ar CH(C*H*$_3$)$_2$).

***N*-(4-Toluenesulfonyl)-4-nitro-2,6-diisopropylaniline, 4-NO$_2$-2,6-^{i}Pr$_2$C$_6$H$_2$NHSO$_2$C$_6$H$_4$Me.** This procedure was adapted from a previous report.[45] 7.01 g (0.021 mol) of *N*-(4-toluenesulfonyl)-2,6-diisopropylaniline was added to a solution of 129 mL of H$_2$O, and 41 mL of HNO$_3$ (50–70%). 140 mL of glacial acetic acid was added to the solution, followed by addition of 2.23 g (0.032 mol) of sodium nitrite. The mixture was heated under reflux for 12 h, allowed to cool for 1 h and then poured over 400 mL of ice water. An off-white solid precipitated, which was separated by filtration, washed with water, and then dried in *vacuo* overnight. Yield: 2.76 g (35%). ^{1}H NMR (300 MHz, CDCl$_3$, δ): 7.97 (s, 2H, Ar H), 7.58 (d, J = 8.1 Hz, 2H, Ar H), 7.28 (d, J = 8.4 Hz, Ar H, this signal overlaps with the residual solvent peak), 6.07 (s, 1H, NH), 3.17 (sept, J = 6.9 Hz, 2H, Ar C*H*(CH$_3$)$_2$), 2.43 (s, 3H, Ar CH$_3$), 1.05 (d, J = 6.6 Hz, 12H, Ar CH(C*H*$_3$)$_2$).

4-Nitro-2,6-diisopropylaniline, 4-NO_2-2,6-^{i}$Pr_2C_6H_2NH_2$. This procedure was adapted from a previous report.[45] A solution of 0.416 g (0.0011 mol) of *N*-(4-toluenesulfonyl)-4-nitro-2,6-diisopropylaniline in 2.2 mL of 95% H_2SO_4 was stirred for 24 h at 20 °C. The solution was then poured over ice and made basic by a slow dropwise addition of 10 M NaOH. The product was extracted from the aqueous solution with two 20 mL portions of dichloromethane, and the combined organic phases were dried over $MgSO_4$ and evaporated to dryness, yielding 0.146 g (60%) of a yellow solid. ^{1}H NMR (300 MHz, $CDCl_3$, δ): 7.98 (s, 2H, Ar H), 4.46 (s, 2H, NH_2), 2.87 (sept, J = 6.9 Hz, 2H, Ar C*H*(CH_3)$_2$), 1.31 (d, J = 6.9 Hz, 12H, Ar CH(C*H*$_3$)$_2$).

***N*-(4-Toluenesulfonyl)-4-amino-2,6-diisopropylaniline, 4-NH_2-2,6-^{i}$Pr_2C_6H_2NHSO_2C_6H_4Me$.** This procedure was adapted from a previous report.[45] 1.42 g (0.0038 mol) of *N*-(4-toluenesulfonyl)-4-nitro-2,6-diisopropylaniline was added to a solution of 4.30 g (0.023 mol) of $SnCl_2$ in 20 mL of ethanol. This solution was heated under reflux and held for 90 min. The solution was cooled to 20 °C and poured over ice. 10M NaOH was added dropwise to the solution until it was basic. The aqueous phase was washed with three 20mL portions of dichloromethane, and the yellow organic phase was dried over $MgSO_4$ and evaporated to dryness, yielding 1.07 g (82%) of a red orange solid. ^{1}H NMR (300 MHz, $CDCl_3$, δ): 7.60 (d, J = 8.4 Hz, 2H, Ar H), 7.24 (d, J = 8.4 Hz, Ar H, this signal overlaps with the residual solvent peak), 6.39 (s, 2H, Ar H), 5.75 (s, 1H, NH), 3.66 (s, 2H, Ar NH_2), 3.02 (sept, J = 6.9 Hz, 2H, Ar C*H*(CH_3)$_2$), 2.47 (s, 3H, Ar CH_3), 0.95 (d, J = 6.6 Hz, 12H, Ar CH(*C*H$_3$)$_2$,).

***N*-(4-Toluenesulfonyl)-4-dimethylamino-2,6-diisopropylaniline, 4-N(Me_2)-2,6-^{i}$Pr_2C_6H_2NHSO_2C_6H_4Me$.** This procedure was adapted from a previous report.[45] A slurry

was made of 0.500 g (0.00144 mol) of N-(4-Toluenesulfonyl)-4-amino-2,6-diisopropylaniline and 0.768 g (0.02 mol) of $NaBH_4$ in 10 mL of diethyl ether. This was slowly added dropwise to a mixture of 2.4 mL of 3M H_2SO_4 and 1.5 mL (0.018 mol) of (37 wt% in H_2O, stabilized with MeOH) formaldehyde under stirring in an ice bath to keep the mixture cool. An additional 10 mL of diethyl ether (20 mL total) was added to the $NaBH_4$ slurry, and over the course of 20 min was added to the mixture. After the addition, the mixture was stirred for 30 min on ice. The mixture was then neutralized with 10M NaOH. The organic phase was separated and the aqueous phase was washed twice with diethyl ether. The combined organic phases were dried over $MgSO_4$ and evaporated to dryness to leave an orange solid, which was dried in *vacuo* overnight. Yield: 0.271 g (50%). ^{1}H NMR (300 MHz, $CDCl_3$, δ): 7.61 (d, J = 8.4 Hz, 2H, Ar H), 7.24 (d, Ar H, this signal overlaps with the residual solvent peak), 6.41 (s, 2H, Ar H), 5.75 (s, 1H, NH), 3.06 (sept, J = 6.9 Hz, 2H, Ar C*H*$(CH_3)_2$), 2.95 (s, 6H, NCH_3), 2.40 (s, 3H, Tos CH_3), 0.98 (d, J = 6.9 Hz, 12H, Ar CH(CH_3)$_2$,).

4-Dimethylamino-2,6-diisopropylaniline, 4-N(Me$_2$)-2,6-^{i}Pr$_2$C$_6$H$_2$NH$_2$. This procedure was adapted from a previous report.[45] A solution of 0.341 g (0.0009 mol) of *N*-(4-toluenesulfonyl)-4-dimethylamino-2,6-diisopropylaniline in 3 mL of 95% H_2SO_4 was stirred for 24 h at 20 °C. The brown solution was poured onto ice and 10M NaOH was added until the mixture was basic. The product was extracted with three 20 mL portions of dichloromethane, the combined organic phases were dried with $MgSO_4$ and evaporated to dryness, giving 0.138 g (69%) of a purple oil. ^{1}H NMR (300 MHz, $CDCl_3$, δ): 6.60 (s, 2H, Ar H), 3.40 (s, 2H, NH_2), 2.97 (sept, J = 6.9 Hz, 2H, Ar C*H*$(CH_3)_2$), 2.85 (s, 6H, NCH_3), 1.27 (d, J = 6.6 Hz, 12H, Ar CH(CH_3)$_2$).

2,6-Diacetylpyridine-d_6, 2,6-{$CD_3C(O)$}$_2C_5H_3N$. This procedure was adapted from a previous report.[46] A solution of 0.50 g (3.06 mmol) of 2,6-diacetylpyridine in 9 mL of a 50:50 mixture of ethanol-d_1 and D_2O was refluxed for 48 h under an Ar atmosphere. The solution was then cooled to 20 °C, and the volatiles were removed under reduced pressure. A yellow solid was obtained which was recrystallized from hexanes at –25 °C to yield an off white solid. Yield: 0.29 g (56%). ^{1}H NMR (300 MHz, $CDCl_3$, δ): 8.22 (d, J = 7.8 Hz, 2H, Ar H), 7.99 (t, J = 6.6 Hz, 1H, Ar H). The integration of the peak of the residual acetyl protons ($COCH_3$) at 2.80 ppm indicates that ca. 5% of the undeuterated 2,6-diacetylpyridine remains.

[Ni{2,6-(2,6-^{i}Pr$_2C_6H_3N$=CMe)$_2C_5H_3N$}Cl_2] (1). The synthesis of this compound was reported, previously;[21] here, a different procedure[47] was adapted. A solution of 0.50 g (3.06 mmol) of 2,6-diacetylpyridine, 1.25 mL (1.18 g, 6.10 mmol) of 2,6-diisopropylaniline (92%) and 0.40 g (3.09 mmol) of $NiCl_2$ in 15 mL of glacial acetic acid was heated under reflux for 4 h. The solution was allowed to cool to room temperature, and 10 mL of diethyl ether was added, causing the formation of a red precipitate. The precipitate was separated by filtration, washed three times with diethyl ether and dried *in vacuo* to yield 1.54 g (83%) of a red-brown powder. Red orange single crystals of X-ray diffraction quality were obtained within ca. one week by vapor diffusion of diethylether into a dichloromethane solution at 4 °C. Anal. Calcd for $C_{33}H_{43}Cl_2N_3Ni\cdot 0.5H_2O$: C, 63.89; H, 7.15; N, 6.77; Cl, 11.43. Found: C, 63.49; H, 7.10; N, 6.51; Cl, 12.17. ESI(+)MS (CH_3CN) (m/z): {M – Cl}$^+$ calcd for $C_{33}H_{43}Cl_2N_3Ni$, 574.25; found, 574.2.IR (KBr, cm^{-1}): 3632, 3462, 3063, 2964 (s), 2927, 2867, 1621, 1583 (s), 1466 (s), 1446,

1371, 1330, 1317, 1262 (s), 1206, 1194, 1103, 1089, 1057, 1033, 937, 818, 804, 796, 777 (s), 760, 746, 719.

[Ni{2,6-(2,6-^{i}Pr$_2$C$_6$H$_3$N=CCD$_3$)$_2$C$_5$H$_3$N}Cl$_2$] (2). A solution of 0.200 g (1.18 mmol) 2,6-diacetylpyridine-d_6, 0.153 g (1.18 mmol) $NiCl_2$, and 0.485 mL (0.00236 mmol) 2,6-diisopropylaniline (92%) in 20 mL glacial acetic acid-d_1 was heated under reflux for 4 h. The solution was allowed to cool to room temperature, concentrated under reduced pressure, and 10 mL of diethyl ether was added causing the formation of a red precipitate. The precipitate was separated by filtration, washed three times with diethyl ether and dried in *vacuo* to yield 0.633 g (87%) of a red microcrystalline solid. Red orange single crystals were obtained within ca. one week by vapor diffusion of diethylether into a dichloromethane solution at 4 °C. Anal. Calcd for $C_{33}H_{43}Cl_2N_3Ni{\cdot}0.5H_2O$: C, 63.89; H, 7.15; N, 6.77; Cl, 11.43. Found: C, 63.60; H, 7.05; N, 6.62; Cl, 11.61 (Note: D atoms treated as H atoms for elemental analysis). ESI(+)MS (CH_3CN) (*m*/*z*): $\{M - Cl\}^+$ calcd for $C_{33}H_{37}D_6Cl_2N_3Ni$, 580.29; found, 580.2. IR (KBr, cm^{-1}): 3632, 3463, 3061, 2964 (s), 2928, 2868, 1616, 1586 (s), 1466 (s), 1444, 1379, 1359, 1329, 1318, 1262 (s), 1212, 1100, 1036, 898, 850, 798, 784, 758, 743, 671.

General Procedure for the Synthesis of [Ni{2,6-(4-X-2,6-^{i}Pr$_2$C$_6$H$_3$N=CMe)$_2$C$_5$H$_3$N}Cl$_2$] Complexes 3-6. In a typical procedure, a solution of 0.200 g (1.23 mmol) of 2,6-diacetylpyridine, 0.159 g (1.23 mmol) $NiCl_2$, and 2 equiv of the appropriate 4-X-2,6-diisopropylaniline (X = Cl, Br, NO_2, $N(CH_3)_2$) in 20 mL glacial acetic acid was heated under reflux for 4 h. The solution was allowed to cool to room temperature, concentrated under reduced pressure, and 10 mL of diethyl ether was added

causing the formation of a precipitate. The precipitate was separated by filtration, washed three times with diethyl ether and dried in *vacuo* to yield a microcrystalline solid.

[Ni{2,6-(4-Cl-2,6-^{i}Pr$_2$C$_6$H$_2$N=CMe)$_2$C$_5$H$_3$N}Cl$_2$] (3). Yield: 0.684 g (82%) of a red microcrystalline solid. Orange single crystals of X-ray diffraction quality were obtained within ca. one week by vapor diffusion of diethylether into a dichloromethane solution at 4 °C. Samples submitted for elemental analysis were dried in *vacuo* for 24 h. Anal. Calcd for $C_{33}H_{41}Cl_4N_3Ni$: C, 58.27; H, 6.08; N, 6.18; Cl, 20.85. Found: C, 57.99; H, 6.25; N, 6.17; Cl, 20.57. ESI(+)MS (CH_3CN) (*m*/*z*): $\{M - Cl\}^+$ calcd for $C_{33}H_{41}Cl_4N_3Ni$, 642.17; found, 642.3. IR (KBr, cm^{-1}): 3084, 2963 (s), 2930, 2867, 1625, 1589 (s), 1466 (s), 1438, 1381, 1371 (s), 1330, 1319, 1262 (s), 1210 (s), 1192, 1069, 1033, 944, 896, 871, 851, 810 (s), 755, 747, 730, 573, 456.

[Ni{2,6-(4-Br-2,6-^{i}Pr$_2$C$_6$H$_2$N=CMe)$_2$C$_5$H$_3$N}Cl$_2$] (4). Yield: 0.759 g (80%) of a red microcrystalline solid. Orange red single crystals of X-ray diffraction quality were obtained within ca. one week by vapor diffusion of diethylether into a dichloromethane solution at 4 °C. Samples submitted for elemental analysis were dried in *vacuo* for 24 h. Anal. Calcd for $C_{33}H_{41}Br_2Cl_2N_3Ni{\cdot}CH_2Cl_2$: C, 47.82; H, 5.07; N, 4.92; Cl, 16.60; Br, 18.71. Found: C, 47.94; H, 5.35; N, 4.88; Cl, 16.33; Br, 18.83. ESI(+)MS (CH_3CN) (*m*/*z*): $\{M - Cl\}^+$ calcd for $C_{33}H_{41}Br_2Cl_2N_3Ni$, 730.07; found, 730.1. IR (KBr, cm^{-1}): 3069, 3048, 2964 (s), 2927, 2865, 1631, 1589 (s), 1574, 1463, 1438, 1382, 1370 (s), 1327, 1314, 1259, 1209, 1190, 1067, 1034, 980, 941, 878, 861, 807, 794, 740, 730 (s), 699, 564.

[Ni{2,6-(4-NO$_2$-2,6-^{i}Pr$_2$C$_6$H$_2$N=CMe)$_2$C$_5$H$_3$N}Cl$_2$] (5). Yield: 0.231 g (27%) of a brown solid. ESI(+)MS (CH_3CN) (*m*/*z*): $\{M - Cl\}^+$ calcd for $C_{33}H_{41}Cl_2N_5NiO_4$, 664.22; found, 664.2.

[Ni{2,6-(4-NMe$_2$-2,6-^{i}Pr$_2$C$_6$H$_2$N=CMe)$_2$C$_5$H$_3$N}Cl$_2$] (6). Yield: 0.742 g (86%) of a brown microcrystalline solid. ESI(+)MS (CH_3CN) (*m*/*z*): $\{M - Cl\}^+$ calcd for $C_{37}H_{53}Cl_2N_5Ni$, 660.33; found, 660.5.

[Ni{2,6-(2,6-^{i}Pr$_2$C$_6$H$_2$BrN=CMe)C$_5$H$_3$NC(O)Me}Cl$_2$] (7). When the synthesis of **4** was attempted using 4-bromo-2,6-diisopropylaniline hydrobromide in place of 4-bromo-2,6-diisopropylaniline, 0.616 g of an orange brown solid was obtained, which appears to be a mixture of three products on the basis of mass spectrometric analysis. Recrystallization of this solid by vapor diffusion of diethylether into a dichloromethane solution at 4 °C afforded orange single crystals of **7**. ESI(+)MS (CH_3CN) (*m*/*z*): calcd for $C_{33}H_{41}Br_2Cl_2N_3Ni$ (**4**), 730.07; calcd for $C_{33}H_{41}Br_4N_3Ni$ (**4** – 2Cl + 2Br), 774.02; calcd for $C_{21}H_{25}Br_3N_2NiO$ (**7**), 536.97; found, 730.1 $\{$**4** – Cl$\}^+$, 774.1 $\{$**4** – 2Cl + Br$\}^+$, 537 $\{$**7** – Br$\}^+$.

X-ray Crystallographic Analyses. A single crystal of each compound was coated with Paratone N oil and mounted on a glass capillary for data collection at 190(2) K on a Bruker Nonius Kappa APEX II diffractometer (**1, 3** and **4**) or at 180(2) K on a Nonius KappaCCD diffractometer (**7**), using Mo *Kα* radiation (graphite monochromator). The temperature was controlled by an Oxford Cryostream Cooler (700 series, N_2 gas). Data collection, data reduction, and absorption correction were carried out following standard CCD techniques using the APEX2 software package (**1, 3** and **4**) or using the software packages Collect and HKL-2000 (**7**).[48-50] Final cell constants were calculated from 4432 (**1**·0.5H_2O), 8554 (**3**·CH_2Cl_2), 9981 (**4**·CH_2Cl_2) or 7413 (**7**) reflections from the complete data set. The space groups of *P*–1 (**1**·0.5H_2O), $P2_1$/m (**3**·CH_2Cl_2 and **4**·CH_2Cl_2), and $P2_1/c$ (**7**) were determined based on systematic absences or lack thereof

and intensity statistics. The structures were solved by direct methods and refined by full-matrix least-squares minimization and difference Fourier methods (SHELXTL v.6.12).[51,52] All non-hydrogen atoms were refined with anisotropic displacement parameters. All hydrogen atoms were placed in ideal positions and refined as riding atoms with relative isotropic displacement parameters. In **1**·0.5H_2O, the hydrogen atoms on the solvent molecule were omitted, and the occupancy of the oxygen atom in the solvent molecule was refined and then fixed to 50%. A couple of reflections with intensities that were severely affected by the beamstop were omitted in the final stage of the refinement. The final full-matrix least-squares refinement converged to $R1 = 0.0450$ and $wR2 = 0.0818$ [F^2, $I > 2\sigma(I)$]. In **3**·CH_2Cl_2 and **4**·CH_2Cl_2, the carbon atom and one of the chlorine atoms of the dichloromethane solvent molecule is disordered about the mirror plane, with 50% occupancy modeled on each side of the mirror plane, and the other chlorine atom is located on the mirror plane. For **3**·CH_2Cl_2, the final full-matrix least-squares refinement converged to $R1 = 0.0406$ and $wR2 = 0.0960$ [F^2, $I > 2\sigma(I)$]. The highest residual electron density peak was located 0.92 Å from Cl4 and the deepest hole was located 0.35 Å from Cl4. For **4**·CH_2Cl_2, the final full-matrix least-squares refinement converged to $R1 = 0.0407$ and $wR2 = 0.0904$ [F^2, $I > 2\sigma(I)$]. The highest residual electron density peak was located 0.92 Å from Cl3 and the deepest hole was located 0.42 Å from Cl3. For **7**, a couple of reflections with intensities that were severely affected by the beamstop were omitted in the final stage of the refinement. The final full-matrix least-squares refinement converged to $R1 = 0.0536$ and $wR2 = 0.1236$ [F^2, $I > 2\sigma(I)$]. The highest residual electron density peak was located 1.34 Å from H2 and the deepest hole

was located 0.85 Å from Br1. Additional information about the refinement is provided in section 3.3.3 and in Tables 1, 5 and 9.

3.3 Results and Discussion

3.3.1 Synthesis and Isolation of 4-Substituted 2,6-Diisopropylanilines

2,6-diisopropylaniline is readily available commercially, however the 4-X-2,6-diisopropylaniline (X = Br, Cl, NO_2, or $N(CH_3)_2$) derivatives must be synthesized as none are available commercially. All four aniline derivatives have been reported previously in the literature.[43-45] A new method was adapted for the synthesis of 4-chloro-2,6-diisopropylaniline using a chloride transfer reagent, iodobenzene dichloride.[42] The reaction of 1 equiv iodobenzene dichloride with 2,6-diisopropylaniline (after neutralization with sodium hydroxide) generated a mixture of 2,6-diisopropylaniline and 4-chloro-2,6-diisopropylaniline (Scheme 10). The mixture could be separated by column chromatography using a silica gel stationary phase and a 2:1 hexanes-dichloromethane mobile phase, with 52% overall yield. It should be noted that 2,6-diisopropylaniline and 4-chloro-2,6-diisopropylaniline have similar retention factors, so a longer column for the separation is preferred.

4-bromo-2,6-diisopropylaniline was synthesized from a reaction of 2,6-diisopropylaniline and Br_2, followed by neutralization with sodium hydroxide (Scheme 11). Here, the method was modified for scale, time, and solvents employed for the

reaction and recrystallization.[44] The hydrobromic acid salt of 2,6-diisopropylanline obtained in the first step could be easily recrystallized from ethanol at -25 °C in a 47% yield. The hydrobromic acid salt of 2,6-diisopropylaniline was neutralized with sodium hydroxide to generate 4-bromo-2,6-diisopropylaniline with a 78% yield for the neutralization step.

Scheme 10. Synthesis of 4-Chloro-2,6-diisopropylaniline.

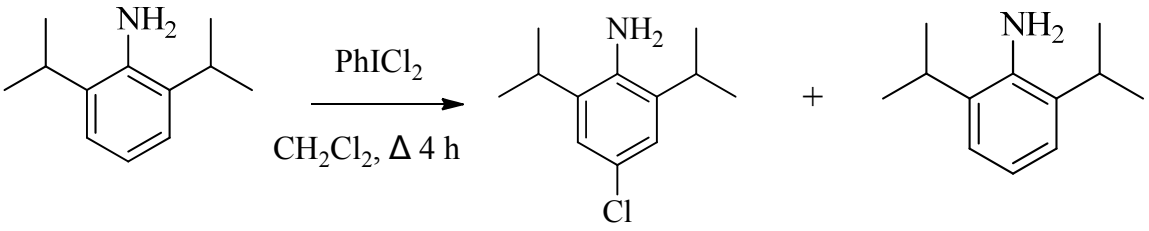

Scheme 11. Synthesis of 4-Bromo-2,6-diisopropylaniline.

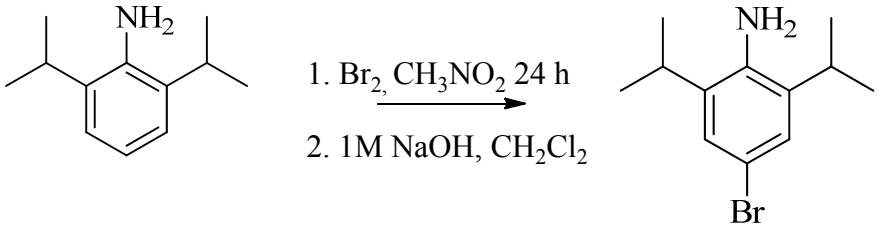

The synthetic route to prepare 4-nitro-2,6-diisopropylaniline and 4-dimethylamino-2,6-diisopropylaniline has been reported previously,[45] and used with only alterations to the scale of the reactions, with the exception of a minor alterations to one of the steps. In the synthesis of 4-dimethylamino-2,6-diisopropylaniline, the fourth step involving the methylation of the 4-amino group was altered to use a greater excess of sodium borohydride and formaldehyde. Using the literature condition, ^{1}H NMR

spectroscopy post isolation identified a mixture of three aniline products when the original method was used, which were identified as the starting material, a monomethyl substituted intermediate, and the final product where both methyl groups had been successfully transferred. Increasing the excess of sodium borohydride and formaldehyde enabled the reaction to proceed to completion, with 100% of the isolated material being identified as the dimethylamino product.

Scheme 12. Synthesis of 4-Nitro-2,6-diisopropylaniline and 4-Dimethylamino-2,6-diisopropylaniline.

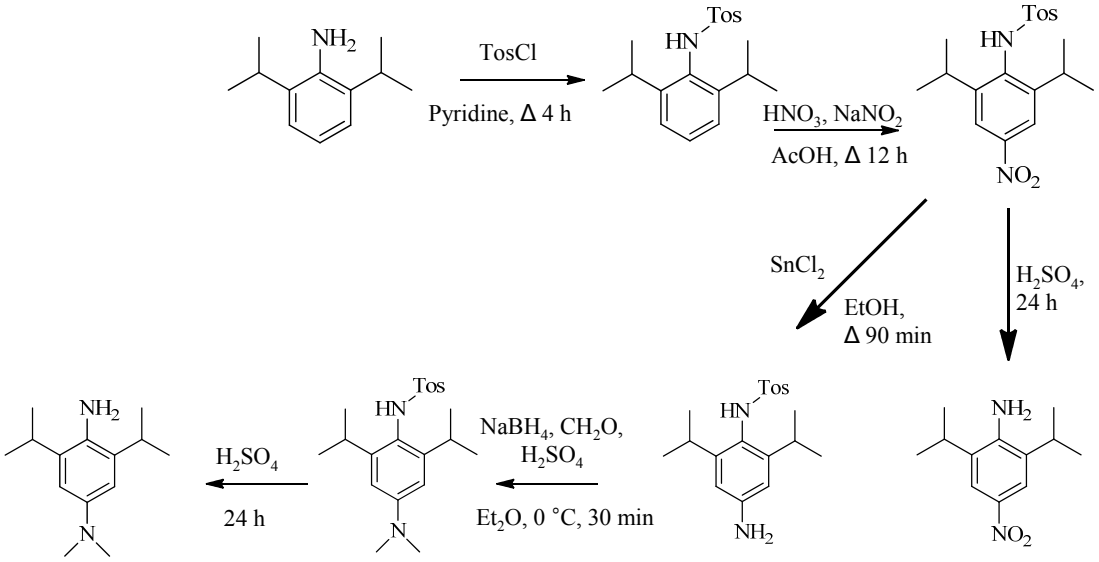

3.3.2 Synthesis and Characterization of Bis(arylimino)pyridine Complexes of Nickel(II)

As discussed in Chapter 2, a wide variety of transition metal complexes with bis(arylimino)pyridine ligands have been synthesized, and typically this process involves

synthesis of the ligand by condensation of 2 equiv of an aniline and 1 equiv of a diisopropylaniline. The completed ligand forms a complex with a metal center in a second reaction.[5,20] Complex **1** has been previously reported and crystallographically characterized using this method.[21] A template reaction has been reported where the condensation of the ligand occurs with complexation to the metal center in one step using the appropriate ratios of 2,4,6-trimethylaniline, 2,6-diacetylpyridine, and $NiCl_2$ in an acetic acid solution heated under reflux for 4 h.[47] This approach was used for the synthesis of complex **1** in this work (Scheme 13). A microcrystalline solid was obtained from this synthesis and was recrystallized from a dichloromethane solution with diethylether diffusion at 4 °C to afford crystals of X-ray diffraction quality.

Scheme 13. Synthesis of Complex **1**.

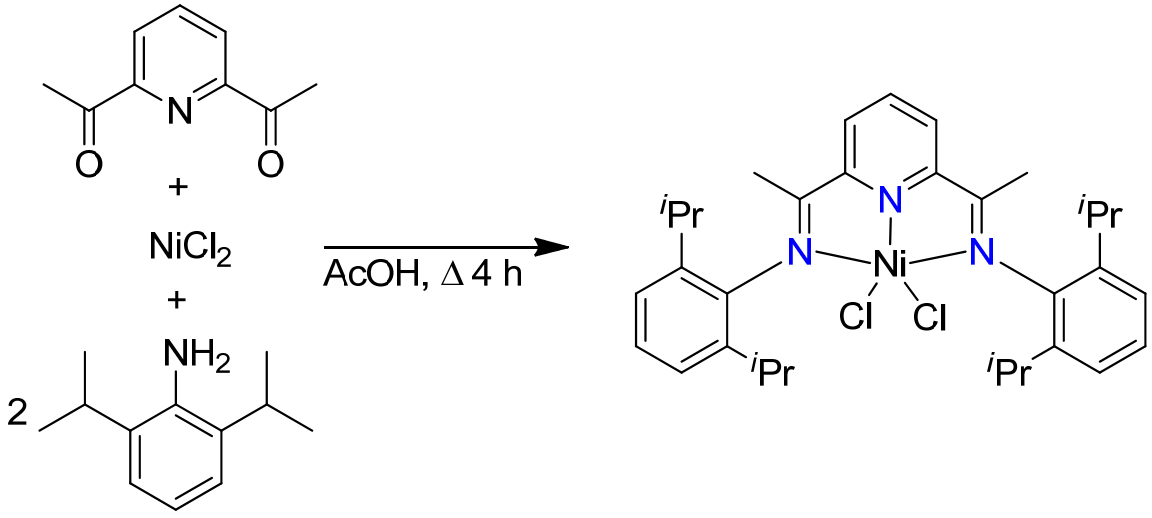

The synthesis of **2** requires the deuterium label to be placed on the 2,6-diacetylpyridine prior to the template reaction. The synthesis of diacetylpyridine-d_6 has been described previously, and the method was used as reported.[46] The reaction is based

on a simple exchange of deuterium for hydrogen using a mixture of ethanol-d_1 and D_2O at reflux (Scheme 14). As a result of this method, the final product was not 100% enriched in deuterium. On the basis of ^1H NMR integration, comparing the integration of the pyridine ^1H peaks to that of the integration of the residual ^1H CH_3 peak, the enrichment of the deuterium label on the aniline is ca. 95%. In addition to using diacetylpyridine-d_6 in the template reaction to form **2**, acetic acid-d_1 was used to ensure that the deuterium label was not lost. A microcrystalline solid was obtained from this synthesis and was recrystallized from a dichloromethane solution with diethylether diffusion at 4 °C.

Scheme 14. Synthesis of 2,6-Diacetylpyridine-d_6.

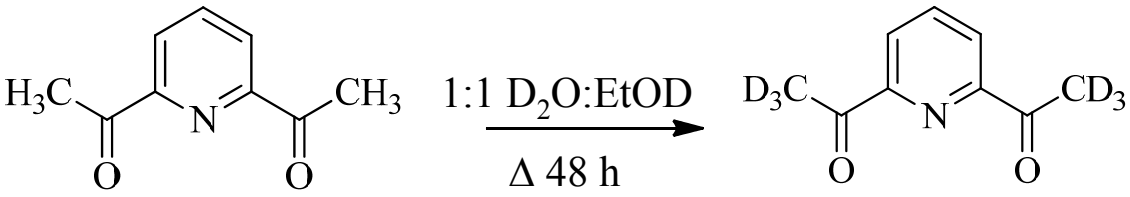

Complexes **3** – **6** were also synthesized using the template reaction as shown in Scheme 15, with the appropriate 2,6-diisopropylaniline derivative used for each reaction. The products from the synthesis of **3** and **4** were recrystallized from a dichloromethane solution with diethylether diffusion at 4 °C to afford crystals of X-ray diffraction quality. Attempts to recyrstallize **5** and **6** from a variety of solvents were unsuccessful.

Electrospray ionization mass spectrometry analysis of complexes **1**-**6** was conducted, and even pre recrystallization, the results typically showed that there was only one ionized species present. The peak observed was the $\{M - Cl\}^+$ peak, with the

molecule losing a chloride anion to gain a positive charge, and the bis(arylimino)pyridine ligand remaining intact.

Scheme 15. Synthesis of Complexes **3**-**6** and Ligand Abbreviations Used in Chapter 3.

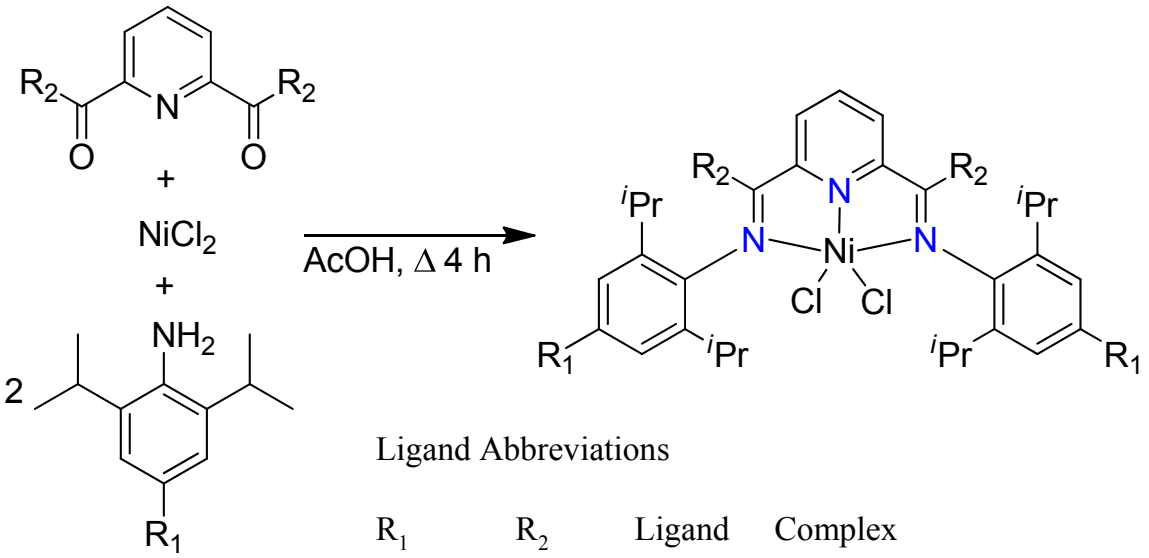

Ligand Abbreviations

R_1	R_2	Ligand	Complex
H	CH_3	L1	**1**
H	CD_3	L2	**2**
Cl	CH_3	L3	**3**
Br	CH_3	L4	**4**
NO_2	CH_3	L5	**5**
$N(CH_3)_2$	CH_3	L6	**6**

The synthesis of **4** was attempted using 4-bromo-2,6-diisopropylaniline hydrobromide. A mixture was observed in the mass spectrum of the product material. The expected $\{M - Cl\}^+$ peak corresponding to $[Ni(L4)Cl_2]$ was present, but from the mass spectroscopy data it also is clear that the chloro ligands exchanged with bromine in a portion of the sample forming $[Ni(L4)Br_2]$, and also that the ligand did not fully form in some of the molecules resulting in $[Ni(L7)Br_2]$. The mixture observed likely arises from a

difference in the aniline used for the complexation reaction, and the presence of HBr is likely the source of the bromide ligand exchange on the metal, and also would seem to reduce the efficiency of the ligand condensation. This reaction and the observed products are highlighted in Scheme 16.

Scheme 16. Synthesis of Bis(arylimino)pyridine Complexes of Ni^{II} using 4-Bromo-2,6-diisopropylaniline Hydrobromide.

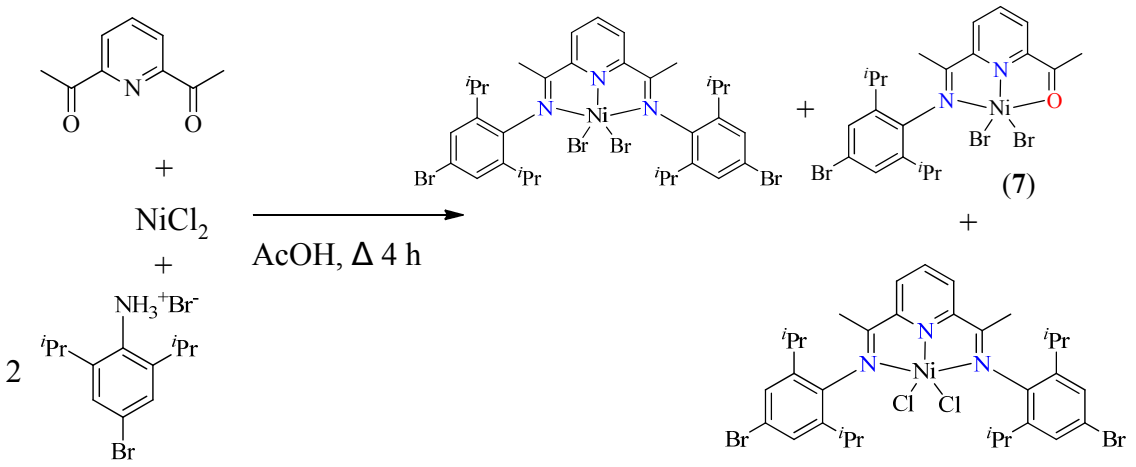

Complexes **1-4** were analyzed using IR spectroscopy. Figures 1 and 2 contain the IR spectra of complexes **1-4**. The bands observed in the IR spectra of the $[Ni(L)Cl_2]$ complexes are listed in the experimental section (Chapter 3.2). For $[Ni(L1)Cl_2]\cdot 0.5H_2O$, the bands above 1500 cm^{-1} can be assigned to ν_{OH} (3632, 3462 cm^{-1}), aromatic ν_{CH} (3063 cm^{-1}), saturated ν_{CH} (2964, 2927, 2867 cm^{-1}), ν_{CN} (1621 cm^{-1}), and aromatic ν_{CC} (1583 cm^{-1}). While the complex itself does not have any OH functionality, the bands in the ν_{OH} region are consistent with the 0.5 equiv of lattice water found in the crystal structure. Overall, the IR spectrum agrees with the previously reported data[43] of

$[Ni(L1)Cl_2]\cdot 0.5H_2O$. The ν_{CN} band was previously reported at 1624 cm^{-1}, which compares favorably with the 1621 cm^{-1} for ν_{CN} observed here.

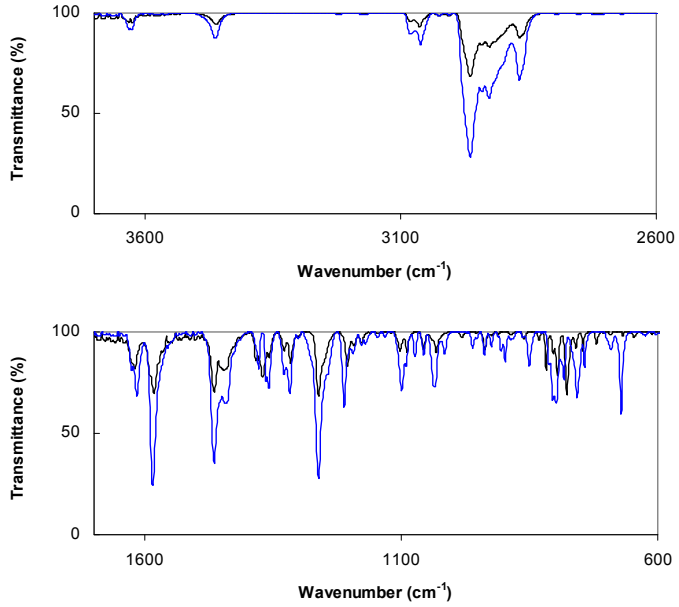

Figure 1. IR spectra of $[Ni(L1)Cl_2]\cdot 0.5H_2O$ (—, black) and $[Ni(L2)Cl_2]\cdot 0.5H_2O$ (—, blue) showing the ranges of 2600-3700 cm^{-1} (top) and 600-1700 cm^{-1} (bottom).

The IR spectrum of $[Ni(L2)Cl_2]\cdot 0.5H_2O$ is very similar to that of $[Ni(L1)Cl_2]\cdot 0.5H_2O$. The CN stretching vibration is shifted from 1621 to 1616 cm^{-1}, consistent with a slightly heavier substituent on the C=N group (CH_3 vs. CD_3). In the fingerprint region, bands at 1371, 1089, 1057, 937, 777 cm^{-1} lost intensity, while new bands appeared at 1358, 898, 850, 671 cm^{-1}, and the band at 758 cm^{-1} gained intensity.

The IR spectra of $[Ni(L3)Cl_2]$ and $[Ni(L4)Cl_2]$ are similar to that of $[Ni(L1)Cl_2]\cdot 0.5H_2O$, but 4-X substitution is noticeable in ν_{CH} (aromatic), ν_{CN}, and in the 700–1200 cm^{-1} region. The CN stretching vibration is shifted to higher energies in both

cases, 1625 cm^{-1} for $[Ni(L3)Cl_2]$ and 1631 cm^{-1} for $[Ni(L4)Cl_2]$ compared to 1621 cm^{-1} for $[Ni(L1)Cl_2]\cdot 0.5H_2O$. There are no bands in the OH stretching region, which is consistent with the lack of lattice water in the crystal structures of these complexes. Compared to each other, the IR spectra of $[Ni(L3)Cl_2]$ and $[Ni(L4)Cl_2]$ are similar, with the most significant changes observed in the region of 700–900 cm^{-1}. These differences are presumably due to ν_{CX} (ν_{CCl} vs. ν_{CBr}) and influences of the C–X group on skeletal vibrations.

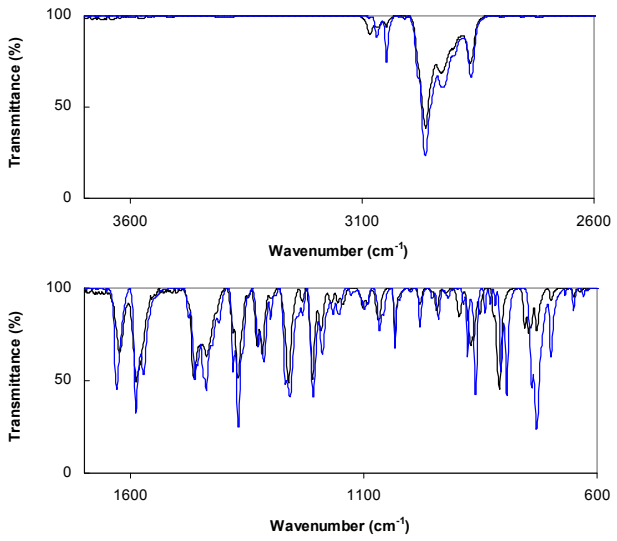

Figure 2. IR spectra of $[Ni(L3)Cl_2]$ (—, black) and $[Ni(L4)Cl_2]$ (—, blue) showing the ranges of 2600-3700 cm^{-1} (top) and 600-1700 cm^{-1} (bottom).

3.3.3 Crystal Structures

Crystals of $[Ni(L1)Cl_2]\cdot 0.5H_2O$ (red orange plates), $[Ni(L3)Cl_2]\cdot CH_2Cl_2$ (orange plates), $[Ni(L4)Cl_2]\cdot CH_2Cl_2$ (orange red plates), and $[Ni(L7)Br_2]$ (orange blades) were all grown by vapor diffusion of diethyl ether into a solution of dichloromethane upon

standing at 4 °C. Crystal structures of $[Ni(L1)Cl_2]\cdot CH_3CN$[21] and $[Ni(L1)Cl_2]\cdot 0.5H_2O$[53] were reported previously. However, the data for each structure was acquired at 293 K, resulting in reported structures of lower quality. The structure was redetermined here with the data acquired at 190 K, because the C–C and C=N distances are of interest for comparison to the structure of the reduced complex presented in Chapter 4.

The unit cell of $[Ni(L1)Cl_2]\cdot 0.5H_2O$ was found to be very similar to the previously reported structure of $[Ni(L1)Cl_2]\cdot 0.5H_2O$,[53] as they have the same space group (*P*–1) and differ only in the first or second decimal place for each parameter. The difference in the volume of the unit cells between the data set previously collected at 293 K[53] and the data set collected at 190 K is 2.6%.

Selected bond lengths and angles for $[Ni(L1)Cl_2]\cdot 0.5H_2O$ are presented in Tables 2-4, and the molecular structure is presented in Figure 3. The Ni–N1 (pyridine) bond length of 1.978(2) Å is shorter than the Ni–N2 (imine) and Ni–N3 (imine) bond lengths of 2.166(2) Å and 2.157(2) Å. This difference is presumably in part due to geometric constraints of the bis(arylimino)pyridine ligand. The Ni–Cl1 and Ni–Cl2 distances are 2.2338(8) Å and 2.2832(9) Å, respectively. The cis-angles about the Ni center all deviate significantly from 90 °, revealing distortion from an ideal coordination geometry (Table 3). These angles include N1–Ni–N2, N1–Ni–N3, N1–Ni–Cl2, N2–Ni–Cl1, N2–Ni–Cl2, N3–Ni–Cl1, N3–Ni–Cl2, and Cl1–Ni–Cl2. Calculation of the τ parameter, where $\tau = (\beta - \alpha)/60$, can be used to distinguish between square pyramidal ($\tau = 0$) and trigonal bipyramidal ($\tau = 1$) coordination geometries.[54] The variables, β and α, are angles about the metal center, where the two largest angles are selected and set into the equation such that the calculated τ is a positive value. The τ value calculated for $[Ni(L1)Cl_2]\cdot 0.5H_2O$

is 0.084, fairly close to the ideal value of 0 for square pyramidal geometry. However, the Ni atom lies outside of the N1–N2–N3 plane, 0.374(2) Å out of the plane in the direction of Cl2, and the cis-angles about Ni deviate significantly from 90 ° so the geometry is best described as distorted square pyramidal.

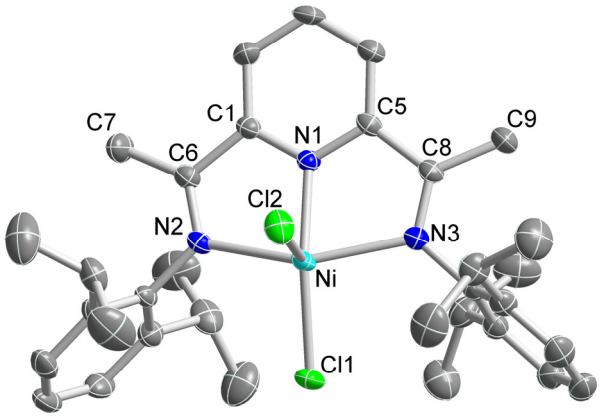

Figure 3. Molecular structure of [Ni{2,6-(2,6-^{i}Pr$_2$C$_6$H$_3$N=CMe)$_2$C$_5$H$_3$N}Cl$_2$]·0.5H$_2$O, **1**·0.5H$_2$O. Displacement ellipsoids are drawn at the 50% probability level. Hydrogen atoms and the solvent oxygen atom have been omitted for clarity. Color key: turquoise = Ni, blue = N, green = Cl, gray = C.

On the ligand there are a few sets of bond lengths that are important for the comparison to the reduced complexes in Chapter 4. The first set includes N2–C6 (1.287(3) Å) and N3–C8 (1.289(3) Å), the imine double bonds. The next set of bond lengths of interest are the C–C bonds adjacent to the pyridine ring, C1–C6 (1.493(4) Å) and C5–C8 (1.486(4) Å), the distances are consistent with single bond character. The distances for C6–C7 (1.495(4) Å) and C8–C9 (1.498(4) Å), are also consistent with single bond character. There are a couple of notable dihedral angles, taking the plane, N1, N2, and N3, and the least squares planes of the aryl rings C10→C15 and C22→C27.

These angles are 78.99(8)° and 77.07(11)°, indicating that the aryl rings of the aniline groups are fairly close to perpendicular to the NiN_3 plane.

Table 1. Crystallographic data and structure refinement for [Ni{2,6-(2,6-$^{i}Pr_2C_6H_3N$=CMe)$_2C_5H_3N$}Cl_2]·0.5H_2O, **1**·0.5H_2O.

	1·0.5H_2O
Empirical formula[a]	$C_{33}H_{44}Cl_2N_3NiO_{0.50}$
Formula weight[a]	620.32
Crystal habit, color	plate, red orange
Crystal size	0.42 x 0.36 x 0.03 mm^3
Temperature, T	190(2) K
Wavelength, λ	0.71073 Å
Crystal system	triclinic
Space group	P–1
Unit cell dimensions	a = 8.7004(9) Å b = 9.7565(10) Å c = 20.844(2) Å α = 83.730(5)° β = 88.156(5)° γ = 65.550(5)°
Volume, V	1600.9(3) $Å^3$
Z	2
Calculated density[a]	1.287 $Mg·m^{-3}$
Absorption coefficient, μ	0.801 mm^{-1}
F(000)	658
θ range for data collection	2.74 to 25.39°
Limiting indices	$-10 \le h \le 10$, $-11 \le k \le 11$, $-25 \le l \le 25$
Reflections collected / unique	19669 / 5862 [R(int) = 0.0530]
Completeness to θ	99.4 % (θ = 25.39°)
Max. and min. transmission	0.9803 and 0.7298
Refinement method	Full-matrix least-squares on F^2
Data / restraints / parameters	5862 / 0 / 372
Goodness-of-fit on F^2	1.014
Final R indices [I>2sigma(I)]	R1 = 0.0450, wR2 = 0.0818
R indices (all data)	R1 = 0.0770, wR2 = 0.0916
Largest diff. peak and hole	0.301 and –0.389 $e·A^{-3}$

[a] The formula, formula weight, and calc. density account for the presence of 0.5 H2O per formula unit, however, the water H atoms were not included in the refinement.

Table 2. Selected interatomic distances (Å) for [Ni{2,6-(2,6-^{i}Pr$_2$C$_6$H$_3$N=CMe)$_2$C$_5$H$_3$N}Cl$_2$]·0.5H$_2$O, **1**·0.5H$_2$O.[a]

1·0.5H$_2$O		**1**·0.5H$_2$O	
Ni–N1	1.978(2)	N1–C1	1.336(3)
Ni–N2	2.166(2)	N1–C5	1.338(3)
Ni–N3	2.157(2)	N2–C6	1.287(3)
Ni–Cl1	2.2338(8)	N2–C10	1.448(3)
Ni–Cl2	2.2832(9)	N3–C8	1.289(3)
		N3–C22	1.442(3)
		C1–C6	1.493(4)
		C5–C8	1.486(4)
		C6–C7	1.495(4)
		C8–C9	1.498(4)

[a] Numbers in parentheses are standard uncertainties in the last significant figures. Atoms are labeled as indicated in Figure 3.

Table 3. Selected angles (°) for [Ni{2,6-(2,6-^{i}Pr$_2$C$_6$H$_3$N=CMe)$_2$C$_5$H$_3$N}Cl$_2$]·0.5H$_2$O, **1**·0.5H$_2$O.[a]

1·0.5H$_2$O		**1**·0.5H$_2$O	
N1–Ni–N2	76.52(9)	N1–C1–C2	120.9(2)
N1–Ni–N3	76.63(9)	N1–C1–C6	113.4(2)
N1–Ni–Cl2	91.99(7)	C2–C1–C6	125.7(3)
N1–Ni–Cl1	154.08(7)	N1–C5–C4	120.8(3)
N2–Ni–Cl1	99.05(6)	N1–C5–C8	112.8(2)
N2–Ni–Cl2	98.57(6)	C4–C5–C8	126.4(2)
N3–Ni–Cl1	98.37(6)	N2–C6–C1	114.9(2)
N3–Ni–Cl2	97.45(6)	N2–C6–C7	126.3(3)
N3–Ni–N2	149.06(8)	C1–C6–C7	118.8(2)
Cl1–Ni–Cl2	113.93(3)	N3–C8–C5	115.7(2)
		N3–C8–C9	125.4(3)
C1–N1–C5	121.0(2)	C5–C8–C9	118.8(2)
C1–N1–Ni	118.91(18)		
C5–N1–Ni	118.87(19)		
C6–N2–C10	119.9(2)		
C6–N2–Ni	114.21(18)		
C10–N2–Ni	125.89(17)		
C8–N3–C22	119.7(2)		
C8–N3–Ni	113.64(19)		
C22–N3–Ni	126.58(17)		

[a] Numbers in parentheses are standard uncertainties in the last significant figures. Atoms are labeled as indicated in Figure 3.

Table 4. Selected dihedral angles (°) for [Ni{2,6-(2,6-$^{i}Pr_2C_6H_3N$=CMe)$_2C_5H_3N$}Cl_2]·0.5H_2O, **1**·0.5H_2O.[a]

1·0.5H_2O	
(N1,N2,N3) / (C10→C15)[b]	78.99(8)
(N1,N2,N3) / (C22→C27)[b]	77.07(11)
(C10→C15) / (C22→C27)[c]	79.65(9)

[a] Numbers in parentheses are standard uncertainties in the last significant figures. Atoms are labeled as indicated in Figure 3. [b] Angle between the plane of the ligand nitrogen atoms (N1, N2, and N3) and a least-squares plane of aryl ring atoms (*e.g.*, C10, C11, C12, C13, C14, and C15). [c] Angle between the least-squares planes of the aryl ring atoms.

The crystal structures of [Ni(L3)Cl_2]·CH_2Cl_2 and [Ni(L4)Cl_2]·CH_2Cl_2 both were solved in the $P2_1/m$ space group, and the unit cells differ only in the first or second decimal place for each parameter. The difference in the volume of the unit cells between the two structures is 0.9%. There is crystallographically imposed symmetry on the molecules, and atoms located on special sites (i.e. the mirror plane) include C4, N1, Ni, Cl1 and C12. The dichloromethane solvent molecule is disordered about the mirror plane in both structures (1 chlorine atom is on the plane), with 50% occupancy on each side of the mirror plane for the carbon atom and the other chlorine atom.

Selected bond lengths and angles for [Ni(L3)Cl_2]·CH_2Cl_2 and [Ni(L4)Cl_2]·CH_2Cl_2 are presented in Tables 6-8, and the molecular structures are presented in Figure 4 and Figure 5. The structural features are very similar to each other. For [Ni(L3)Cl_2]·CH_2Cl_2, the Ni–N1 (pyridine) bond length is 1.971(2), which is shorter than Ni–N2 (imine) bond length of 2.1535(16). For [Ni(L4)Cl_2]·CH_2Cl_2, the Ni–N1 (pyridine) bond length is 1.972(2), which is shorter than Ni–N2 (imine) bond length of 2.1512(19). The Ni–Cl1 and Ni–Cl2 distances in [Ni(L3)Cl_2]·CH_2Cl_2 are 2.2126(8) Å and 2.2798(8) Å, respectively, and in [Ni(L4)Cl_2]·CH_2Cl_2 are 2.2126(9) Å and 2.2790(9), respectively, which are consistent with nickel halogen single bonds. The cis-angles about the Ni center

N1–Ni–N2, N1–Ni–Cl2, N2–Ni–Cl1, N2–Ni–Cl2, and Cl1–Ni–Cl2 in both complexes all deviate significantly from 90 °, revealing distortion from an ideal coordination geometry (Table 7). The calculated τ parameter for $[Ni(L3)Cl_2]\cdot CH_2Cl_2$ is 0.078 and for $[Ni(L4)Cl_2]\cdot CH_2Cl_2$ is 0.082, indicating the geometry for both complexes is square pyramidal. However, the Ni atom in $[Ni(L3)Cl_2]\cdot CH_2Cl_2$ lies outside of the N1–N2–N2#1 plane, 0.277(2) Å out of the plane in the direction of Cl2, and in $[Ni(L4)Cl_2]\cdot CH_2Cl_2$ it is 0.283(3) Å out of the N1–N2–N2#1 plane in the direction of Cl2. As the cis-angles also deviate from 90 °, the geometry for both complexes is best described as distorted square pyramidal.

It is only when the halogen atom on the ligand is considered that the identity of each compound is confirmed. In $[Ni(L3)Cl_2]\cdot CH_2Cl_2$, the C9–Cl3 bond length is 1.748(2) Å, which is consistent with a C–Cl bond. In $[Ni(L4)Cl_2]\cdot CH_2Cl_2$, the C9–Br bond length is 1.907(2) Å, which is consistent with a C–Br bond. In $[Ni(L3)Cl_2]\cdot CH_2Cl_2$, the N2–C4 bond length is 1.281(3) Å, consistent with a carbon–nitrogen double bond. In $[Ni(L4)Cl_2]\cdot CH_2Cl_2$, the N2–C4 bond length is 1.278(3) Å, also consistent with a carbon–nitrogen double bond. The bond length of C1–C4, which is adjacent to the pyridine ring in $[Ni(L3)Cl_2]\cdot CH_2Cl_2$ is 1.496(3) Å, and in $[Ni(L4)Cl_2]\cdot CH_2Cl_2$ is 1.495(3) Å, consistent with single bond character. The C4–C5 distances of 1.496(3) Å in $[Ni(L3)Cl_2]\cdot CH_2Cl_2$ and 1.494(3) Å in $[Ni(L4)Cl_2]\cdot CH_2Cl_2$ is also consistent with single bond character. The dihedral angle, taking the plane of N1, N2, and N2#1 and the least squares plane of the aryl ring C6→C11, is 75.21(8)° in $[Ni(L3)Cl_2]\cdot CH_2Cl_2$ and 74.78(10)° in $[Ni(L4)Cl_2]\cdot CH_2Cl_2$.

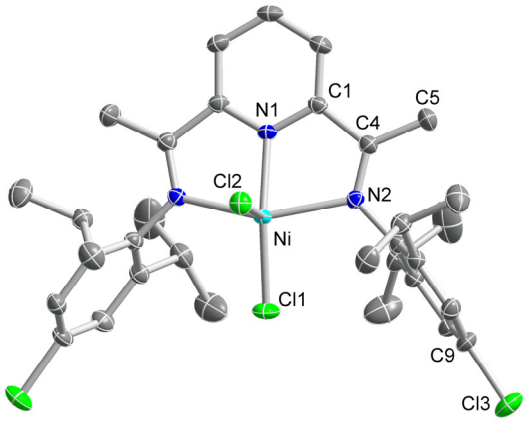

Figure 4. Molecular structure of [Ni{2,6-(4-Cl-2,6-^{i}Pr$_2$C$_6$H$_3$N=CMe)$_2$C$_5$H$_3$N}Cl$_2$] ·CH$_2$Cl$_2$, **3**·CH$_2$Cl$_2$. Displacement ellipsoids are drawn at the 50% probability level. Hydrogen atoms and the solvent molecule have been omitted for clarity. Color key: turquoise = Ni, blue = N, green = Cl, gray = C.

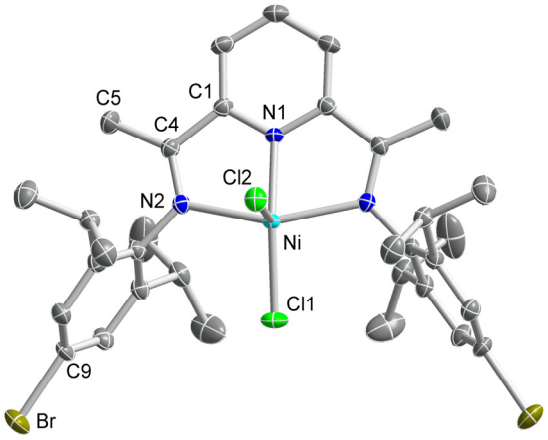

Figure 5. Molecular structure of [Ni{2,6-(4-Br-2,6-^{i}Pr$_2$C$_6$H$_3$N=CMe)$_2$C$_5$H$_3$N}Cl$_2$] ·CH$_2$Cl$_2$, **4**·CH$_2$Cl$_2$. Displacement ellipsoids are drawn at the 50% probability level. Hydrogen atoms and the solvent molecule have been omitted for clarity. Color key: turquoise = Ni, blue = N, green = Cl, gray = C, dark yellow = Br

Table 5. Crystallographic data and structure refinement for [Ni{2,6-(4-Cl-2,6-$^{i}Pr_2C_6H_2N{=}CMe)_2C_5H_3N$}$Cl_2$]·$CH_2Cl_2$, **3**·$CH_2Cl_2$, and [Ni{2,6-(4-Br-2,6-$^{i}Pr_2C_6H_2N{=}CMe)_2C_5H_3N$}$Cl_2$]·$CH_2Cl_2$, **4**·$CH_2Cl_2$.

	3·CH_2Cl_2	**4**·CH_2Cl_2
Empirical formula	$C_{34}H_{43}Cl_6N_3Ni$	$C_{34}H_{43}Br_2Cl_4N_3Ni$
Formula weight	765.12	854.04
Crystal habit, color	plate, orange	plate, orange red
Crystal size	0.25 x 0.21 x 0.06 mm^3	0.50 x 0.30 x 0.16 mm^3
Temperature, T	190(2) K	190(2) K
Wavelength, λ	0.71073 Å	0.71073 Å
Crystal system	monoclinic	monoclinic
Space group	$P2_1/m$	$P2_1/m$
Unit cell dimensions	a = 8.7155(9) Å b = 24.127(3) Å c = 9.0166(9) Å β = 105.837(5)°	a = 8.7538(9) Å b = 24.293(3) Å c = 8.9821(9) Å β = 105.448(5)°
Volume, V	1824.0(3) $Å^3$	1841.1(3) $Å^3$
Z	2	2
Calculated density	1.393 $Mg·m^{-3}$	1.541 $Mg·m^{-3}$
Absorption coefficient, μ	0.999 mm^{-1}	3.015 mm^{-1}
F(000)	796	868
θ range for data collection	1.69 to 29.01°	1.68 to 30.54°
Limiting indices	$-11 \le h \le 11$, $-32 \le k \le 32$, $-12 \le l \le 12$	$-12 \le h \le 12$, $-34 \le k \le 34$, $-12 \le l \le 12$
Reflections collected / unique	31023 / 4970 [R(int) = 0.0375]	41661 / 5749 [R(int) = 0.0352]
Completeness to θ	100.0 % (θ = 29.01°)	99.9 % (θ = 30.54°)
Max. and min. transmission	0.9425 and 0.7882	0.6440 and 0.3140
Refinement method	Full-matrix least-squares on F^2	Full-matrix least-squares on F^2
Data / restraints / parameters	4970 / 0 / 222	5749 / 0 / 222
Goodness-of-fit on F^2	1.041	1.032
Final R indices [I>2sigma(I)]	$R1$ = 0.0406, $wR2$ = 0.0960	$R1$ = 0.0407, $wR2$ = 0.0904
R indices (all data)	$R1$ = 0.0551, $wR2$ = 0.1037	$R1$ = 0.0592, $wR2$ = 0.0988
Largest diff. peak and hole	1.479 and –1.507 e·$Å^{-3}$	1.715 and –1.734 e·$Å^{-3}$

Table 6. Selected interatomic distances (Å) for [Ni{2,6-(4-Cl-2,6-$^{i}Pr_2C_6H_2N{=}CMe)_2C_5H_3N$}$Cl_2$]·$CH_2Cl_2$, **3**·$CH_2Cl_2$, and [Ni{2,6-(4-Br-2,6-$^{i}Pr_2C_6H_2N{=}CMe)_2C_5H_3N$}$Cl_2$]·$CH_2Cl_2$, **4**·$CH_2Cl_2$.[a]

3·CH_2Cl_2		**4**·CH_2Cl_2	
Ni–N1	1.971(2)	Ni–N1	1.972(2)
Ni–N2	2.1535(16)	Ni–N2	2.1512(19)
Ni–Cl1	2.2126(8)	Ni–Cl1	2.2126(9)
Ni–Cl2	2.2798(8)	Ni–Cl2	2.2790(9)
N1–C1	1.333(2)	N1–C1	1.334(2)
N2–C4	1.281(3)	N2–C4	1.278(3)
N2–C6	1.437(2)	N2–C6	1.437(3)
C1–C4	1.496(3)	C1–C4	1.495(3)
C4–C5	1.496(3)	C4–C5	1.494(3)
C9–Cl3	1.748(2)	C9–Br	1.907(2)

[a] Numbers in parentheses are standard uncertainties in the last significant figures. Atoms are labeled as indicated in Figures 4 and 5.

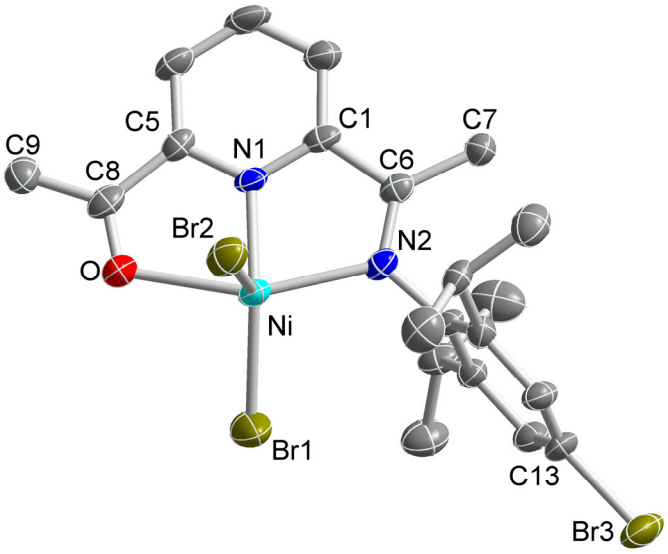

Figure 6. Molecular structure of [Ni{6-(2,6-$^{i}Pr_2C_6H_3N{=}CMe)C_5H_3N$-2-C(O)Me}$Cl_2$], **7**. Displacement ellipsoids are drawn at the 50% probability level. Hydrogen atoms have been omitted for clarity. Color key: turquoise = Ni, blue = N, gray = C, dark yellow = Br.

Table 7. Selected angles (°) for [Ni{2,6-(4-Cl-2,6-^{i}Pr$_2$C$_6$H$_2$N=CMe)$_2$C$_5$H$_3$N}Cl$_2$]·CH$_2$Cl$_2$, **3**·CH$_2$Cl$_2$, and [Ni{2,6-(4-Br-2,6-^{i}Pr$_2$C$_6$H$_2$N=CMe)$_2$C$_5$H$_3$N}Cl$_2$]·CH$_2$Cl$_2$, **4**·CH$_2$Cl$_2$.[a]

3·CH$_2$Cl$_2$		**4**·CH$_2$Cl$_2$	
N1–Ni–N2	77.12(4)	N1–Ni–N2	77.02(5)
N1–Ni–Cl2	92.81(7)	N1–Ni–Cl2	93.20(8)
N1–Ni–Cl1	156.46(7)	N1–Ni–Cl1	156.42(8)
N2–Ni–Cl1	99.50(4)	N2–Ni–Cl1	99.54(5)
N2–Ni–Cl2	96.27(4)	N2–Ni–Cl2	96.47(5)
N2#1–Ni–N2	151.79(9)	N2–Ni–N2#1	151.53(10)
Cl1–Ni–Cl2	110.73(3)	Cl1–Ni–Cl2	110.38(4)
C1–N1–C1#1	121.6(2)	C1#1–N1–C1	121.6(3)
C1–N1–Ni	118.92(12)	C1–N1–Ni	118.89(13)
C4–N2–C6	123.42(17)	C4–N2–C6	123.46(19)
C4–N2–Ni	114.04(13)	C4–N2–Ni	114.23(15)
C6–N2–Ni	122.47(12)	C6–N2–Ni	122.26(14)
N1–C1–C2	120.63(19)	N1–C1–C2	120.5(2)
N1–C1–C4	113.62(17)	N1–C1–C4	113.54(19)
C2–C1–C4	125.74(18)	C2–C1–C4	126.0(2)
N2–C4–C1	115.10(17)	N2–C4–C1	115.1(2)
N2–C4–C5	126.12(19)	N2–C4–C5	126.2(2)
C1–C4–C5	118.78(17)	C5–C4–C1	118.7(2)

[a] Numbers in parentheses are standard uncertainties in the last significant figures. Atoms are labeled as indicated in Figures 4 and 5.Symmetry operations: #1, x, –y+1/2, z.

Table 8. Selected dihedral angles (°) for [Ni{2,6-(4-Cl-2,6-^{i}Pr$_2$C$_6$H$_2$N=CMe)$_2$C$_5$H$_3$N}Cl$_2$]·CH$_2$Cl$_2$, **3**·CH$_2$Cl$_2$, and [Ni{2,6-(4-Br-2,6-^{i}Pr$_2$C$_6$H$_2$N=CMe)$_2$C$_5$H$_3$N}Cl$_2$]·CH$_2$Cl$_2$, **4**·CH$_2$Cl$_2$.[a]

3·CH$_2$Cl$_2$		**4**·CH$_2$Cl$_2$	
(N1,N2,N2#1) / (C6→C11)[b]	75.21(8)	(N1,N2,N2#1) / (C6→C11)[b]	74.78(10)
(C6→C11) / (C6#1→C11#1)[c]	79.48(5)	(C6→C11) / (C6#1→C11#1)[c]	78.84(6)

[a] Numbers in parentheses are standard uncertainties in the last significant figures. Atoms are labeled as indicated in Figures 4 and 5. Symmetry operation: #1, x, –y+1/2, z. [b] Angle between the plane of the ligand nitrogen atoms (N1, N2, and N2#1) and the least-squares plane of the aryl ring atoms (C6, C7, C8, C9, C10, and C11). [c] Angle between the least-squares planes of the aryl ring atoms.

The crystal structure of [Ni(L7)Cl_2] was solved in the $P2_1/c$ space group. Selected bond lengths and angles for [Ni(L7)Cl_2] are presented in Tables 10-12, and the molecular structure is presented in Figure 6. The Ni–N1 (pyridine) and Ni–N2 (imine) bond lengths are 1.968(5) Å and 2.111(5) Å, respectively. The Ni–O bond length is 2.253(5) Å, indicating a weaker interaction. The Ni–Br1 and Ni–Br2 distances are 2.3269(11) Å and 2.4094(11) Å, respectively, are longer than the Ni–Cl distances in [Ni(L1)Cl_2]·0.5H_2O, [Ni(L3)Cl_2]·CH_2Cl_2, and [Ni(L4)Cl_2]·CH_2Cl_2. The cis-angles about the Ni center all deviate significantly from 90°, revealing distortion from an ideal coordination geometry (Table 11). These angles include N1–Ni–N2, N1–Ni–O, N1–Ni–Br2, N2–Ni–Br1, N2–Ni–Br2, O–Ni–Br1, O–Ni–Br2, and Br1–Ni–Br2. The calculated τ parameter for [Ni(L7)Cl_2] is 0.215 indicating the geometry is distorted square pyramidal. On the basis of the calculation of the τ parameter, [Ni(L7)Cl_2] has the most distorted square pyramidal geometry of the four complexes. The calculation of the τ parameter for all four complexes is summarized in Table 13. The Ni atom also lies outside of the N1–N2–O plane, 0.206(5) Å out of the plane in the direction of Br2.

On the ligand, a notable bond length to highlight is C8–O, 1.222(7) Å, which is consistent with a carbon–oxygen double bond, and shorter than the typical imine double bond. The N3–C8 distance of 1.283(8) Å is consistent with an imine double bond. The bond lengths of the C–C bonds adjacent to the pyridine ring, C1–C6 (1.491(8) Å) and C5–C8 (1.498(9) Å), are consistent with single bond character. The C6–C7 (1.494(9) Å) and C8–C9 (1.460(9) Å) distances are also consistent with single bond character. The C13–Br3 bond length is 1.912(6) Å, which is consistent with a C–Br bond length. The dihedral angle, taking the plane of N1, N2, and O and the least squares plane of the aryl

ring C10→C15 is 84.2(2)°, indicating that the aryl ring of the aniline group is fairly close to perpendicular to the NiN_2O plane.

Table 9. Crystallographic data and structure refinement for [Ni{6-(4-Br-2,6-$^{i}Pr_2C_6H_2N$=CMe)C_5H_3N-2-C(O)Me}Br_2], **7**.

	7
Empirical formula	$C_{21}H_{25}Br_3N_2NiO$
Formula weight	619.87
Crystal habit, color	blade, orange
Crystal size	0.28 x 0.10 x 0.01 mm^3
Temperature, T	180(2) K
Wavelength, λ	0.71073 Å
Crystal system	monoclinic
Space group	$P2_1/c$
Unit cell dimensions	a = 17.5083(18) Å b = 8.2313(8) Å c = 18.0872(18) Å β = 115.359(5)°
Volume, V	2355.5(4) $Å^3$
Z	4
Calculated density	1.748 $Mg \cdot m^{-3}$
Absorption coefficient, μ	5.926 mm^{-1}
F(000)	1224
θ range for data collection	2.77 to 25.35°
Limiting indices	$-21 \le h \le 21$, $-9 \le k \le 9$, $-21 \le l \le 21$
Reflections collected / unique	14658 / 4262 [R(int) = 0.0565]
Completeness to θ	99.0 % (θ = 25.35°)
Max. and min. transmission	0.9431 and 0.2877
Refinement method	Full-matrix least-squares on F^2
Data / restraints / parameters	4262 / 0 / 259
Goodness-of-fit on F^2	1.077
Final R indices [I>2sigma(I)]	$R1$ = 0.0536, $wR2$ = 0.1236
R indices (all data)	$R1$ = 0.0847, $wR2$ = 0.1366
Largest diff. peak and hole	1.574 and –1.252 $e \cdot A^{-3}$

Table 10. Selected interatomic distances (Å) for [Ni{6-(4-Br-2,6-$^{i}Pr_2C_6H_2N$=CMe)C_5H_3N-2-C(O)Me}Br_2], **7**.[a]

7		**7**	
Ni–N1	1.968(5)	C1–C6	1.491(8)
Ni–N2	2.111(5)	C5–C8	1.498(9)
Ni–O	2.253(5)	C6–C7	1.494(9)
Ni–Br1	2.3269(11)	C8–C9	1.460(9)
Ni–Br2	2.4094(11)		
		C13–Br3	1.912(6)
N1–C1	1.335(8)		
N1–C5	1.347(8)		
N2–C6	1.283(8)		
N2–C10	1.455(7)		
C8–O	1.222(7)		

[a] Numbers in parentheses are standard uncertainties in the last significant figures. Atoms are labeled as indicated in Figure 6.

Table 11. Selected angles (°) for [Ni{6-(4-Br-2,6-$^{i}Pr_2C_6H_2N$=CMe)C_5H_3N-2-C(O)Me}Br_2], **7**.[a]

7		**7**	
N1–Ni–N2	78.0(2)	N1–C1–C2	120.6(6)
N1–Ni–O	75.26(19)	N1–C1–C6	114.1(5)
N1–Ni–Br2	96.91(14)	C2–C1–C6	125.3(6)
N1–Ni–Br1	139.11(15)	N1–C5–C4	120.8(6)
N2–Ni–Br1	101.76(13)	N1–C5–C8	113.0(5)
N2–Ni–Br2	102.04(14)	C4–C5–C8	126.2(6)
O–Ni–Br1	93.20(12)	N2–C6–C1	114.5(5)
O–Ni–Br2	89.29(14)	N2–C6–C7	127.0(5)
N2–Ni–O	151.98(18)	C1–C6–C7	118.5(5)
Br1–Ni–Br2	122.45(5)	O–C8–C5	117.1(6)
		O–C8–C9	122.2(6)
C1–N1–C5	121.2(5)	C9–C8–C5	120.7(6)
C1–N1–Ni	117.7(4)		
C5–N1–Ni	120.8(4)		
C6–N2–C10	120.8(5)		
C6–N2–Ni	114.7(4)		
C10–N2–Ni	124.5(4)		
C8–O–Ni	113.5(4)		

[a] Numbers in parentheses are standard uncertainties in the last significant figures. Atoms are labeled as indicated in Figure 6.

Table 12. Selected dihedral angle (°) for [Ni{6-(4-Br-2,6-$^{i}Pr_2C_6H_2N$=CMe)C_5H_3N-2-C(O)Me}Br_2], **7**.[a]

7	
(N1,N2,O) / (C10→C15)[b]	84.2(2)

[a] Numbers in parentheses are standard uncertainties in the last significant figures. Atoms are labeled as indicated in Figure 6. [b] Angle between the plane of the ligand nitrogen and oxygen atoms (N1, N2, and O) and the least-squares plane of the aryl ring atoms (C10, C11, C12, C13, C14, and C15).

Table 13. Calculated τ Values for Five-Coordinate Bis(arylimino)pyridine Complexes of Nickel(II).

Complex	β	α	τ
[Ni(L1)Cl_2]·0.5H_2O	N1–Ni–Cl1, 154.08°	N3–Ni–N2, 149.06°	0.084
[Ni(L3)Cl_2]·CH_2Cl_2	N1–Ni–Cl1, 156.46°	N2#1–Ni–N2, 151.79°	0.078
[Ni(L4)Cl_2]·CH_2Cl_2	N1–Ni–Cl1, 156.42°	N2#1–Ni–N2, 151.53°	0.082
[Ni(L7)Br_2]	N2–Ni–O, 151.98°	N1–Ni–Br1, 139.11°	0.215

3.3.4 Electrochemical Characterization of Bis(arylimino)pyridine Complexes of Nickel(II)

Differential pulse voltammograms (DPV) for [Ni^{II}(L1)Cl_2], [Ni^{II}(L2)Cl_2], [Ni^{II}(L3)Cl_2], and [Ni^{II}(L4)Cl_2] revealed a reduction event, DPV for [Ni^{II}(L5)Cl_2] and [Ni^{II}(L6)Cl_2] revealed no such event. The results are summarized in Table 14. The halogen substituted complexes, [Ni^{II}(L3)Cl_2] and [Ni^{II}(L4)Cl_2], have slightly lower reduction potentials than [Ni^{II}(L1)Cl_2] and [Ni^{II}(L2)Cl_2], but this difference is only 20 mV between [Ni^{II}(L1)Cl_2] and [Ni^{II}(L3)Cl_2].

Table 14. Reduction Potentials of Bis(arylimino)pyridine complexes of Ni^{II} (V vs. $[FeCp_2]/[FeCp_2]^+$) in CH_2Cl_2.

Complex	V vs. $[FeCp_2]/[FeCp_2]^+$
$[Ni^{II}(L4)Cl_2]$	-0.92 V
$[Ni^{II}(L3)Cl_2]$	-0.94 V
$[Ni^{II}(L1)Cl_2]$	-0.96 V
$[Ni^{II}(L2)Cl_2]$	-0.98 V
$[Ni^{II}(L5)Cl_2]$	not observed
$[Ni^{II}(L6)Cl_2]$	not observed

Cyclic voltammograms of $[Ni^{II}(L1)Cl_2]$, $[Ni^{II}(L2)Cl_2]$, $[Ni^{II}(L3)Cl_2]$, and $[Ni^{II}(L4)Cl_2]$ were investigated using a scan rate of 0.1 $V \cdot s^{-1}$. The peak to peak separation observed for $[Ni^{II}(L1)Cl_2]$, $[Ni^{II}(L2)Cl_2]$, and $[Ni^{II}(L3)Cl_2]$ compares favorably to the $[FeCp_2]/[FeCp_2]^+$ standard peak to peak separation, therefore they are quasi-reversible. For $[Ni^{II}(L4)Cl_2]$, the cathodic peak was barely detected, the event observed in this case is irreversible.

Scheme 17. Electrochemical Characterization of a 2:1 Bis(arylimino)pyridine Complex of Ni.

$$[Ni^{III}(L^0)_2]^{3+} \underset{-e^-}{\overset{+e^-}{\rightleftharpoons}} [Ni^{II}(L^0)_2]^{2+} \underset{-e^-}{\overset{+e^-}{\rightleftharpoons}} [Ni^{I}(L^0)_2]^{+} \underset{-e^-}{\overset{+e^-}{\rightleftharpoons}} [Ni^{I}(L^0)(L^{\bullet -})]^0$$

+ 1.19 V - 1.30 V -1.82 V

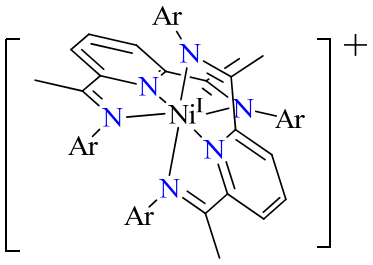

Ar = 4-$MeOC_6H_5$

There has only been one previous example of cyclic voltammetry of bis(arylimino)pyridine complex of Ni previously reported in the literature. It is very different than the complexes in this project, in that there are no isopropyl groups on the ligand, enabling formation of a 2:1 complex with two bis(arylimino)pyridine ligands bound to the Ni center.[45] Three reversible one-electron events were observed for this complex, which is highlighted in Scheme 17. The first event observed at a potential of +1.19 V $[FeCp_2]/[FeCp_2]^+$ was described as a one-electron oxidation of Ni. The second event, a one-electron reduction, was observed at a potential of -1.30 V vs. $[FeCp_2]/[FeCp_2]^+$. The third event, also a one-electron reduction was observed at a potential of -1.82 V vs. $[FeCp_2]/[FeCp_2]^+$. The reduction potential of the second event, the first one-electron reduction, compares reasonably well to the Ni complexes characterized in this work, but it should be noted that first reduction of the 2:1 complex was considered to be metal centered, with the second reduction occurring on the ligand. A major topic in Chapter 4 will be identifying whether the one-electron reduction of $[Ni^{II}(L1)Cl_2]$ is ligand-centered or metal-centered.

3.4 Conclusion

The synthesis and characterization of six bis(arylimino)pyridine complexes of Ni^{II} and one aryliminopyridine complex of Ni^{II} was described in this chapter. XRD analysis of complexes **1, 3** and **4** reveals that these complexes have distorted square pyramidal geometry about the nickel center on the basis of calculated τ values. IR spectroscopy of complexes **1-4** shows a CN stretching vibration that changes slightly with substitution of

the ligand. Complex **7** was revealed to be a mixture of three components on the basis of ESI(+)MS, and shows why neutral anilines must be used in place of acid salts of anilines in the synthesis of these complexes. Complexes **5** and **6** were unable to be crystallized, so the characterization of these complexes was limited and the purity was not confirmed as of yet. However, based on ^{1}H NMR of the aniline precursors and ESI(+)MS of the complexes, the synthesis of these complexes was at least achieved. Electrochemical characterization of complexes **1-4** revealed a one electron reduction event between -0.92 V and -0.98 V vs. $[FeCp_2]/[FeCp_2]^+$, with substitution resulting in only minor changes to the reduction potential. The electrochemical characterization of **5** and **6** did not reveal a one electron reduction event, implying that chemical reduction of these complexes may not be possible.

CHAPTER 4

SYNTHESIS AND CHARACTERIZATION OF BIS(ARYLIMINO)PYRIDINE RADICAL ANION COMPLEXES OF NICKEL(II)

4.1 Introduction

The one-electron reduction of Ni^{II} complexes supported by bis(arylimino)pyridine derivatives will be the focus of Chapter 4. The general method for reducing these complexes involves reaction with a sodium amalgam, and the new complexes **8-11** were isolated upon recrystallization from toluene or *n*-pentane. For the characterization of these complexes mass spectrometry, infrared spectroscopy, X-ray diffraction, electron paramagnetic resonance spectroscopy, and UV-Vis spectroscopy will be used. The synthesis and characterization of complex **8** was published in 2009.[55]

A topic that will be explored in this Chapter is the question of whether the reduction of these complexes is ligand-centered or metal-centered. Electron paramagnetic resonance spectroscopy of **8** will elucidate whether the unpaired electron density is localized in a metal based or ligand based orbital in these complexes. This work will be the focus of section 4.3.1. Section 4.3.2 will focus on X-ray crystallography. Single crystal X-ray diffraction of **8** and **9** will be used in order to confirm the identity of these complexes. Comparing key bond lengths of the reduced complexes to corresponding bond lengths of the unreduced complex (**1**) from Chapter 3 will also provide an insight into the whether these complexes are best described as ligand radical complexes or Ni^{I} complexes.

4.2 Experimental Section

Materials. All reagents and solvents were purchased from commercial sources and were used as received, unless noted otherwise. Toluene was deoxygenated by sparging with N_2 and purified by passage through two packed columns of molecular sieves under an N_2 pressure (MBraun solvent purification system). *n*-Pentane was dried over Na and distilled under N_2 prior to use. Preparation and handling of air- and moisture-sensitive materials were carried out under an inert gas atmosphere by using either standard Schlenk and vacuum line techniques or a glovebox. Elemental analysis was performed by Atlantic Microlab, Inc., Norcross, GA.

Physical Methods. Mass spectral data were acquired on a single quadrupole ThermoFinnigan Voyager mass spectrometer using an electron impact ionization source (equipped with a solids probe). UV–Visible spectra were recorded on an HP 8453A diode array spectrophotometer (Agilent Technologies). IR spectra were recorded on a Bruker Vertex 70 Fourier-transform IR spectrometer using samples prepared by mixing the solid compound with KBr in a glovebox and pressing the mixture into a disk. Continuous-wave (CW) EPR spectra were obtained at 77 K on a Bruker EMX-61 spectrometer equipped with a liquid N_2 cold-finger Dewar flask. Typical EPR spectral parameters were an X-band microwave frequency of 9.30 GHz, a modulation frequency of 100 kHz, a modulation amplitude of 10 G, and a microwave power of 2.0 mW (sample concentration, 5 mM in toluene).

[Ni{2,6-(2,6-^{i}Pr$_2$C$_6$H$_3$N=CMe)$_2$C$_5$H$_3$N}Cl] (8). A 0.5 wt % sodium amalgam was prepared under an N_2 atmosphere by mixing 3.8 mg (0.165 mmol) of Na into 760 mg

of Hg for 15 min. A solution of 100 mg (0.164 mmol) of **1** in 5 mL of toluene was added dropwise to the amalgam over 5 min. The resulting solution was stirred for 24 h. After ca. 15–20 min, the solution turned black, followed by a gradual color change to dark orange-black and formation of a white precipitate over the course of 24 h. The solution was removed from the amalgam and filtered through a celite pad. The solvent was removed under reduced pressure to afford 47 mg (50%) of an orange-black solid. The residue was recrystallized from toluene by preparing a concentrated solution at 20 °C and storing it at –30 °C. Black single crystals of X-ray diffraction quality were typically obtained within several days. (Note that **2** is stable in toluene solution for a limited time but degrades if stored over an extended period (several weeks), as indicated by the disappearance of its EPR signal.) Anal. Calcd for $C_{33}H_{43}ClN_3Ni$: C, 68.83; H, 7.53; N, 7.30. Found: C, 68.16; H, 7.43; N, 7.01. EIMS (70 eV) *m*/*z*: $M^{+\bullet}$ calcd for $C_{33}H_{43}ClN_3Ni$, 574.25; found, 574.3 ($M^{+\bullet}$), 481.4 ($M^{+\bullet}$ – Ni – Cl), 466.4 ($M^{+\bullet}$ – Ni – Cl – 15). UV–Vis (toluene) λ_{max}, nm (ε): 465 (1100), 505 (1000), 730 (630), 820 (830). IR (KBr, cm^{-1}): 3062, 2961 (s), 2926, 2866, 1629, 1586, 1466, 1442, 1380, 1364, 1323, 1261, 1208, 1102, 1057, 1042, 1002, 938, 794, 775, 761, 731, 695.

[Ni{2,6-(2,6-^{i}Pr$_2$C$_6$H$_3$N=CCD$_3$)$_2$C$_5$H$_3$N}Cl] (9). This compound was synthesized following the procedure of **8** using 100 mg (0.162 mmol) of **2**. Yield: 58 mg (62%) of an orange-black solid. The product was recrystallized from toluene by preparing a concentrated solution at 20 °C and storing it at –15 °C. Black single crystals of X-ray diffraction quality were typically obtained within several days. EIMS (70 eV) *m*/*z*: $M^{+\bullet}$ calcd for $C_{33}H_{47}D_6ClN_3Ni$, 580.29; found, 579.5 ($M^{+\bullet}$). UV–Vis (toluene) λ_{max}, nm (ε): 465 (1200), 505 (1100), 730 (710), 825 (920). IR (KBr, cm^{-1}): 3055, 2960 (s), 2926,

2865, 1624, 1588, 1523, 1495, 1466, 1441, 1406, 1381, 1361, 1324, 1262, 1243, 1214, 1099, 1074, 1057, 1038, 1002, 962, 898, 799, 756, 731, 695, 669, 522, 465.

[Ni{2,6-(4-Cl-2,6-^{i}Pr$_2$C$_6$H$_2$N=CMe)$_2$C$_5$H$_3$N}Cl] (10). This compound was synthesized following the procedure of **8** using 100 mg (0.147 mmol) of **3**. The amalgam was prepared by mixing 3.6 mg (0.157 mmol) of Na into 700 mg of Hg. Yield: 34 mg (36%) of an orange-black solid. The product was recrystallized from *n*-pentane by preparing a concentrated solution at 20 °C and storing it at –15 °C. A black microcrystalline solid was obtained within several weeks. EIMS (70 eV) *m*/*z*: $M^{+\bullet}$ calcd for $C_{33}H_{41}Cl_3N_3Ni$, 642.17; found, 642.3 ($M^{+\bullet}$), 549.5 ($M^{+\bullet}$ – Ni – Cl), 534.4 ($M^{+\bullet}$ – Ni – Cl – 15). UV–Vis (toluene) λ_{max}, nm (ε): 465 (1200), 505 (1100), 705 (850), 815 (880).

[Ni{2,6-(4-Br-2,6-^{i}Pr$_2$C$_6$H$_2$N=CMe)$_2$C$_5$H$_3$N}Cl] (11). This compound was synthesized following the procedure of **8** using 100 mg (0.117 mmol) of **4**·CH_2Cl_2. The amalgam was prepared by mixing 2.7 mg (0.117 mmol) of Na into 540 mg of Hg. Yield: 45 mg (52%) of an orange-black solid. The product was recrystallized from *n*-pentane by preparing a concentrated solution at 20 °C and storing it at –15 °C. A black microcrystalline solid was obtained within several weeks. EIMS (70 eV) *m*/*z*: $M^{+\bullet}$ calcd for $C_{33}H_{41}Br_2ClN_3Ni$, 730.07; found, 730.2 ($M^{+\bullet}$), 637.3 ($M^{+\bullet}$ – Ni – Cl), 622.3 ($M^{+\bullet}$ – Ni – Cl – 15). UV–Vis (toluene) λ_{max}, nm (ε): 465 (1300), 505 (1200), 725 (700), 815 (950).

X-ray Crystallographic Analyses. A single crystal of each compound was coated with Paratone N oil and mounted on a glass capillary for data collection at 190(2) K on a Bruker Nonius Kappa APEX II diffractometer (**9**·$2C_7H_8$) or on a Nonius KappaCCD diffractometer (**8**·$2C_7H_8$), using Mo *Kα* radiation (graphite monochromator). The temperature was controlled by an Oxford Cryostream Cooler (700 series, N_2 gas).

Data collection, data reduction, and absorption correction were carried out following standard CCD techniques using the software packages Collect and HKL-2000 (**8**·2C_7H_8) or the APEX2 software package (**9**·2C_7H_8) .[48-50] Final cell constants were calculated from 20011 (**8**·2C_7H_8) or 9919 (**9**·2C_7H_8) reflections from the complete data set. In each case, the space group $P2_1/c$ was determined based on systematic absences and intensity statistics. The structures were solved by direct methods and refined by full-matrix least-squares minimization and difference Fourier methods (SHELXTL v.6.12).[51,52] All non-hydrogen atoms were refined with anisotropic displacement parameters. All hydrogen atoms were placed in ideal positions and refined as riding atoms with relative isotropic displacement parameters. In **8**·2C_7H_8, the two solvent molecules are disordered and each one was modeled with two components (70.5:29.5 and 64.3:35.7). The parameters of the toluene carbon atoms were refined with restrained C–C distances (1.38(2) and 2.40(4) Å for aromatic 1,2- and 1,3-distances, respectively, and 1.50(2) and 2.50(4) Å for distances involving a methyl carbon atom) and rigid-bond restraints. The final full-matrix least-squares refinement converged to $R1 = 0.0577$ and $wR2 = 0.1296$ [F^2, $I > 2\sigma(I)$]. In **9**·2C_7H_8, one of the disordered two solvent molecules was modeled with two components (71.3:28.7) and the other one with three components (64.0:14.4:21.6). The aromatic rings were constrained to regular hexagons, and C–C distances involving a methyl carbon atom were restrained to 1.50(2) Å. The carbon atoms of the two minor components of the second solvent molecule were refined with isotropic displacement parameters. Appropriate constraints and restraints were applied to the displacement parameters of all solvent carbon atoms. The final full-matrix least-squares refinement converged to $R1 =$

0.0469 and $wR2 = 0.1252$ [F^2, $I > 2\sigma(I)$]. Crystallographic data and additional information about the refinement is provided in Table 15 in section 4.3.2.

4.3 Results and Discussion

4.3.1 Synthesis and Characterization of [$Ni^{II}(L^{\bullet -})Cl$] Complexes

Complexes **1-4**, described in Chapter 3, were reduced with 1 equiv of sodium amalgam, a method that was reported previously for the reduction of bis(arylimino)pyridine complexes of Co.[32] Scheme 17 provides an outline for the general method of the reaction, along with numbering used for complexes in this Chapter. The new complexes **8-11** were obtained as orange-black solids and were recrystallized from toluene or *n*-pentane to give black crystalline solids. The composition of these complexes was established by electron impact mass spectrometry for **8-11** and by elemental analysis for **8**. Complexes **8** and **9** were also characterized by IR spectroscopy (see below) and X-ray crystallography (section 4.3.2). Complex **8** was further characterized by EPR spectroscopy (see below). Attempts at the reduction of complexes **5** and **6** using this method were unsuccessful. Complexes **5** and **6** also did not have an observable one-electron reduction event with either cyclic voltammetry or differential pulse voltammetry. The issue of whether the reduction of these complexes is ligand-centered or metal-centered will be explored in this Chapter, and Scheme 19 shows resonance structures for these complexes that must be considered.

The new complexes **8-11** were characterized by electron impact mass spectrometry. In all cases, the molecular ion $[Ni(L)Cl]^{+\bullet}$ was observed in the mass spectrum. In complexes **8**, **10**, and **11**, the loss of NiCl could be observed as well. No trace of unreduced complexes was observed in the spectra of complexes **8-11**.

Scheme 18. One Electron Reduction of Bis(arylimino)pyridine Complexes of Ni^{II}.

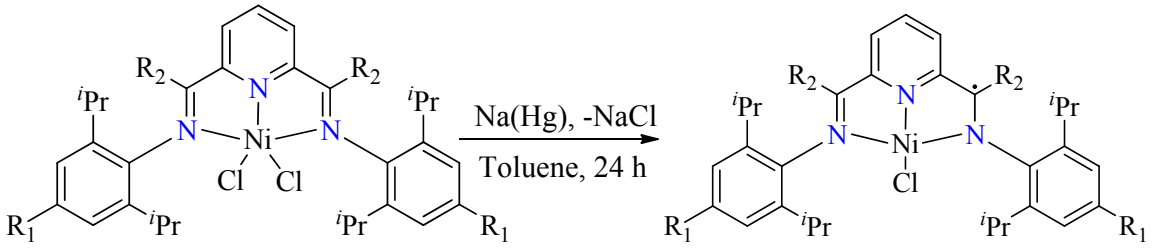

R_1	R_2	Ligand	Complex
H	CH_3	L1	**8**
H	CD_3	L2	**9**
Cl	CH_3	L3	**10**
Br	CH_3	L4	**11**

Scheme 19. Resonance Structures for the One Electron Reduction of Bis(arylimino)pyridine complexes of Ni^{II}.

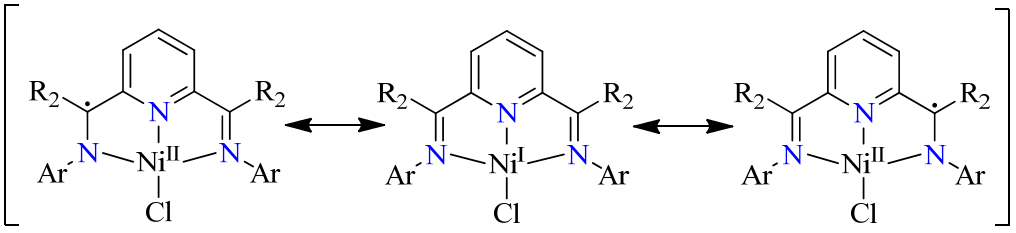

$[Ni^{II}(L^{\bullet-})Cl]$ $[Ni^{I}(L)Cl]$ $[Ni^{II}(L^{\bullet-})Cl]$

$R_2 =$ CH_3 or CD_3 Ar = 2,6-^{i}Pr$_2$C$_6$H$_3$
4-Cl-2,6-^{i}Pr$_2$C$_6$H$_2$
4-Br-2,6-^{i}Pr$_2$C$_6$H$_2$

The IR spectra of [Ni(L1$^{\bullet-}$)Cl] and [Ni(L2$^{\bullet-}$)Cl] have similar ν_{CH} (aromatic) and ν_{CH} (saturated) bands to [Ni(L1)Cl_2] and [Ni(L2)Cl_2]. Bands at 1629 and 1624 cm^{-1} can be assigned to the CN stretching vibration. These bands are shifted by 8 cm^{-1} to higher energies, and have decreased intensities compared to the unreduced complexes. In the IR spectra of the ligand radical anion complexes, the intensities of the bands below 1700 cm^{-1} are generally lower relative to the ν_{CH} (aromatic) and ν_{CH} (saturated) bands than in the unreduced complexes. New bands appeared at 1002, 731, and 695 cm^{-1} in both ligand radical anion complexes, whereas bands at 1089 and 746 cm^{-1} (for [Ni(L1)Cl_2]) and at 850 and 743 cm^{-1} (for [Ni(L2)Cl_2]) disappeared upon reduction of the dichloride complexes. Key differences between the two ligand radical anion complexes [Ni(L1$^{\bullet-}$)Cl] and [Ni(L2$^{\bullet-}$)Cl] are that the bands at 1057, 938 and 775 cm^{-1} lost intensity while new bands at 898 and 669 cm^{-1} appeared upon deuteration.

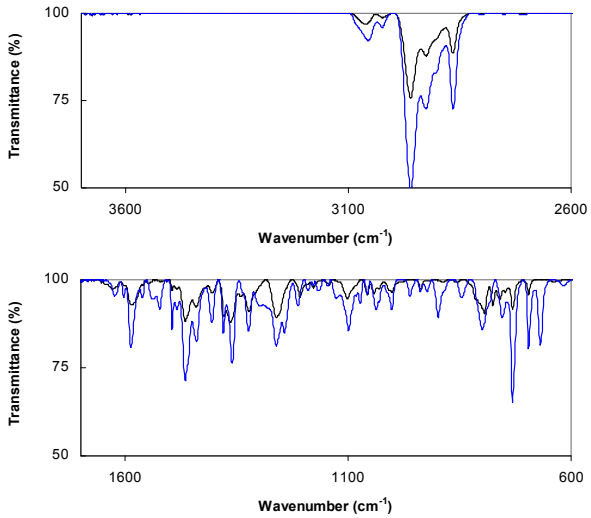

Figure 7. IR spectra of [Ni(L1$^{\bullet-}$)Cl] (—, black) and [Ni(L2$^{\bullet-}$)Cl] (—, blue) showing the ranges of 2600-3700 cm^{-1} (top) and 600-1700 cm^{-1} (bottom).

Complex **8** was characterized by electron paramagnetic resonance spectroscopy in order to elucidate the electronic structure of the complex and gain insight into whether the reduction was ligand centered (i.e. $[Ni^{II}(L^{\bullet-})Cl]$) or metal centered (i.e. $[Ni^{I}(L)Cl]$). The EPR spectrum of **8** (Figure 8) displayed an isotropic resonance signal centered at g = 2.016 with a peak to peak separation of ≈ 25 G. This isotropic signal and g value near 2.002 are consistent with an organic radical. The EPR signal does not show any fine structure, therefore the unpaired electron density is not located on a nitrogen atom on the ligand. If the unpaired electron density were located in a metal-based orbital (i.e. $[Ni^{I}(L)Cl]$), a more distorted signal (e.g. axial or rhombic) with a larger g value and a broader line width may be expected. This is one key piece of evidence establishing that the location of the added electron is on the ligand and not the metal center. This is in contrast to two other reduced bis(arylimino)pyridine complexes of Ni that were reported previously. Those complexes have key structural differences, however, as the first example is the 2:1 bis(arylimino)pyridine:nickel complex, $[Ni^{I}(L)_2]^{+}$, discussed in Section 3.3.4. This complex had an axial EPR signal with $g_{\parallel}$ = 2.213, and $g_{\perp}$ = 2.115.[26] The second example, $[Ni^{I}(L)(SPh)_2]^{-}$, is a Ni complex supported by thiolate ligands on the Ni center instead of chloride, and has a completely unsubstituted aniline ring. This complex had a rhombic EPR signal with g = 2.28, 2.20, and 2.16.[23] So these complexes are best formulated as Ni^{I} complexes. The electronic structure of **8** is consistent, however, with other $[M^{II}(L^{\bullet-})Cl]$ complexes of Cr, Fe, and Co which have been described as ligand radical complexes on the basis of crystallographic data.[19,33,34]

Crystallographic evidence for complexes **8** and **9** will be presented in the next section in order to help confirm the location of the radical on the ligand in these complexes. Complexes **8-11** all exhibit similar features in the Vis-NIR region of their absorption spectra, which may be a characteristic signature of these ligand radical complexes. Therefore complexes **10** and **11**, which have not yet been characterized by EPR spectroscopy or X-ray crystallography, may also be considered ligand radical complexes.

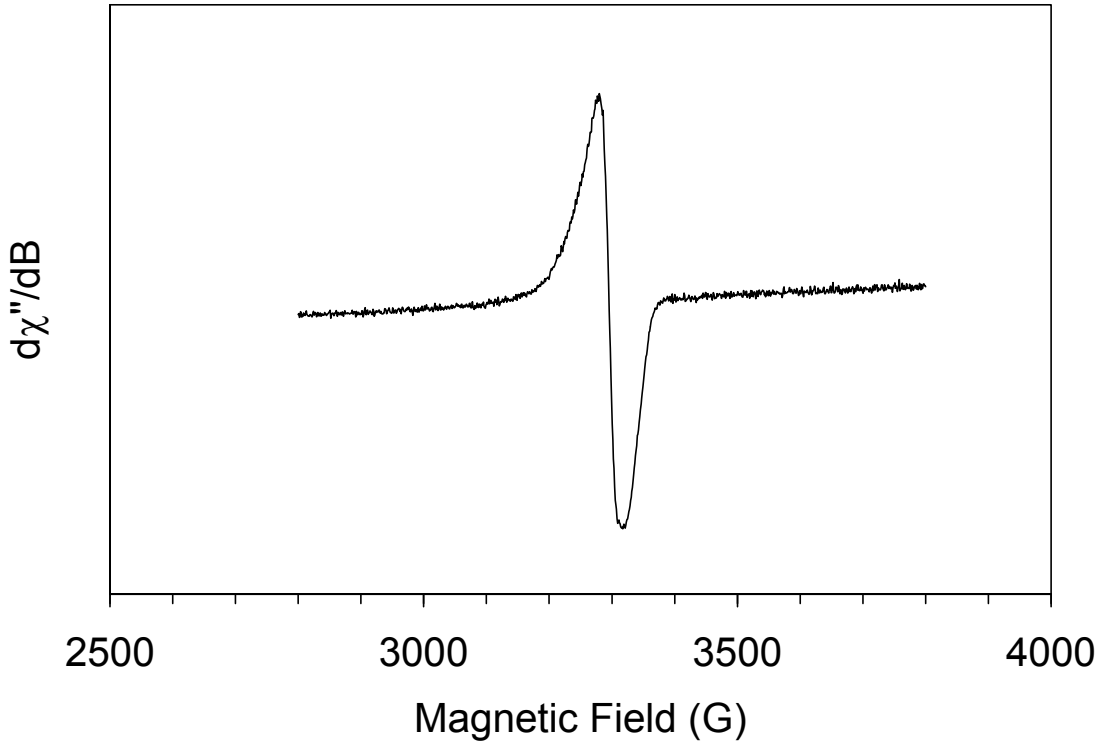

Figure 8. EPR spectrum of 5 mM [Ni(L1$^{\bullet-}$)Cl] in toluene at 77 K (X-band microwave frequency, 9.30 GHz; modulation frequency. 100 kHz; modulation amplitude, 10 G; and microwave power, 2.0 mW).

4.3.2 Crystal Structures

Crystals of $[Ni(L1^{\bullet-})Cl]\cdot 2C_7H_8$ (black needles) and $[Ni(L2^{\bullet-})Cl]\cdot 2C_7H_8$ (dark green blocks) were grown from concentrated toluene solutions upon standing at –30 °C for $[Ni(L1^{\bullet-})Cl]\cdot 2C_7H_8$ or –15 °C for $[Ni(L2^{\bullet-})Cl]\cdot 2C_7H_8$. As expected, there is high agreement in the unit cell constants of the two structures, with differences only in the second decimal places. The cell volume differs by 0.3%. The molecular structures of the complexes are nearly identical, with only minor differences in bond lengths and angles (Tables 16-18). This is to be expected as the only difference is a deuterium label on two methyl groups, which should have negligible, if any, influences on the structural parameters. Selected bond lengths and angles for $[Ni(L1^{\bullet-})Cl]\cdot 2C_7H_8$ and $[Ni(L2^{\bullet-})Cl]\cdot 2C_7H_8$ are presented in Tables 16-18, and the molecular structures are presented in Figures 9 and 10. The coordination geometry in both complexes is best described as distorted square planar, with angles distorted from the ideal 90 °C around Ni (Table 17). In contrast to the unreduced structures, the Ni atom lies in the N1–N2–N3 plane in the reduced complexes. In $[Ni(L1^{\bullet-})Cl]\cdot 2C_7H_8$, the Ni–N1 (pyridine) bond length of 1.833(2) Å is shorter than the Ni–N2 and Ni–N3 (imine) bond lengths of 1.941(2) Å and 1.943(2) Å. The Ni–Cl distance is 2.1688(8) Å. These distances are all shorter than found on the corresponding unreduced complex $[Ni(L1)Cl_2]\cdot 0.5H_2O$. On the ligand, the first set of notable bond lengths include the imine double bonds, N2–C6 (1.318(4) Å) and N3–C8 (1.324(4) Å), which are slightly longer than observed for $[Ni(L1)Cl_2]\cdot 0.5H_2O$ (Table 19), indicating less double bond character. The next set of bond lengths of interest are the C–C bonds adjacent to the pyridine ring, C1–C6 (1.451(4) Å) and C5–C8 (1.446(4) Å),

which are shorter than found in $[Ni(L1)Cl_2]\cdot 0.5H_2O$. The C–C bond lengths involving the acetimino groups C6–C7 and C8–C9 are 1.468(4) Å and 1.482(4) Å, respectively.

Table 15. Crystallographic data and structure refinement for $[Ni\{2,6\text{-}(2,6\text{-}{}^{i}Pr_2C_6H_3N{=}CCH_3)_2C_5H_3N\}Cl]\cdot 2C_7H_8$, **8**$\cdot 2C_7H_8$, and $[Ni\{2,6\text{-}(2,6\text{-}{}^{i}Pr_2C_6H_3N{=}CCD_3)_2C_5H_3N\}Cl]\cdot 2C_7H_8$, **9**$\cdot 2C_7H_8$.

	8$\cdot 2C_7H_8$	**9**$\cdot 2C_7H_8$
Empirical formula	$C_{47}H_{59}ClN_3Ni$	$C_{47}H_{53}ClD_6N_3Ni$
Formula weight	760.13	766.17
Crystal habit, color	needle, black	block, dark green
Crystal size	0.33 x 0.07 x 0.04 mm^3	0.40 x 0.39 x 0.23 mm^3
Temperature, T	190(2) K	190(2) K
Wavelength, λ	0.71073 Å	0.71073 Å
Crystal system	monoclinic	monoclinic
Space group	$P2_1/c$	$P2_1/c$
Unit cell dimensions	a = 19.115(2) Å b = 13.0015(14) Å c = 19.112(2) Å β = 113.704(5)°	a = 19.1241(19) Å b = 12.9953(13) Å c = 19.1785(19) Å β = 113.767(5)°
Volume, V	4349.3(8) $Å^3$	4362.1(8) $Å^3$
Z	4	4
Calculated density	1.161 $Mg\cdot m^{-3}$	1.167 $Mg\cdot m^{-3}$
Absorption coefficient, μ	0.541 mm^{-1}	0.540 mm^{-1}
$F(000)$	1628	1628
θ range for data collection	2.81 to 27.91°	2.98 to 27.50°
Limiting indices	$-25 \le h \le 25$, $-17 \le k \le 17$, $-25 \le l \le 24$	$-24 \le h \le 24$, $-16 \le k \le 16$, $-22 \le l \le 24$
Reflections collected / unique	37926 / 10390 [R(int) = 0.0989]	74489 / 9985 [R(int) = 0.0306]
Completeness to θ	99.8 % (θ = 27.91°)	99.9 % (θ = 27.50°)
Max. and min. transmission	0.9787 and 0.8416	0.8859 and 0.8131
Refinement method	Full-matrix least-squares on F^2	Full-matrix least-squares on F^2
Data / restraints / parameters	10390 / 120 / 611	9985 / 459 / 534
Goodness-of-fit on F^2	1.000	1.042
Final R indices [I>2sigma(I)]	$R1$ = 0.0577, $wR2$ = 0.1296	$R1$ = 0.0469, $wR2$ = 0.1252
R indices (all data)	$R1$ = 0.1343, $wR2$ = 0.1679	$R1$ = 0.0648, $wR2$ = 0.1384
Largest diff. peak and hole	0.431 and –0.300 $e\cdot Å^{-3}$	0.849 and -0.310 $e\cdot Å^{-3}$

Table 16. Selected interatomic distances (Å) for [Ni{2,6-(2,6-$^{i}Pr_2C_6H_3N{=}CCH_3)_2C_5H_3N$}Cl]·$2C_7H_8$, **8**·$2C_7H_8$, and [Ni{2,6-(2,6-$^{i}Pr_2C_6H_3N{=}CCD_3)_2C_5H_3N$}Cl]·$2C_7H_8$, **9**·$2C_7H_8$.[a]

8·$2C_7H_8$		**9**·$2C_7H_8$	
Ni–N1	1.833(2)	Ni–N1	1.840(2)
Ni–N2	1.941(2)	Ni–N2	1.9529(18)
Ni–N3	1.943(2)	Ni–N3	1.9455(18)
Ni–Cl	2.1688(8)	Ni–Cl	2.1766(7)
N1–C1	1.350(4)	N1–C1	1.360(3)
N1–C5	1.356(4)	N1–C5	1.344(3)
N2–C6	1.318(4)	N2–C6	1.313(3)
N2–C10	1.445(3)	N2–C10	1.446(3)
N3–C8	1.324(4)	N3–C8	1.323(3)
N3–C22	1.436(4)	N3–C22	1.445(3)
C1–C6	1.451(4)	C1–C6	1.445(3)
C5–C8	1.446(4)	C5–C8	1.442(3)
C6–C7	1.468(4)	C6–C7	1.494(3)
C8–C9	1.482(4)	C8–C9	1.484(3)

[a] Numbers in parentheses are standard uncertainties in the last significant figures. Atoms are labeled as indicated in Figures 9 and 10.

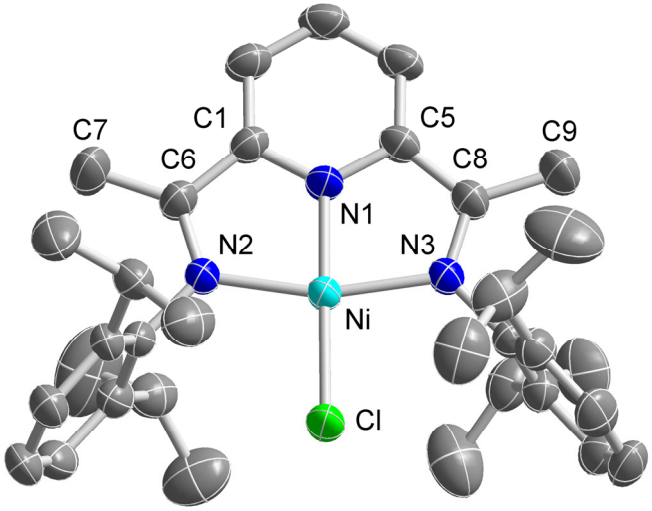

Figure 9. Molecular structure of [Ni{2,6-(2,6-$^{i}Pr_2C_6H_3N{=}CCH_3)_2C_5H_3N$}Cl]·$2C_7H_8$, **8**·$2C_7H_8$. Displacement ellipsoids are drawn at the 50% probability level. Hydrogen atoms and the solvent toluene molecules have been omitted for clarity. Color key: turquoise = Ni, blue = N, green = Cl, gray = C.

Table 17. Selected angles (°) for [Ni{2,6-(2,6-$^{i}Pr_2C_6H_3N{=}CCH_3)_2C_5H_3N$}Cl]·$2C_7H_8$, **8**·$2C_7H_8$, and [Ni{2,6-(2,6-$^{i}Pr_2C_6H_3N{=}CCD_3)_2C_5H_3N$}Cl]·$2C_7H_8$, **9**·$2C_7H_8$.[a]

8·$2C_7H_8$		**9**·$2C_7H_8$	
N1–Ni–N2	81.26(10)	N1–Ni–N2	80.95(8)
N1–Ni–N3	81.29(10)	N1–Ni–N3	81.11(8)
N2–Ni–Cl	99.17(7)	N2–Ni–Cl	98.76(6)
N3–Ni–Cl	98.31(7)	N3–Ni–Cl	99.21(6)
N1–Ni–Cl	179.03(10)	N1–Ni–Cl	178.71(8)
N2–Ni–N3	162.45(9)	N2–Ni–N3	161.95(8)
C1–N1–C5	121.9(2)	C1–N1–C5	121.8(2)
C1–N1–Ni	119.02(19)	C1–N1–Ni	119.07(16)
C5–N1–Ni	119.0(2)	C5–N1–Ni	119.10(16)
C6–N2–C10	119.7(2)	C6–N2–C10	120.02(19)
C6–N2–Ni	115.32(19)	C6–N2–Ni	115.18(15)
C10–N2–Ni	125.01(18)	C10–N2–Ni	124.80(14)
C8–N3–C22	119.5(2)	C8–N3–C22	120.32(18)
C8–N3–Ni	115.14(19)	C8–N3–Ni	114.76(15)
C22–N3–Ni	125.39(17)	C22–N3–Ni	124.90(14)
N1–C1–C2	119.6(3)	N1–C1–C2	119.8(2)
N1–C1–C6	111.1(2)	N1–C1–C6	110.8(2)
C2–C1–C6	129.3(3)	C2–C1–C6	129.4(2)
N1–C5–C4	119.7(3)	N1–C5–C4	119.9(2)
N1–C5–C8	111.2(2)	N1–C5–C8	111.2(2)
C4–C5–C8	129.2(3)	C4–C5–C8	128.9(2)
N2–C6–C1	113.3(3)	N2–C6–C1	114.0(2)
N2–C6–C7	125.4(3)	N2–C6–C7	125.1(2)
C1–C6–C7	121.3(3)	C1–C6–C7	120.9(2)
N3–C8–C5	113.4(2)	N3–C8–C5	113.8(2)
N3–C8–C9	124.7(3)	N3–C8–C9	124.8(2)
C5–C8–C9	121.9(3)	C5–C8–C9	121.4(2)

[a] Numbers in parentheses are standard uncertainties in the last significant figures. Atoms are labeled as indicated in Figures 9 and 10.

Table 18. Selected dihedral angles (°) for [Ni{2,6-(2,6-$^{i}Pr_2C_6H_3N{=}CCH_3)_2C_5H_3N$}Cl]·$2C_7H_8$, **8**·$2C_7H_8$, and [Ni{2,6-(2,6-$^{i}Pr_2C_6H_3N{=}CCD_3)_2C_5H_3N$}Cl]·$2C_7H_8$, **9**·$2C_7H_8$.[a]

8·$2C_7H_8$		**9**·$2C_7H_8$	
(N1,N2,N3) / (C10→C15)[b]	85.6(1)	(N1,N2,N3) / (C10→C15)[b]	87.5(1)
(N1,N2,N3) / (C22→C27)[b]	87.3(1)	(N1,N2,N3) / (C22→C27)[b]	85.31(9)
(C10→C15) / (C22→C27)[c]	83.2(1)	(C10→C15) / (C22→C27)[c]	83.24(8)

[a] Numbers in parentheses are standard uncertainties in the last significant figures. Atoms are labeled as indicated in Figures 9 and 10. [b] Angle between the plane of the ligand nitrogen atoms (N1, N2, and N3) and a least-squares plane of aryl ring atoms (*e.g.*, C10, C11, C12, C13, C14, and C15). [c] Angle between the least-squares planes of the aryl ring atoms.

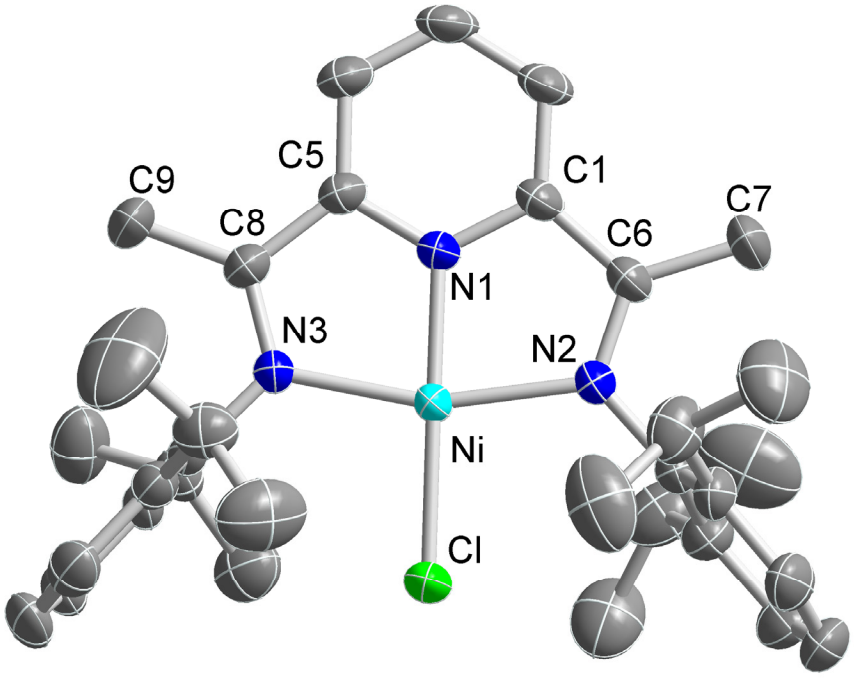

Figure 10. Molecular structure of [Ni{2,6-(2,6-$^{i}Pr_2C_6H_3N{=}CCD_3)_2C_5H_3N$}Cl]·$2C_7H_8$, **9**·$2C_7H_8$. Displacement ellipsoids are drawn at the 50% probability level. Hydrogen atoms and the solvent toluene molecules have been omitted for clarity. Color key: turquoise = Ni, blue = N, green = Cl, gray = C.

In [Ni(L2$^{\bullet-}$)Cl]·$2C_7H_8$, the Ni–N1 (pyridine) bond length is 1.840(2) Å, is shorter than the Ni–N2 and Ni–N3 (imine) bond lengths of 1.9529(18) Å and 1.9455(18) Å. The

Ni–Cl bond length is 2.1766(7) Å, all of which are similar to [Ni(L1$^{\bullet-}$)Cl]·2C_7H_8. On the ligand, the first set of notable bond lengths include the imine double bonds N2–C6 (1.313(3) Å) and N3–C8 (1.323(3) Å), again similar to [Ni(L1$^{\bullet-}$)Cl]·2C_7H_8 (Table 19). The next set of bond lengths of interest are the C–C bonds adjacent to the pyridine ring, C1–C6 (1.445(3) Å) and C5–C8 (1.442(3) Å), again similar to [Ni(L1$^{\bullet-}$)Cl]·2C_7H_8. The C–C bond lengths of the involving the acetimino groups C6–C7 and C8–C9 are 1.494(3) Å and 1.484(3) Å, respectively.

Table 19. Comparison of Key Intraligand Distances (Å) for Complexes **1**, **8** and **9**.

	1	**8**	**9**
N2–C6	1.287(3)	1.318(4)	1.313(3)
N3–C8	1.289(3)	1.324(4)	1.323(3)
C1–C6	1.493(4)	1.451(4)	1.445(3)
C5–C8	1.486(4)	1.446(4)	1.442(3)
C6–C7	1.495(4)	1.468(4)	1.494(3)
C8–C9	1.498(4)	1.482(4)	1.484(3)

The contraction of the C1–C6 and C5–C8 distances along with the lengthening of the N2–C6 and N3–C8 distances in these complexes is an important clue in determining the location of the unpaired electron density (Table 19). Related bis(arylimino)pyridine complexes of Cr, Fe and Co ([M(L)Cl]) that have been reduced have also shown a similar contraction of C1–C6 and C5–C8 distances and a similar lengthening of N2–C6 and N3–C8 distances which were attributed to the presence of an unpaired electron on the ligand.[19,33,34] These complexes were ultimately described as ligand radical complexes,

which was also confirmed by DFT calculations.[34] This observation is also consistent with the EPR spectrum of $[Ni(L1^{\bullet-})Cl]\cdot 2C_7H_8$.

4.4 Conclusion

The reduction of bis(arylimino)pyridine complexes of nickel(II) was discussed in this chapter. Complexes **1-4** were successfully reduced using 1 equiv of a sodium amalgam under an inert atmosphere. Complexes **5** and **6** were unable to be chemically reduced, consistent with the lack of a reduction event seen in the electrochemical characterization of these complexes. The new reduced complexes **8**-**11** were isolated and characterized as ligand radical anion complexes of Ni^{II}, $[Ni^{II}(L^{\bullet-})Cl]$. Electron paramagnetic resonance spectroscopy of **1** gave an isotropic signal centered at $g = 2.016$, consistent with an organic radical. The C–C bonds adjacent to the imine group were shown by single crystal X-ray diffraction of **8** and **9** to contract upon reduction, and the C=N bonds of the imine were shown to lengthen, consistent with unpaired electron density on the ligand. These results show that the reduction of these bis(arylimino)pyridine complexes of Ni^{II} is a ligand centered reduction, not a metal centered reduction. Infrared spectroscopy of **8** and **9** revealed a decrease in the intensity of the CN stretching vibration as compared to the unreduced complexes. On the basis of electronic absorption spectroscopy, complexes **10** and **11** can also be assigned as ligand radical complexes as they give the same signature in the Vis-NIR region as complexes **8** and **9**. The reactivity of the new reduced complexes towards O_2 was investigated and is described in Chapter 5.

CHAPTER 5

REACTIONS OF BIS(ARYLIMINO)PYRIDINE RADICAL ANION COMPLEXES OF NICKEL(II) WITH DIOXYGEN

5.1 Introduction

The reactions of bis(arylimino)pyridine radical anion complexes of Ni^{II} with O_2 will be the focus of Chapter 5. These reactions were investigated by UV-Vis spectroscopy. Overall, the O_2 reactions of each of the Ni complexes were similar to each other in terms of the course of the reaction, but the half-life of the reaction was affected by ligand substitution. Reactions were also carried out on a preparative scale, and the new complexes **12-15** were isolated. Single crystal X-ray diffraction of **12** and **13** showed that the coordination environment of the Ni center remained unchanged. However, a C–C bond on the ligand was cleaved resulting in conversion of an acetimino group into a carboxamidato group. A strong band observed with infrared spectroscopy of **12-15** could be assigned to the CO stretching vibration. The ligand was extracted from **12-15**, forming the new compounds **16-19**. ^{1}H nuclear magnetic resonance spectroscopy of **16** confirms the loss of an acetimino group on the ligand. The reaction of **8** with O_2 and the characterization of the product and the isolated ligand was published in 2009.[55] In contrast, in the reaction of a bis(arylimino)pyridine Co complex with O_2 only a one-electron oxidation was observed. The possible mechanisms of the reactions will be discussed. Data from the reaction of O_2 with the deuterium labeled complex **13** are consistent with direct attack of the ligand radical by O_2.

5.2 Experimental Section

Materials. All reagents and solvents were purchased from commercial sources and were used as received, unless noted otherwise. Toluene and acetonitrile were deoxygenated by sparging with N_2 and purified by passage through two packed columns of molecular sieves under an N_2 pressure (MBraun solvent purification system). Nitromethane was purified by flash-freezing with liquid N_2 and decanting the liquid phase upon warming to –20 °C; this procedure was repeated twice, and the resulting solvent was dried over molecular sieves.[56] Preparation and handling of air- and moisture-sensitive materials were carried out under an inert gas atmosphere by using either standard Schlenk and vacuum line techniques or a glovebox.

Physical Methods NMR spectra were recorded on a Bruker Avance II 300 spectrometer at ambient temperature. ^{1}H chemical shifts are reported in parts per million (ppm) and were referenced to residual solvent peaks. Low-resolution mass spectral data were acquired on a quadrupole ion trap ThermoFinnigan LCQ Deca mass spectrometer using an electrospray ionization source or on a single quadrupole ThermoFinnigan Voyager mass spectrometer using an electron impact ionization source (equipped with a solids probe). High-resolution mass spectral data were acquired on a time-of-flight Waters Q-tof Premier mass spectrometer using an electrospray ionization source, on a double-focusing magnetic-sector Micromass, Inc., Autospec mass spectrometer using an electron impact ionization source (equipped with a solids probe), or on a Waters GCT Premier mass spectrometer using an electron impact ionization source (equipped with a solids probe). UV–Visible spectra were recorded on an HP 8453A diode array

spectrophotometer (Agilent Technologies) with samples maintained at the desired temperature using a cryostat/heater from Unisoku Scientific Instruments, Japan. IR spectra were recorded on a Bruker Vertex 70 Fourier-transform IR spectrometer using samples prepared by mixing the solid compound with KBr and pressing the mixture into a disk.

[Ni{6-(2,6-^{i}Pr$_2$C$_6$H$_3$N=CMe)C$_5$H$_3$N-2-C(O)N(2,6-^{i}Pr$_2$C$_6$H$_3$)}Cl] (12). In an N_2 atmosphere, a solution of 29 mg (0.050 mmol) of **8** in 50 mL of toluene was heated to 60 °C. Dioxygen was then purged through the solution for 30 s, and the solution was kept under an O_2 atmosphere and at a temperature of 60 °C throughout the course of the reaction. After 24 h, the solution was allowed to cool to room temperature, concentrated to a volume of 5 mL, and stored at –25 °C. An orange-red precipitate formed within 3 days, which was separated by filtration (yield: 14 mg, 49%) and recrystallized from nitromethane at –25 °C. Within a week, orange-brown cubic crystals of X-ray diffraction quality were obtained. ESI(+)MS (CH_3NO_2) *m*/*z*: $\{M + H\}^+$ calcd for $C_{32}H_{40}ClN_3NiO$, 576.23; found, 576.2 ($\{M + H\}^+$), 540.3 ($\{M – Cl\}^+$). ESI(+)MS (CH_3CN) *m*/*z*: 589.3 ($\{M – Cl + Na + CN\}^+$). High-resolution ESI(+)MS (CH_3NO_2) *m*/*z* calcd for $C_{32}H_{40}ClN_3NiO$: $\{M + H\}^+$, 576.2292; $\{M – Cl\}^+$, 540.2525; $\{M – Ni – Cl + 2H\}^+$, 484.3328. Found: 576.2334; 540.2522; 484.3331. UV–Vis (toluene) λ_{max}, nm (ε): 360 (1100), 470 (390), 515 (420). IR (KBr, cm^{-1}): 3060, 2960 (s), 2928, 2866, 1635 (s), 1604, 1587, 1466, 1442, 1380, 1358, 1325, 1288, 1255, 1058, 937, 818, 798, 791, 762, 741.

[Ni{6-(2,6-^{i}Pr$_2$C$_6$H$_3$N=CCD$_3$)C$_5$H$_3$N-2-C(O)N(2,6-^{i}Pr$_2$C$_6$H$_3$)}Cl] (13). This compound was synthesized following the method for **12** using 29.1 mg (0.050 mmol) of **9.** Yield: 8 mg (28%) of a red orange solid. Red-orange crystals of X-ray diffraction quality

were obtained from nitromethane at –25 °C. ESI(+)MS (CH_3CN) *m*/*z*: $\{M + H\}^+$ calcd for $C_{32}H_{37}D_3ClN_3NiO$, 579.25; found, 579.1 ($\{M + H\}^+$). UV–Vis (toluene) λ_{max}, nm: 390, 475, 515. IR (KBr, cm^{-1}): 3071, 3058, 2960 (s), 2927, 2867, 1634 (s), 1602, 1587, 1466, 1443, 1379, 1358, 1326, 1257, 1099, 1073, 1058, 1041, 816, 799, 759, 741, 730, 669, 403.

[Ni{6-(4-Cl-2,6-^{i}Pr$_2$C$_6$H$_2$N=CMe)C$_5$H$_3$N-2-C(O)N(4-Cl-2,6-^{i}Pr$_2$C$_6$H$_2$)}Cl] (14). This compound was synthesized following the method for **12** using 32.2 mg (0.050 mmol) of **10**. Yield: 8 mg (25%) of a red orange solid. ESI(+)MS (CH_3NO_2) *m*/*z*: $\{M + H\}^+$ calcd for $C_{32}H_{38}Cl_3N_3NiO$, 644.15; found, 644 ($\{M + H\}^+$). High-resolution ESI(+)MS (CH_3NO_2) *m*/*z* calcd for $C_{32}H_{38}Cl_3N_3NiO$: $\{M – Cl + K + CN\}^+$, 673.1413; $\{M – Cl + Na + CN\}^+$, 657.1674; $\{M – Ni – Cl + Na + H\}^+$, 574.2368; $\{M – Ni – Cl + 2H\}^+$, 552.2548. Found: 673.1439; 657.1688; 574.2382; 552.2571. UV–Vis (toluene) λ_{max}, nm: 385, 470, 515. IR (KBr, cm^{-1}): 3082, 3062, 2962 (s), 2932, 2867, 1697, 1636 (s), 1604, 1579, 1466, 1448, 1431, 1380, 1359, 1326, 1261, 1232, 1205, 1149, 1089, 1069, 1023, 945, 898, 866, 819, 803, 759, 730, 695, 464, 396.

[Ni{6-(4-Br-2,6-^{i}Pr$_2$C$_6$H$_2$N=CMe)C$_5$H$_3$N-2-C(O)N(4-Br-2,6-^{i}Pr$_2$C$_6$H$_2$)}Cl] (15). This compound was synthesized following the method for **12** using 37 mg (0.050 mmol) of **11**. Yield: 3 mg (8%) of a red orange solid. ESI(+)MS (CH_3NO_2) *m*/*z*: $\{M + H\}^+$ calcd for $C_{32}H_{38}Br_2ClN_3NiO$, 732.05; found, 732 ($\{M + H\}^+$). High-resolution ESI(+)MS (CH_3NO_2) *m*/*z* calcd for $C_{32}H_{38}Br_2ClN_3NiO$: $\{M – Cl + K + CN\}^+$, 761.0403; $\{M – Cl + Na + CN\}^+$, 745.0664; $\{M – Ni – Cl + Na + H\}^+$, 662.1358. Found: 761.0421; 745.0659; 662.1363. UV–Vis (toluene) λ_{max}, nm: 380, 470, 515. IR (KBr, cm^{-1}): 2960 (s),

2926 (s), 2855, 1745, 1635 (s), 1572, 1465, 1446, 1379, 1359, 1325, 1261, 1204, 1150, 1071, 944, 892, 865, 823, 799, 760, 463, 380.

Isolation of 6-(2,6-^{i}Pr$_2$C$_6$H$_3$N=CMe)C$_5$H$_3$N-2-C(O)NH(2,6-^{i}Pr$_2$C$_6$H$_3$) (16). A total of 5 mg (0.009 mmol) of **12** was dissolved in 1 mL of 1:1 CH_3CN/H_2O. A white precipitate formed, which was isolated by filtration, washed three times with 1:1 CH_3CN/H_2O, and dried *in vacuo*. Yield: 4 mg. High-resolution EIMS (70 eV) *m*/*z*: $M^{+\bullet}$ calcd for $C_{32}H_{41}N_3O$, 483.3250; found, 483.3257. ^{1}H NMR (300 MHz, $CDCl_3$, δ): 9.44 (s, 1H, NH), 8.58 (d, *J* = 7.9 Hz, 1H, Py H), 8.40 (d, *J* = 7.7 Hz, 1H, Py H), 8.04 (t, *J* = 7.7 Hz, 1H, Py H), 7.35–7.07 (6H, Ar H), 3.15 (sept, *J* = 6.8 Hz, 2H, Ar C*H*$(CH_3)_2$, *N*-arylcarboxamide), 2.73 (sept, *J* = 6.9 Hz, 2H, Ar C*H*$(CH_3)_2$, *N*-arylimine), 2.23 (s, 3H, N=CC*H*$_3$), 1.23 (d, *J* = 6.8 Hz, 12H, Ar CH(C*H*$_3)_2$, *N*-arylcarboxamide), 1.15 (d, *J* = 6.8 Hz, 12H, Ar CH(C*H*$_3)_2$, *N*-arylimine).

Isolation of 6-(2,6-^{i}Pr$_2$C$_6$H$_3$N=CCD$_3$)C$_5$H$_3$N-2-C(O)NH(2,6-^{i}Pr$_2$C$_6$H$_3$) (17). This compound was isolated following the method for **16**, with the exception of using D_2O in place of H_2O, using 5 mg (0.009 mmol) of **13**. Yield: 3 mg. EIMS (70 eV) *m*/*z*: $M^{+\bullet}$ calcd for $C_{32}H_{37}D_4N_3O$, 487.4; found, 487.7. The second most abundant peak in this envelope was at *m*/*z* = 484.7 (35% rel. abundance). ^{1}H NMR (300 MHz, $CDCl_3$, δ): 9.44 (s, NH; H residual peak), 8.60 (d, *J* = 7.8 Hz, 1H, Py H), 8.42 (d, *J* = 7.5 Hz, 1H, Py H), 8.05 (t, *J* = 7.8 Hz, 1H, Py H), 7.34–7.14 (Ar H; these signals overlap with the residual solvent peak), 3.17 (sept, *J* = 6.9 Hz, 2H, Ar C*H*$(CH_3)_2$, *N*-arylcarboxamide), 2.75 (sept, *J* = 6.9 Hz, 2H, Ar C*H*$(CH_3)_2$, *N*-arylimine), 2.27 (s, N=CC*H*$_3$; H residual peak), 1.25 (d, *J* = 6.9 Hz, 12H, Ar CH(C*H*$_3)_2$, *N*-arylcarboxamide), 1.17 (d, *J* = 6.6 Hz, 12H, Ar CH(C*H*$_3)_2$, *N*-arylimine).

Isolation of 6-(4-Cl-2,6-^{i}Pr$_2$C$_6$H$_2$N=CMe)C$_5$H$_3$N-2-C(O)NH(4-Cl-2,6-^{i}Pr$_2$C$_6$H$_2$) (18). A total of 5 mg (0.008 mmol) of **14** was dissolved in 1 mL of 1:1 CH_3CN/H_2O. The solution was allowed to stand for 16 h. The solution was evaporated to dryness, and 3 mL of H_2O was added. The product was extracted with two 3 mL portions of CH_2Cl_2, and the combined organic phases were evaporated to dryness. Yield: ca. 2 mg. High-resolution EIMS (70 eV) *m*/*z*: $M^{+\bullet}$ calcd for $C_{32}H_{39}N_3OCl_2$, 551.2470; found, 551.2448. ^{1}H NMR (300 MHz, $CDCl_3$, δ): 9.33 (s, 1H, NH), 8.58 (d, *J* = 7.2 Hz, 1H, Py H), 8.41 (d, *J* = 7.2 Hz, 1H, Py H), 8.06 (t, *J* = 7.8 Hz, 1H, Py H), 7.20 (s, 2H, Ar H), 7.14 (s, 2H, Ar H), 3.13 (sept, *J* = 6.9 Hz, 2H, Ar C*H*$(CH_3)_2$, *N*-arylcarboxamide), 2.71 (sept, *J* = 6.9 Hz, 2H, Ar C*H*$(CH_3)_2$, *N*-arylimine), 2.25 (s, 3H, N=CC*H*$_3$), 1.23 (d, *J* = 6.9 Hz, 12H, Ar CH(C*H*$_3)_2$, *N*-arylcarboxamide), 1.15 (d, *J* = 6.6 Hz, 12H, Ar CH(C*H*$_3)_2$, *N*-arylimine).

Isolation of 6-(4-Br-2,6-^{i}Pr$_2$C$_6$H$_2$N=CMe)C$_5$H$_3$N-2-C(O)NH(4-Br-2,6-^{i}Pr$_2$C$_6$H$_2$) (19). This compound was isolated following the method for **18** using 3 mg (0.004 mmol) of **15**. Yield: ca. 1 mg. High-resolution EIMS (70 eV) *m*/*z*: $M^{+\bullet}$ calcd for $C_{32}H_{39}N_3OBr_2$, 639.1460; found, 639.1438.

[Co{2,6-(2,6-^{i}Pr$_2$C$_6$H$_3$N=CMe)$_2$C$_5$H$_3$N}Cl$_2$] (20). The synthesis of this compound was reported, previously;[57] here, a different procedure[47] was adapted. A solution of 0.20 g (1.23 mmol) of 2,6-diacetylpyridine, 0.50 mL (0.47 g, 2.44 mmol) of 2,6-diisopropylaniline and 0.16 g (1.23 mmol) of $CoCl_2$ in 15 mL of glacial acetic acid was heated under reflux for 4 h. The solution was allowed to cool to room temperature, and 10 mL of diethyl ether was added, causing the formation of a golden-brown precipitate. The precipitate was separated by filtration, washed three times with diethyl

ether and dried *in vacuo* to yield 0.70 g (94%) of a golden-brown powder. ESI(+)MS (*m*/*z*): $\{M - Cl\}^+$ calcd for $C_{33}H_{43}Cl_2CoN_3$, 575.25; found, 575.4. UV–Vis (CH_2Cl_2) λ_{max}, nm (ε): 350 (sh, 1500), 440 (sh, 620), 700 (120).

[Co{2,6-(2,6-^{i}Pr$_2$C$_6$H$_3$N=CMe)$_2$C$_5$H$_3$N}Cl] (21). The synthesis of this compound was reported, previously;[32] here, the procedure used for the synthesis of **8** was employed. A 0.5 wt % sodium amalgam was prepared under an N_2 atmosphere by mixing 3.8 mg (0.165 mmol) of Na into 760 mg of Hg for 15 min. A solution of 100 mg (0.164 mmol) of **20** in 5 mL of toluene was added dropwise to the amalgam over 5 min. The resulting solution was stirred for 24 h. After ca. 15–20 min, the solution turned black, followed by a gradual color change to dark purple and formation of a white precipitate over the course of 24 h. The solution was removed from the amalgam and filtered through a celite pad. The solvent was removed under reduced pressure to afford 55 mg (58%) of a dark purple-red solid. EIMS (70 eV) *m*/*z*: $M^{+\bullet}$ calcd for $C_{33}H_{43}ClCoN_3$, 575.25; found, 575.3 ($M^{+\bullet}$), 481.4 ($M^{+\bullet}$ – Co – Cl), 466.4 ($M^{+\bullet}$ – Co – Cl – 15). UV–Vis (toluene) λ_{max}, nm (ε): ca. 350 (sh, 1400), 530 (600).

General Procedure for O_2 Reactions Monitored by UV-Vis Spectroscopy. A 1 mM solution of **8-11** or **21** (0.002 mmol) in 2 mL of toluene was placed in a 0.5-cm UV–Vis cuvette and warmed to 60 °C. The solution was purged with O_2 for 15 s and kept under an O_2 atmosphere. The half-lives of the reactions were determined by UV-Vis spectroscopy, and the reported values for the reactions of **8-11** with O_2 represent the averages of three runs. Bubbling times for O_2 of up to 2 min were explored, and did not yield any significant changes to the half-life of the reactions.

X-ray Crystallographic Analyses. A single crystal of each compound was coated with Paratone N oil and mounted on a glass capillary for data collection at 190(2) K on a Nonius KappaCCD diffractometer (**12**·$2CH_3NO_2$) or on a Bruker Nonius Kappa APEX II diffractometer (**13**·$2CH_3NO_2$), using Mo $K\alpha$ radiation (graphite monochromator). The temperature was controlled by an Oxford Cryostream Cooler (700 series, N_2 gas). Data collection, data reduction, and absorption correction were carried out following standard CCD techniques using the software packages Collect and HKL-2000 (**12**·$2CH_3NO_2$) or the APEX2 software package (**13**·$2CH_3NO_2$).[48-50] Final cell constants were calculated from 15615 (**12**·$2CH_3NO_2$) or 9945 (**13**·$2CH_3NO_2$) reflections from the complete data set. In each case, the space group $P2_1/c$ was determined based on systematic absences and intensity statistics. The structures were solved by direct methods and refined by full-matrix least-squares minimization and difference Fourier methods (SHELXTL v.6.12).[51,52] All non-hydrogen atoms were refined with anisotropic displacement parameters. All hydrogen atoms were placed in ideal positions and refined as riding atoms with relative isotropic displacement parameters. For **12**·$2CH_3NO_2$, the final full-matrix least-squares refinement converged to $R1 = 0.0403$ and $wR2 = 0.0904$ [F^2, $I > 2\sigma(I)$]. For **13**·$2CH_3NO_2$, the final full-matrix least-squares refinement converged to $R1 = 0.0463$ and $wR2 = 0.0989$ [F^2, $I > 2\sigma(I)$]. Crystallographic data and additional information about the refinement is provided in Table 22 in section 5.3.4.

5.3 Results and Discussion

5.3.1 Reaction of the Ligand Radical Complex $[Ni^{II}(L1^{\bullet-})Cl]$ with Dioxygen

Complex **8** is stable in toluene, but reacted with O_2. The reaction of $[Ni^{II}(L1^{\bullet-})Cl]$, **8**, in toluene with O_2 at 60 °C was monitored by UV-Vis spectroscopy. UV-Vis spectra and the time course of the reaction are shown in Figures 11 and 12. The absorption bands characteristic of $[Ni^{II}(L1^{\bullet-})Cl]$ at 465, 505, 730, and 820 nm disappeared, with concomitant formation of new bands at 400, 480, and 515 nm. Isosbestic points were observed at 375 and 430 nm, suggesting the formation of a new species. The half-life of the reaction was 1850 s, and was determined from the time course of the decay of the 820 nm peak.

Scheme 20. Reaction of **8** with O_2.

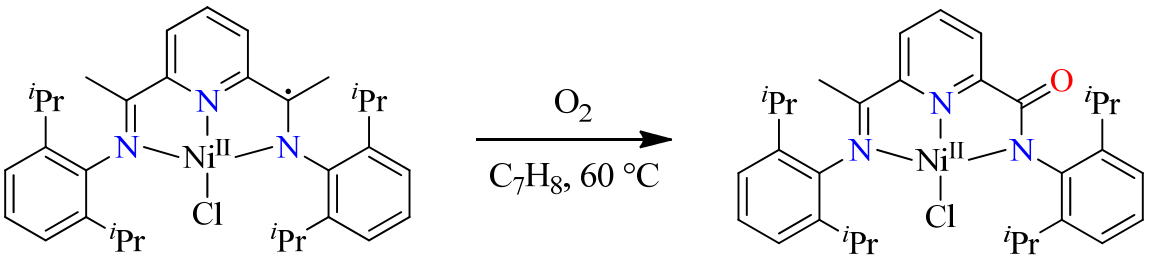

The product of the reaction, **12**, was first characterized by ESIMS, and peaks were found at m/z = 540 with an isotope distribution pattern consistent with the presence of Ni, and m/z = 576 with an isotope distribution pattern consistent with the presence of Ni and

Cl. Peaks are assigned to $\{\mathbf{12} - Cl\}^+$ and $\{\mathbf{12} + H\}^+$, respectively. The *m*/*z* values indicate that the ligand gained a mass unit, which is explained by the loss of a methyl group and the introduction of an oxygen atom. The reaction of O_2 with **8** was also done on a preparative scale, and the product was isolated. Single crystals were obtained from a nitromethane solution at -25 °C (Section 5.3.4). The product, **12**, is $[Ni^{II}(L1^{ox})Cl]$ which is the result of conversion of an acetimino group into a carboxamidato group (Scheme 20). High-resolution ESI MS of isolated **12** is shown in Figure 13. The EPR signal of **8** disappeared, indicating loss of the ligand radical in the product complex.

The fate of the acetimino methyl group was explored by running the O_2 reaction in a deuterated solvent, C_6D_6, suitable for NMR spectroscopy and by GCMS analysis of the headspace of the sealed reaction vessel immediately following the O_2 reaction. As there is a methyl group unaccounted for after the reaction and an excess of O_2 was used, likely products could include methanol, formaldehyde or formic acid. The combination of two methyl groups to form ethane should also be considered. However, the ^1H NMR spectrum of the reaction solution following the O_2 reaction did not show any of the expected product outcomes for the acetimino methyl group, and GCMS analysis of the atmosphere above the reaction mixture also did not show any of these expected outcomes.

The product, $[Ni^{II}(L1^{ox})Cl]$, **12**, was characterized by infrared spectroscopy (Figure 14). The feature of note is the strong band at 1635 cm^{-1}, which is characteristic of an amidato CO stretching vibration (ν_{CO}). The CN stretching vibration should be present in the spectrum as one imine group is still present in the complex. The CN stretching vibration was observed at 1621 cm^{-1} for $[Ni^{II}(L1)Cl_2]\cdot 0.5H_2O$, and at 1629 cm^{-1} for

[$Ni^{II}(L1^{\bullet-})Cl$], but is not observed in this spectrum, as it is presumably hidden by the CO stretching vibration.

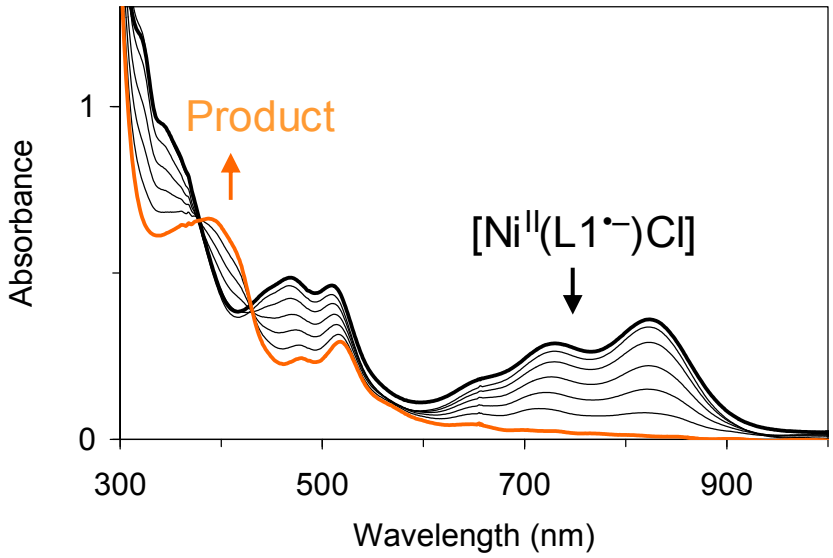

Figure 11. Reaction of 1 mM [$Ni^{II}(L1^{\bullet-})Cl$] (—, black) in toluene with dioxygen at 60 °C, as monitored by electronic absorption spectroscopy (path length, 0.5 cm).

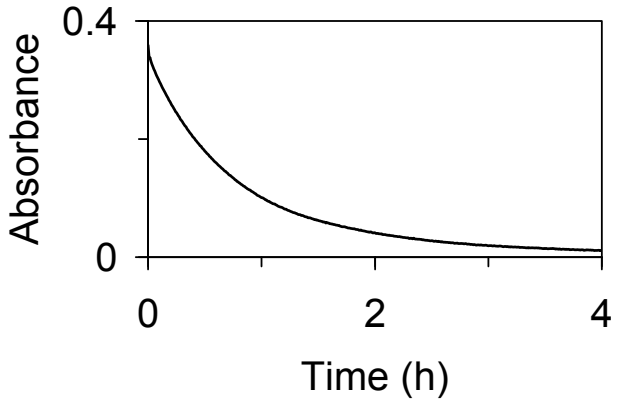

Figure 12. Time course of the decay of 1 mM [$Ni^{II}(L1^{\bullet-})Cl$] in toluene at 60 °C after dioxygen addition (λ = 820 nm (—, black), as monitored by electronic absorption spectroscopy (path length = 0.5 cm).

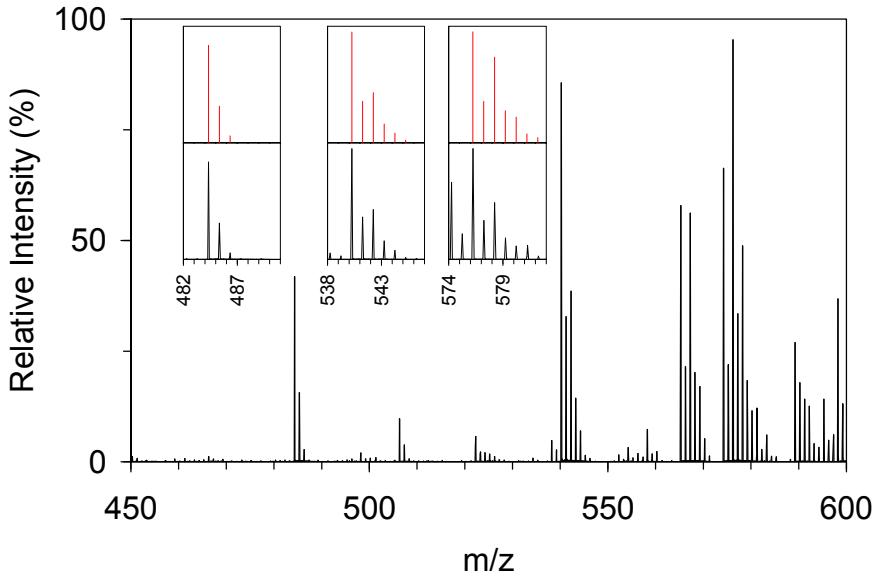

Figure 13. High-resolution electrospray ionization mass spectrum of [Ni{6-(2,6-^{i}Pr$_2$C$_6$H$_3$N=CMe)C$_5$H$_3$N-2-C(O)N(2,6-^{i}Pr$_2$C$_6$H$_3$)}Cl], **12**, in nitromethane. Insets: Expanded views of the features attributed to {**12** + H}$^+$, {**12** – Cl}$^+$ and {**12** – Ni – Cl + 2H}$^+$ (bottom, —, black) and their calculated isotope distribution patterns (top, —, red).

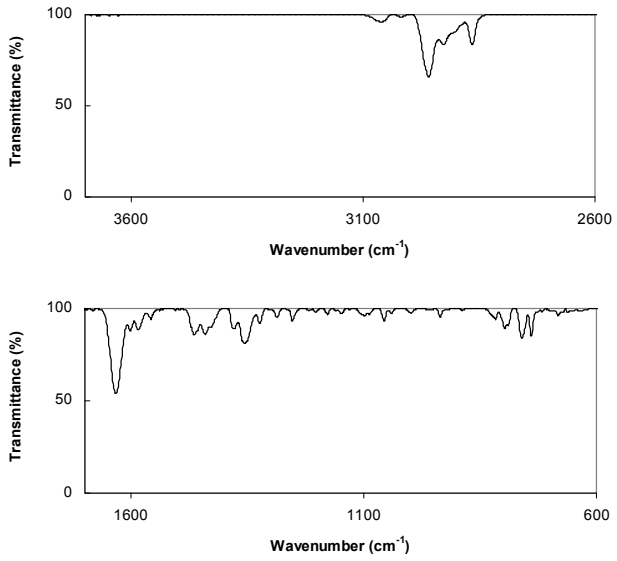

Figure 14. IR spectrum of [Ni(L1^{ox})Cl] (—, black) showing the ranges of 2600–3700 cm^{-1} and 600–1700 cm^{-1}.

Scheme 21. Extraction of $HL1^{ox}$.

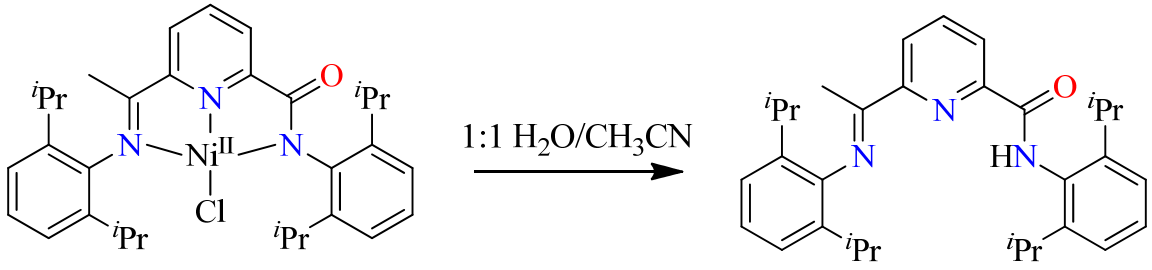

Table 20. ^{1}H NMR Assignments of $HL1^{ox}$.

δ (ppm)	Integration, multiplicity	Assignment
9.44	1H, s	N*H*
8.58	1H, d	Py H
8.4	1H, d	Py H
8.04	1H, t	Py H
7.35-7.07	6H	Ar H
3.15	2H, sept	Ar C*H*(CH_3), *N*-arylcarboxamide
2.73	2H, sept	Ar C*H*(CH_3), *N*-arylimine
2.23	3H, s	N=CC*H*$_3$
1.23	12H, d	Ar CH(C*H*$_3$), *N*-arylcarboxamide
1.15	12H, d	Ar CH(C*H*$_3$), *N*-arylimine

For further analysis the ligand, $HL1^{ox}$, was extracted by 1:1 CH_3CN/H_2O in nearly quantitative yield (Scheme 21). A white precipitated formed, and $HL1^{ox}$ was isolated in the form of a colorless solid. $HL1^{ox}$ was characterized by ^{1}H NMR spectroscopy, the results of which are summarized in Table 20. The ^{1}H NMR spectrum of **16** exhibits the expected resonance signals of an asymmetrically disubstituted pyridine ring and of two sets of isopropyl substituents. The presence of only one acetimino group is evidenced by the intensity ratio of the peaks arising from the N=CC*H*$_3$ and ArCH(C*H*$_3$)$_2$ protons of

1:4:4. $HL1^{ox}$ was characterized by high-resolution electron impact mass spectrometry, and *m*/*z* of 483.3257 for $M^{+\bullet}$ was found, consistent with the theoretical value of 483.3250, for the loss of a methyl group and addition of an oxygen atom on the ligand.

5.3.2 Reaction of the Deuterium-Labeled Ligand Radical Complex $[Ni^{II}(L2^{\bullet-})Cl]$ with Dioxygen

The reaction of $[Ni^{II}(L2^{\bullet-})Cl]$, **9**, in toluene with O_2 at 60 °C was monitored by UV-Vis spectroscopy. UV-Vis spectra and the time course of the reaction are shown in Figures 15 and 16. The absorption bands characteristic of $[Ni^{II}(L2^{\bullet-})Cl]$ at 465, 505, 730, and 825 nm disappeared, with concomitant formation of new bands at 400, 480, and 520 nm. Isosbestic points were observed at 380 and 430 nm. The half-life of the reaction was determined from the time course of the decay of the 825 nm peak. The half-life, as compared to the reaction of $[Ni^{II}(L1^{\bullet-})Cl]$ with O_2, is similar (2000 s compared to 1850 s for the reaction involving $[Ni^{II}(L1^{\bullet-})Cl]$), as is the overall course of the reaction.

The product of the reaction, **12**, was characterized by ESIMS, and a peak was found at *m*/*z* = 579, $\{\mathbf{13} + H\}^+$, with a complicated isotope distribution pattern due to the presence of d_0, d_1 and d_2 labeled species since the complex is not 100% deuterium labeled. The *m*/*z* value indicates that the ligand has gained a mass unit, similar to what was observed for **12**. The reaction of O_2 with **9** was also done on a preparative scale, and the product was isolated. Single crystals were obtained from a nitromethane solution at -25 °C (Section 5.3.4).

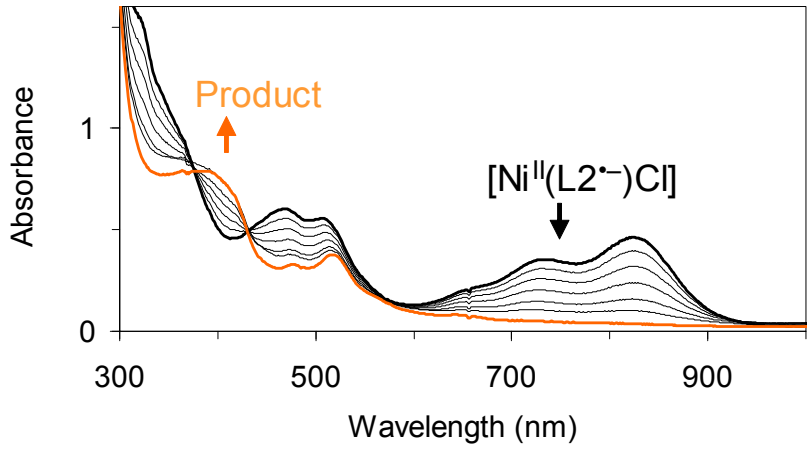

Figure 15. Reaction of 1 mM [$Ni^{II}(L2^{\bullet-})Cl$] (—, black) in toluene with dioxygen at 60 °C, as monitored by electronic absorption spectroscopy (path length, 0.5 cm).

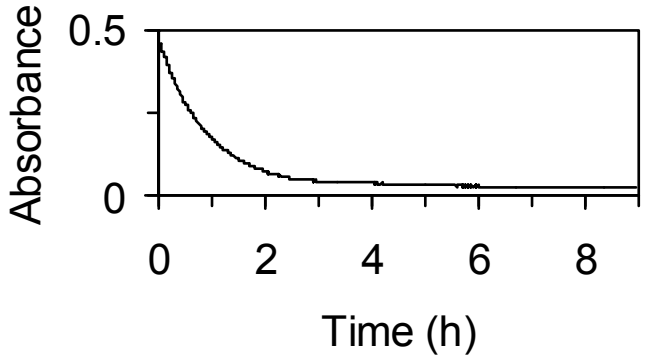

Figure 16. Time course of the decay of 1 mM [$Ni^{II}(L2^{\bullet-})Cl$] in toluene at 60 °C after dioxygen addition (λ = 825 nm (—, black), as monitored by electronic absorption spectroscopy (path length = 0.5 cm).

The product, [$Ni^{II}(L2^{ox})Cl$], **13**, was characterized by infrared spectroscopy (Figure 17). The feature of note is the strong band at 1634 cm^{-1}, which is characteristic of an amidato CO stretching vibration (ν_{CO}). This band is similar the band observed for complex **12**. The CN stretching vibration should be present in the spectrum as one imine

group is still present in the complex. The CN stretching vibration was observed at 1616 cm^{-1} for $[Ni(L2)Cl_2]\cdot 0.5H_2O$, and at 1624 cm^{-1} for $[Ni^{II}(L2^{\bullet-})Cl]$, but is not observed in this spectrum, as it is presumably hidden by the CO stretching vibration.

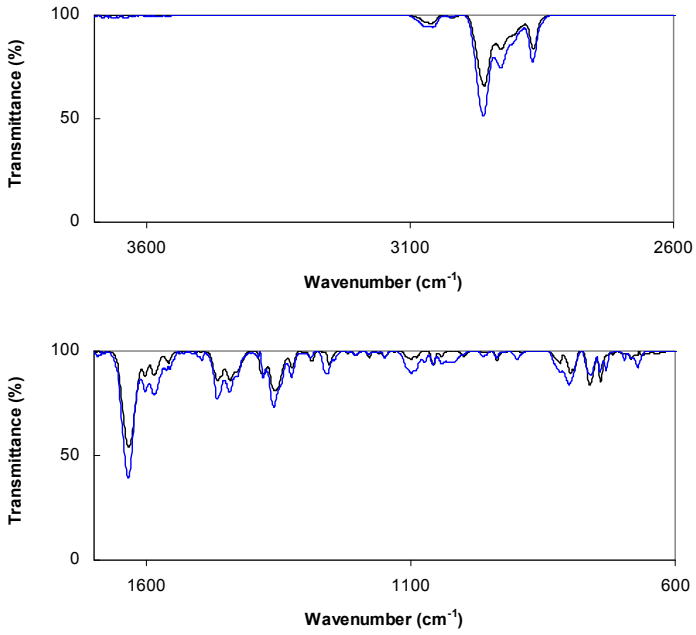

Figure 17. IR spectra of $[Ni(L1^{ox})Cl]$ (—, black) and $[Ni(L2^{ox})Cl]$ (—, blue) showing the ranges of 2600-3700 cm^{-1} (top) and 600-1700 cm^{-1} (bottom).

For further analysis the ligand, $HL2^{ox}$, was extracted by 1:1 CH_3CN/D_2O. A white precipitated formed, and $HL2^{ox}$ was isolated in the form of a colorless solid. $HL2^{ox}$ was characterized electron impact mass spectrometry, and *m*/*z* of 487.7 for $M^{+\bullet}$ was found, consistent with the theoretical value of 487.4. This peak is consistent with the loss of a methyl group and addition of an oxygen atom on the ligand along with deuterium labeling of the remaining acetimino group and of the NH group of the carboxamide. The second most abundant peak in this envelope was at *m*/*z* = 484.7 (35% rel. abundance).

$HL2^{ox}$ was characterized by ^1H NMR spectroscopy. The ^1H NMR spectrum of **17** exhibits the expected resonance signals of an asymmetrically disubstituted pyridine ring and of two sets of isopropyl substituents, which was also observed in Section 5.3.1. Residual peaks for the remaining N=CCH_3 group and the NH group were observed as the deuterium labeling of the complex is not 100%.

5.3.3 Reactions of the Substituted Ligand Radical Complexes $[Ni^{II}(L3^{\bullet-})Cl]$ and $[Ni^{II}(L4^{\bullet-})Cl]$ with Dioxygen

The reactions of $[Ni^{II}(L3^{\bullet-})Cl]$ (**10**) and $[Ni^{II}(L4^{\bullet-})Cl]$ (**11**) in toluene with O_2 at 60 °C were monitored by UV-Vis spectroscopy. UV-Vis spectra and time courses of the reactions are shown in Figures 18-21. For **10**, the absorption bands characteristic of $[Ni^{II}(L3^{\bullet-})Cl]$ at 465, 505, 705, and 815 nm disappeared, with concomitant formation of new bands at 400, 480, and 520 nm. Isosbestic points were observed at 380 and 430 nm. For **11**, the absorption bands characteristic of $[Ni^{II}(L4^{\bullet-})Cl]$ at 465, 505, 725, and 815 nm disappeared, with concomitant formation of new bands at 400, 480, and 520 nm. Isosbestic points were observed at 380 and 430 nm. The half-lives of the reactions were determined by monitoring the time courses of the decay of the 815 nm peak. The half-lives of the reactions are 4100 s for **10** and 2850 s for **11**. Compared to the reaction of $[Ni^{II}(L1^{\bullet-})Cl]$ with O_2 the half-lives of the reactions of $[Ni^{II}(L3^{\bullet-})Cl]$ and $[Ni^{II}(L4^{\bullet-})Cl]$ are longer, but the overall course of the reaction is similar. The half-life for the reaction involving $[Ni^{II}(L4^{\bullet-})Cl]$ is shorter than that for the reaction involving $[Ni^{II}(L3^{\bullet-})Cl]$,

indicating that the substitution of Br on the ligand does not have as much of an effect on the rate of the reaction as substitution of Cl on the ligand.

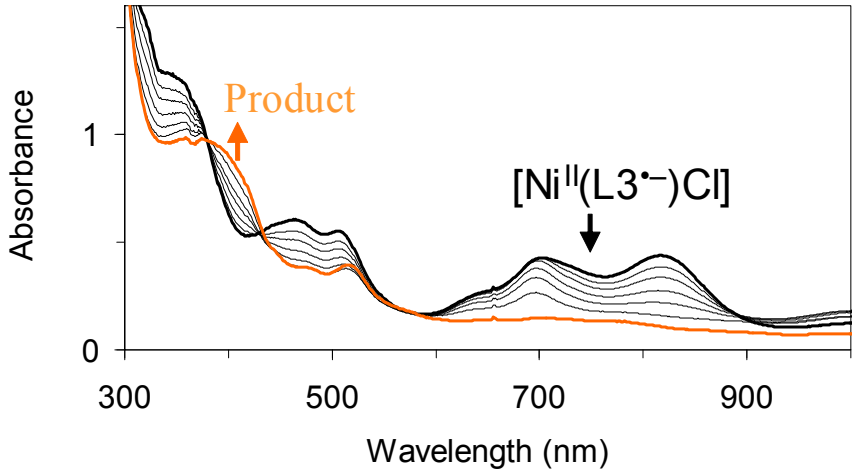

Figure 18. Reaction of 1 mM [Ni^{II}(L3$^{\bullet-}$)Cl] (—, black) in toluene with dioxygen at 60 °C, as monitored by electronic absorption spectroscopy (path length, 0.5 cm).

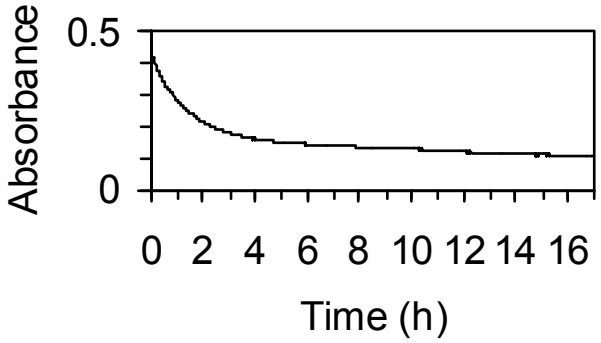

Figure 19. Time course of the decay of 1 mM [Ni^{II}(L3$^{\bullet-}$)Cl] in toluene at 60 °C after dioxygen addition (λ = 815 nm (—, black), as monitored by electronic absorption spectroscopy (path length = 0.5 cm).

The products of the reactions were characterized by ESI MS, and peaks were found at m/z = 644, {**14** + H}$^+$, and at m/z = 732, {**15** + H}$^+$. The isotope distribution pattern for {**14** + H}$^+$ is consistent with the presence of a Ni and three Cl atoms. The isotope distribution pattern for {**15** + H}$^+$ is consistent with the presence of a Ni, a Cl, and two Br atoms. The m/z values in both cases are consistent with loss of a methyl group and the incorporation of an oxygen atom to the ligand.

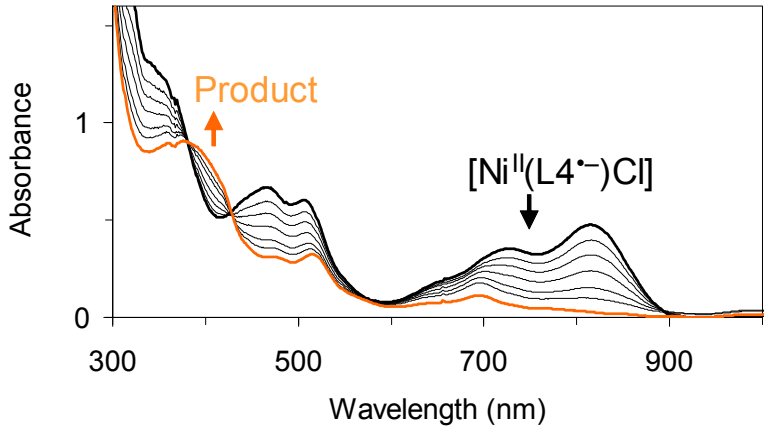

Figure 20. Reaction of 1 mM [Ni^{II}(L4$^{\bullet-}$)Cl] (—, black) in toluene with dioxygen at 60 °C, as monitored by electronic absorption spectroscopy (path length, 0.5 cm).

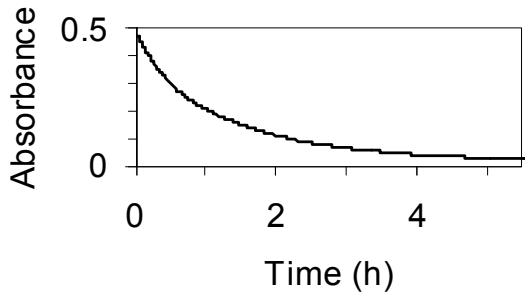

Figure 21. Time course of the decay of 1 mM [Ni^{II}(L4$^{\bullet-}$)Cl] in toluene at 60 °C after dioxygen addition (λ = 815 nm (—, black), as monitored by electronic absorption spectroscopy (path length = 0.5 cm).

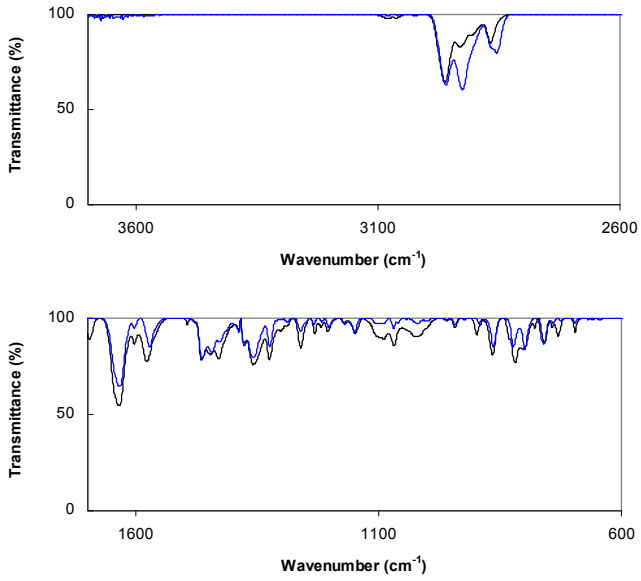

Figure 22. IR spectra of [Ni(L3^{ox})Cl] (—, black) and [Ni(L4^{ox})Cl] (—, blue) showing the ranges of 2600-3700 cm^{-1} and 600-1700 cm^{-1}.

The products [Ni^{II}(L3^{ox})Cl] (**14**) and [Ni^{II}(L3^{ox})Cl] (**15**) were characterized by infrared spectroscopy (Figure 22). The feature of note is the strong band at 1636 cm^{-1} for [Ni^{II}(L3^{ox})Cl] and 1635 cm^{-1} for [Ni^{II}(L4^{ox})Cl], which is characteristic of an amidato CO stretching vibration. The CN stretching vibration should be present in the spectra as an imine group is still present in each complex. The CN stretching vibration was observed at 1625 cm^{-1} for [Ni(L3)Cl$_2$] and at 1631 cm^{-1} for [Ni(L4)Cl$_2$] but is not observed in these spectra, as it is presumably hidden by the CO stretching vibration.

For further analysis the ligands, HL3^{ox} and HL4^{ox}, were extracted by 1:1 CH$_3$CN/H$_2$O. HL3^{ox} and HL4^{ox} were isolated and characterized by high-resolution electron impact mass spectrometry. For HL3^{ox}, *m*/*z* of 551.2448 for M$^{+\bullet}$ was found, consistent with the theoretical value of 551.2470, for the loss of a methyl group and

addition of an oxygen atom on the ligand. For HL4^{ox}, *m*/*z* of 639.1438 for $M^{+\bullet}$ was found, consistent with the theoretical value of 639.1460, for the loss of a methyl group and addition of an oxygen atom on the ligand. HL3^{ox} was characterized by ^{1}H NMR spectroscopy. The ^{1}H NMR spectrum of **18** exhibits the expected resonance signals of an asymmetrically disubstituted pyridine ring and of two sets of isopropyl substituents. The presence of only one acetimino group is evidenced by the intensity ratio of the peaks arising from the N=CC*H*$_3$ and ArCH(C*H*$_3$)$_2$ protons of 1:4:4.

5.3.4 Crystal Structures of the Product Complexes

Crystals of [Ni(L1^{ox})Cl]·2CH_3NO_2, **12**·2CH_3NO_2 (orange prisms) and [Ni(L2^{ox})Cl]·2CH_3NO_2, **13**·2CH_3NO_2 (red orange prisms) were grown from concentrated nitromethane solutions upon standing at –25 °C. As expected, there is high agreement in the unit cell constants of the two structures, with differences only in the second decimal places. The cell volume differs by 0.1%. The molecular structures of the complexes are nearly identical, with only minor differences in bond lengths and angles (Tables 23-25). This is to be expected as the only difference is a deuterium label on the remaining methyl group, which should have negligible, if any, influences on the structural parameters. Selected bond lengths and angles for [Ni(L1^{ox})Cl]·2CH_3NO_2 and [Ni(L2^{ox})Cl]·2CH_3NO_2 are presented in Tables 23-25, and the molecular structures are presented in Figures 23 and 24. The coordination geometry in both complexes is best described as distorted square planar, with angles distorted from the ideal 90 °C around Ni (Table 24). Similar to the reduced complexes, the Ni atom lies in the N1–N2–N3 plane in

both [Ni(L1^{ox})Cl]·2CH_3NO_2 and [Ni(L2^{ox})Cl]·2CH_3NO_2. Importantly, the structure determinations show that one of the two acetimino groups of the tridentate ligand was transformed into an amidato group. The refinement of the structures was attempted with C, N, and O atoms in the terminal position of the bond. The thermal parameters and *R* values best matched an O atom, and the distance is consistent with a C=O double bond.

In [Ni(L1^{ox})Cl]·2CH_3NO_2 the Ni–N1 (pyridine) bond length of 1.8218(15) Å is shorter than the Ni–N2 (imine) and Ni–N3 (amidate) bond lengths of 1.9187(15) Å and 1.8923(15) Å. These distances are all shorter than found for the corresponding reduced complex [Ni(L1$^{\bullet-}$)Cl]·2C_7H_8, as it now contains an anionic amidato donor in place of an imino donor group. The Ni–Cl distance is 2.1439(6) Å. On the ligand, the first set of notable bond lengths include N2–C6 (1.297(2) Å) and N3–C8 (1.348(2) Å). N2–C6 has a distance consistent with an imino double bond, while N3–C8 has lengthened due to the conversion into an amidato group. The next set of bond lengths of interest are the bonds adjacent to the pyridine ring, C1–C6 (1.472(3) Å) and C5–C8 (1.506(3) Å), which have lengthened compared to the reduced complex, indicating loss of the ligand radical anion. The bond length of the remaining acetimino methyl group, C6–C7, is 1.485(3) Å. The bond length on the other side of the molecule (C8–O1) was found to be 1.236(2) Å, consistent with a C=O double bond.

In [Ni(L2^{ox})Cl]·2CH_3NO_2 the Ni–N1 (pyridine) bond length of 1.8259(17) Å is shorter than the Ni–N2 (imine) and Ni–N3 (amidate) bond lengths of 1.9201(18) Å and 1.8907(19) Å. Again, these distances are all shorter than found on the corresponding reduced complex [Ni(L2$^{\bullet-}$)Cl]·2C_7H_8. The Ni–Cl distance is 2.1411(7) Å. On the ligand, the first set of notable bond lengths include N2–C6 (1.300(3) Å) and N3–C8 (1.347(3) Å).

N2–C6 has a distance consistent with an imino double bond, while N3–C8 has lengthened due to the conversion to an amidato group. The next set of bond lengths of interest are the bonds adjacent to the pyridine ring, C1–C6 (1.466(3) Å) and C5–C8 (1.502(3) Å), which have lengthened indicating loss of the ligand radical anion. The bond length of the remaining acetimino methyl group, C6–C7, is 1.487(3) Å. The bond length of C8-O1 is 1.239(3) Å, consistent with the formation of a C=O double bond similar to $[Ni(L1^{ox})Cl]\cdot 2CH_3NO_2$.

Table 21. Comparison of Key Distances (Å) for Complexes **1**, **8**, **9**, **12** and **13**.

	1	**8**	**9**	**12**	**13**
Ni–N1	1.978(2)	1.833(2)	1.840(2)	1.8218(15)	1.8259(17)
Ni–N2	2.166(2)	1.941(2)	1.9529(18)	1.9187(15)	1.9201(18)
Ni–N3	2.157(2)	1.943(2)	1.9455(18)	1.8923(15)	1.8907(19)
Ni–Cl	2.2338(8)	2.1688(8)	2.1766(7)	2.1439(6)	2.1411(7)
	2.2832(9)				
N2–C6	1.287(3)	1.318(4)	1.313(3)	1.297(2)	1.300(3)
N3–C8	1.289(3)	1.324(4)	1.323(3)	1.348(2)	1.347(3)
C1–C6	1.493(4)	1.451(4)	1.445(3)	1.472(3)	1.466(3)
C5–C8	1.486(4)	1.446(4)	1.442(3)	1.506(3)	1.502(3)
C6–C7	1.495(4)	1.468(4)	1.494(3)	1.485(3)	1.487(3)
C8–C9	1.498(4)	1.482(4)	1.484(3)		
C8–O1				1.236(2)	1.239(3)

Table 21 highlights the differences in key distances between $[Ni(L1)Cl_2]\cdot 0.5H_2O$ (**1**), $[Ni(L1^{\bullet-})Cl]\cdot 2C_7H_8$ (**8**), $[Ni(L2^{\bullet-})Cl]\cdot 2C_7H_8$ (**9**), $[Ni(L1^{ox})Cl]\cdot 2CH_3NO_2$ (**12**) and $[Ni(L2^{ox})Cl]\cdot 2CH_3NO_2$ (**13**). The Ni–N distances are shorter in **12** and **13** compared to **1** due to the anionic nature of the ligand. The C1–C6 and C5–C8 distances in **12** and **13** are

similar to those in **1** and are longer than those in **8** and **9**, consistent with the absence of a ligand radical in **12** and **13**. In **12** and **13**, the N2–C6 distance has returned to a length consistent with the imine double bond seen in **1**, while the N3–C8 distance has further lengthened which indicates more single bond character. The C8–O1 distances in **12** and **13** are significantly shorter compared to the C8–C9 distances in **1**, **8** and **9**, which is consistent with the formation of a C=O on the ligand.

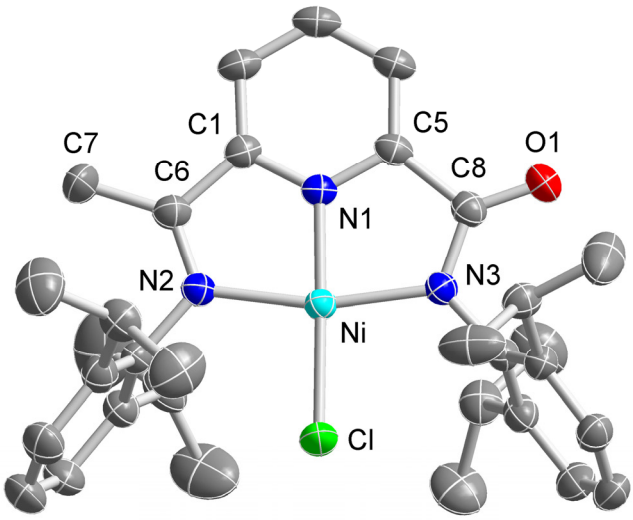

Figure 23. Molecular structure of [Ni{6-(2,6-$^{i}Pr_2C_6H_3N{=}CCH_3$)C_5H_3N-2- C(O)N(2,6-$^{i}Pr_2C_6H_3$)}Cl]·$2CH_3NO_2$, **12**·$2CH_3NO_2$. Displacement ellipsoids are drawn at the 50% probability level. Hydrogen atoms and the solvent toluene molecules have been omitted for clarity. Color key: turquoise = Ni, blue = N, green = Cl, gray = C, red = O.

Table 22. Crystallographic data and structure refinement for [Ni{6-(2,6-$^{i}Pr_2C_6H_3N{=}CCH_3$)C_5H_3N-2-C(O)N(2,6-$^{i}Pr_2C_6H_3$)}Cl]·$2CH_3NO_2$, **12**·$2CH_3NO_2$, and [Ni{6-(2,6-$^{i}Pr_2C_6H_3N{=}CCD_3$)C_5H_3N-2-C(O)N(2,6-$^{i}Pr_2C_6H_3$)}Cl]·$2CH_3NO_2$, **13**·$2CH_3NO_2$.

	12·$2CH_3NO_2$	**13**·$2CH_3NO_2$
Empirical formula	$C_{34}H_{46}ClN_5NiO_5$	$C_{34}H_{43}ClD_3N_5NiO_5$
Formula weight	698.92	701.94
Crystal habit, color	prism, orange	prism, red orange
Crystal size	0.36 x 0.28 x 0.22 mm^3	0.22 x 0.14 x 0.13 mm^3
Temperature, T	190(2) K	190(2) K
Wavelength, λ	0.71073 Å	0.71073 Å
Crystal system	monoclinic	monoclinic
Space group	$P2_1/c$	$P2_1/c$
Unit cell dimensions	a = 14.1976(15) Å b = 15.7496(17) Å c = 16.8785(18) Å β = 107.454(5)°	a = 14.1917(14) Å b = 15.7360(16) Å c = 16.8596(17) Å β = 107.209(5)°
Volume, V	3600.4(7) $Å^3$	3596.5(6) $Å^3$
Z	4	4
Calculated density	1.289 $Mg·m^{-3}$	1.296 $Mg·m^{-3}$
Absorption coefficient, μ	0.659 mm^{-1}	0.659 mm^{-1}
F(000)	1480	1480
θ range for data collection	2.84 to 27.91°	2.84 to 28.37°
Limiting indices	$-18 \le h \le 18$, $-20 \le k \le 20$, $-22 \le l \le 22$	$-18 \le h \le 18$, $-21 \le k \le 20$, $-22 \le l \le 22$
Reflections collected / unique	29201 / 8549 [R(int) = 0.0386]	70679 / 8985 [R(int) = 0.0664]
Completeness to θ	99.4 % (θ = 27.91°)	99.8 % (θ = 28.37°)
Max. and min. transmission	0.8686 and 0.7974	0.9192 and 0.8685
Refinement method	Full-matrix least-squares on F^2	Full-matrix least-squares on F^2
Data / restraints / parameters	8549 / 0 / 426	8985 / 0 / 426
Goodness-of-fit on F^2	1.028	1.005
Final R indices [I>2sigma(I)]	$R1$ = 0.0403, $wR2$ = 0.0904	$R1$ = 0.0463, $wR2$ = 0.0989
R indices (all data)	$R1$ = 0.0637, $wR2$ = 0.1029	$R1$ = 0.0911, $wR2$ = 0.1160
Largest diff. peak and hole	0.343 and –0.411 $e·Å^{-3}$	0.511 and –0.486 $e·Å^{-3}$

Table 23. Selected interatomic distances (Å) for [Ni{6-(2,6-^{i}Pr$_2$C$_6$H$_3$N=CCH$_3$)C$_5$H$_3$N-2-C(O)N(2,6-^{i}Pr$_2$C$_6$H$_3$)}Cl]·2CH$_3$NO$_2$, **12**·2CH$_3$NO$_2$, and [Ni{6-(2,6-^{i}Pr$_2$C$_6$H$_3$N=CCD$_3$)C$_5$H$_3$N-2-C(O)N(2,6-^{i}Pr$_2$C$_6$H$_3$)}Cl]·2CH$_3$NO$_2$, **13**·2CH$_3$NO$_2$.[a]

12·2CH$_3$NO$_2$		**13**·2CH$_3$NO$_2$	
Ni–N1	1.8218(15)	Ni–N1	1.8259(17)
Ni–N2	1.9187(15)	Ni–N2	1.9201(18)
Ni–N3	1.8923(15)	Ni–N3	1.8907(19)
Ni–Cl	2.1439(6)	Ni–Cl	2.1411(7)
N1–C1	1.345(2)	N1–C1	1.344(3)
N1–C5	1.331(2)	N1–C5	1.326(3)
N2–C6	1.297(2)	N2–C6	1.300(3)
N2–C9	1.442(2)	N2–C9	1.444(3)
N3–C8	1.348(2)	N3–C8	1.347(3)
N3–C21	1.434(2)	N3–C21	1.438(3)
C1–C6	1.472(3)	C1–C6	1.466(3)
C5–C8	1.506(3)	C5–C8	1.502(3)
C6–C7	1.485(3)	C6–C7	1.487(3)
C8–O1	1.236(2)	C8–O1	1.239(3)

[a] Numbers in parentheses are standard uncertainties in the last significant figures. Atoms are labeled as indicated in Figures 20 and 21.

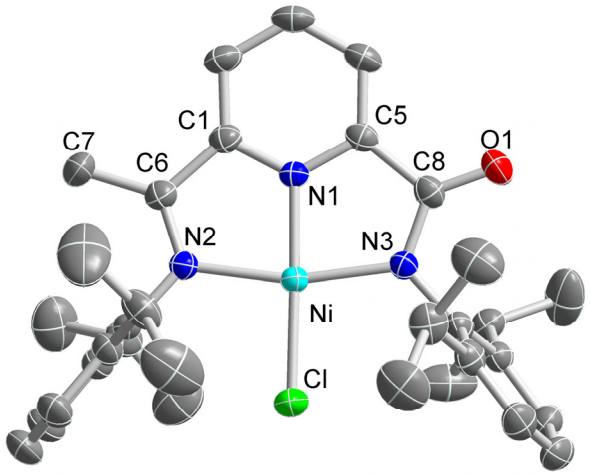

Figure 24. Molecular structure of [Ni{6-(2,6-^{i}Pr$_2$C$_6$H$_3$N=CCD$_3$)C$_5$H$_3$N-2- C(O)N(2,6-^{i}Pr$_2$C$_6$H$_3$)}Cl]·2CH$_3$NO$_2$, **13**·2CH$_3$NO$_2$. Displacement ellipsoids are drawn at the 50% probability level. Hydrogen atoms and the solvent toluene molecules have been omitted for clarity. Color key: turquoise = Ni, blue = N, green = Cl, gray = C, red = O.

Table 24. Selected angles (°) for [Ni{6-(2,6-$^{i}Pr_2C_6H_3N{=}CCH_3$)C_5H_3N-2-C(O)N(2,6-$^{i}Pr_2C_6H_3$)}Cl]·$2CH_3NO_2$, **12**·$2CH_3NO_2$, and [Ni{6-(2,6-$^{i}Pr_2C_6H_3N{=}CCD_3$)C_5H_3N-2-C(O)N(2,6-$^{i}Pr_2C_6H_3$)}Cl]·$2CH_3NO_2$, **13**·$2CH_3NO_2$.[a]

12·$2CH_3NO_2$		**13**·$2CH_3NO_2$	
N1–Ni–N2	82.10(6)	N1–Ni–N2	82.09(8)
N1–Ni–N3	83.10(7)	N1–Ni–N3	83.01(8)
N2–Ni–Cl	96.47(5)	N2–Ni–Cl	96.50(6)
N3–Ni–Cl	98.32(5)	N3–Ni–Cl	98.39(6)
N1–Ni–Cl	178.41(5)	N1–Ni–Cl	178.42(6)
N3–Ni–N2	165.19(6)	N3–Ni–N2	165.09(8)
C5–N1–C1	122.77(16)	C5–N1–C1	123.00(19)
C1–N1–Ni	118.42(13)	C1–N1–Ni	118.28(15)
C5–N1–Ni	118.80(13)	C5–N1–Ni	118.71(15)
C6–N2–C9	119.95(16)	C6–N2–C9	120.32(19)
C6–N2–Ni	115.63(13)	C6–N2–Ni	115.41(16)
C9–N2–Ni	124.41(12)	C9–N2–Ni	124.26(14)
C8–N3–C21	119.03(16)	C8–N3–C21	118.99(19)
C8–N3–Ni	116.16(13)	C8–N3–Ni	116.10(15)
C21–N3–Ni	124.82(12)	C21–N3–Ni	124.91(14)
N1–C1–C2	119.86(18)	N1–C1–C2	119.8(2)
N1–C1–C6	110.69(16)	N1–C1–C6	110.88(19)
C2–C1–C6	129.42(18)	C2–C1–C6	129.3(2)
N1–C5–C4	119.92(18)	N1–C5–C4	119.7(2)
N1–C5–C8	111.41(16)	N1–C5–C8	111.55(19)
C4–C5–C8	128.65(18)	C4–C5–C8	128.7(2)
N2–C6–C1	113.10(17)	N2–C6–C1	113.3(2)
N2–C6–C7	125.83(18)	N2–C6–C7	125.6(2)
C1–C6–C7	121.07(17)	C1–C6–C7	121.1(2)
N3–C8–C5	110.51(16)	N3–C8–C5	110.6(2)
O1–C8–N3	128.32(18)	O1–C8–N3	128.2(2)
O1–C8–C5	121.16(17)	O1–C8–C5	121.1(2)

[a] Numbers in parentheses are standard uncertainties in the last significant figures. Atoms are labeled as indicated in Figures 20 and 21.

Table 25. Selected dihedral angles (°) for [Ni{6-(2,6-$^{i}Pr_2C_6H_3N$=CCH_3)C_5H_3N-2-C(O)N(2,6-$^{i}Pr_2C_6H_3$)}Cl]·$2CH_3NO_2$, **12**·$2CH_3NO_2$, and [Ni{6-(2,6-$^{i}Pr_2C_6H_3N$=CCD_3)C_5H_3N-2-C(O)N(2,6-$^{i}Pr_2C_6H_3$)}Cl]·$2CH_3NO_2$, **13**·$2CH_3NO_2$.[a]

12·$2CH_3NO_2$		**13**·$2CH_3NO_2$	
(N1,N2,N3) / (C9→C14)[b]	83.4(1)	(N1,N2,N3) / (C9→C14)[b]	83.14(9)
(N1,N2,N3) / (C21→C26)[b]	79.1(1)	(N1,N2,N3) / (C21→C26)[b]	79.05(8)
(C9→C14) / (C21→C26)[c]	78.4(1)	(C9→C14) / (C21→C26)[c]	78.51(8)

[a] Numbers in parentheses are standard uncertainties in the last significant figures. Atoms are labeled as indicated in Figures 20 and 21. [b] Angle between the plane of the ligand nitrogen atoms (N1, N2, and N3) and a least-squares plane of aryl ring atoms (*e.g.*, C10, C11, C12, C13, C14, and C15). [c] Angle between the least-squares planes of the aryl ring atoms.

5.3.5 Reaction of a Ligand Radical Anion Complex of Cobalt(II) with Dioxygen

In order to test the effect of the metal center on the reactivity with O_2, a ligand radical anion complex of L1 was prepared with Co, [$Co^{II}(L1^{\bullet-})$Cl], **21**, using the methods from Chapters 3 and 4. This complex has been described extensively by the literature.[32, 58-60] The reaction of [$Co^{II}(L1^{\bullet-})$Cl] in toluene with O_2 at 60 °C was monitored by UV-Vis spectroscopy. The characteristic bands in the UV-Vis spectrum of **21** disappeared rapidly. A very different product was observed with ESI MS as compared to the product found in the reactions of O_2 with the radical anion complexes of Ni. Peaks were found at m/z = 575 and 482. The 575 peak corresponds to a positively charged ion of the metal complex, $[Co^{II}(L1)Cl]^{+}$, and suggests that a one electron oxidation has occurred over the course of the reaction. The 482 peak corresponds to the protonated form of the unmodified ligand, $\{L1 + H\}^{+}$. Thus no cleavage of a C–C bond occurred on the ligand.

Scheme 22. Comparison of the Reactivity of Ligand Radical Anion Complexes of Co^{II} and Ni^{II} with O_2.

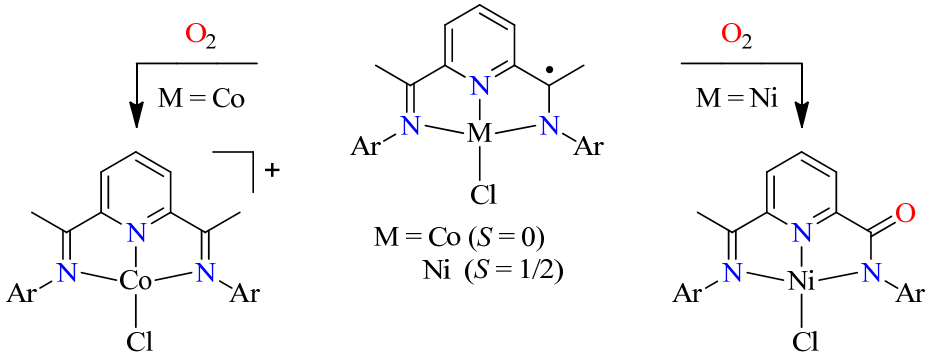

The different outcomes of the reactions of complexes **8** and **21** (Scheme 22) with O_2 imply that the metal center must have an influence on the course of the reaction, even though the added electron is mainly located on the ligand and the C–C bond cleavage observed in the reactivity of Ni complex **8** occurs adjacent to the ligand radical. There are some key differences between the complexes. These differences are the spin state of the complexes (S = 0 for the Co complex, S = 1/2 for the Ni complex), the O_2 affinity of the metal center in each complex, and presumably the degree of ligand radical character in each complex. Each of these factors may play an important role in the reaction with O_2 and may account for the vastly different outcome of the reaction of the two complexes **8** and **21**.

5.3.6 Comparison of the Reactivity Data and Mechanistic Implications

The previous sections of Chapter 5 have been focused on the course of the O_2 reactions of bis(arylimino)pyridine radical anion complexes of Ni^{II} and the identity of the

products of these reactions. Elucidating the mechanism of the reaction would also be useful in order to further our understanding of dioxygen activation with these complexes, and is the focus of this section. The first set of data to look at is the kinetic data in order to see if the substitution of the ligand had any effect on the reaction. It is clear from sections 5.3.1 through 5.3.3 that substitution with either Cl or Br in the aniline groups or with D in the methyl group that is cleaved in the reaction had no effect on the overall outcome of the reaction. However, substitution with the halogens did have an effect on the half-life of the reaction with dioxygen, which is summarized in Table 26. The half-lives of the reactions follow the trend R_1 = H < Br < Cl, which is a trend of increasing electronegativity of the substituent at R_1 on the ligand. As both these groups are electron withdrawing groups, it is possible that the effective radical character at the position of bond cleavage is reduced. Interestingly, the deuterium-labeled complex, [Ni^{II}(L2$^{\bullet-}$)Cl], did not have a significantly different half-life from [Ni^{II}(L1$^{\bullet-}$)Cl]. The presence of a large kinetic isotope effect would indicate that hydrogen atom abstraction is the rate-determining step of the mechanism.[61] Since a large kinetic isotope effect was not observed, hydrogen atom abstraction from the methyl group is ruled out as the rate-determining step of the mechanism of the reactions of these complexes with O_2.

Table 26. Summary of the Kinetic Data from the O_2 Reactions of Bis(arylimino)pyridine Radical Anion Complexes of Ni^{II}.

Reactant Complex	$t_{1/2}$ (s)	Range (s)
[Ni^{II}(L1$^{\bullet-}$)Cl] (**8**)	1850	1680–2040
[Ni^{II} (L2$^{\bullet-}$)Cl] (**9**)	2000	1770–2190
[Ni^{II} (L3$^{\bullet-}$)Cl] (**10**)	4100	3870–4470
[Ni^{II} (L4$^{\bullet-}$)Cl] (**11**)	2850	2520–3270

Scheme 23. Reaction of O_2 with **8** in the Presence of Oxidizable Substrates.

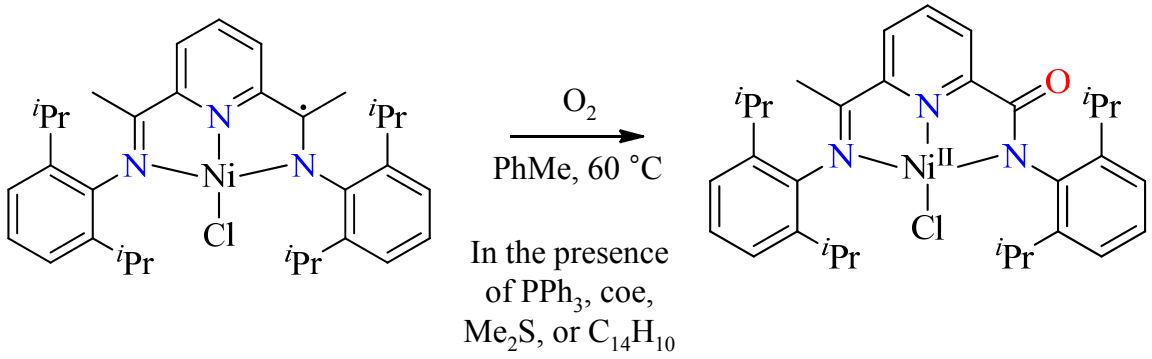

The C–C bond cleavage in the reaction of O_2 with complexes **8-11** differs from the chemistry of reactive Ni–O_x intermediates, which react with C–H bonds that are disposed in close proximity to the Ni center or oxidize external substrates.[62-66] No ligand C–H bond hydroxylation was observed as the methine C–H bonds in the complexes are nearby an open coordination site of the Ni center but remain unaltered in the reaction with O_2. It should be noted that no Ni–O_x intermediates were observed in any of these reactions. However, Ni–O_x intermediates that are too short lived to be observed could exist and have the potential to oxidize external substrates. The oxidation of external substrates was tested by running O_2 reactions with [Ni^{II}($L1^{\bullet-}$)Cl] in the presence of triphenylphosphine, *cis*-cyclooctene (coe), dimethyl sulfide, or dihydroanthracene. The presence of these substrates does not affect the oxidation of **8** to **12** and does not alter the course of the O_2 reaction as observed by UV-Vis spectroscopy (Scheme 23). Also, no oxidation of the external substrates was observed. Thus, on the basis of the lack of chemistry typical of Ni–O_x intermediates and given the ligand-radical character, it is likely that oxidation is initiated by direct attack of the O_2 diradical on an imino carbon atom that perhaps is assisted by coordination to the Ni center.

Scheme 24. Possible Initial Step for O_2 Activation.

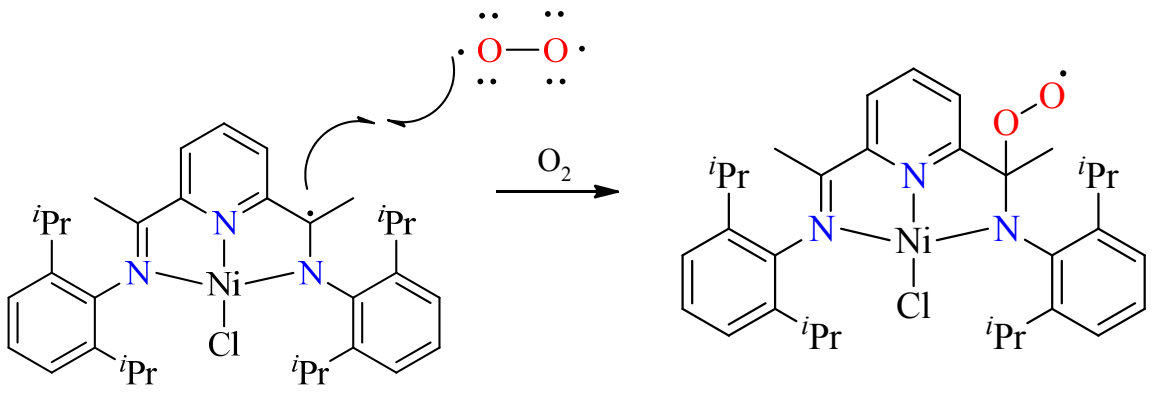

Scheme 24 represents a proposed initial step of a ligand centered mechanism. With formation of an [Ni(L–OO•)Cl] species, one could consider H atom abstraction from the acetiminio methyl group as a possible rate-determining step of the mechanism. However, a primary kinetic isotope effect was not observed, thus H atom abstraction as the rate-determining step is unlikely. Instead, the superoxo group may attack the carbon atom of the acetimino methyl group to initiate C–C bond cleavage. The exact mechanism by which these complexes are oxidized, including the fate of the CH_3 group and the second atom of O_2, is not known, and logical products resulting from the CH_3 group, such as methanol, formaldehyde, formic acid or possibly ethane, were never observed in the experiments discussed in Section 5.3.1. However, the ligand-centered oxygenation is a contrast to the previously observed small molecule activation with bis(arylimino)pyridine complexes presented in Chapter 2, which clearly showed reactivity that would be consistent with metal-centered activation.[9.15] This reactivity is not unprecedented,

however, as the vanadium-catalyzed catechol oxidation presented in Chapter 2 was proposed to entail attack of metal-bound catecholate by O_2.[36,37]

5.4 Conclusion

The reactions of O_2 with bis(arylimino)pyridine radical anion complexes of Ni^{II} was the focus of Chapter 5. The reactions of $[Ni^{II}(L1^{\bullet-})Cl]$, $[Ni^{II}(L2^{\bullet-})Cl]$, $[Ni^{II}(L3^{\bullet-})Cl]$, and $[Ni^{II}(L4^{\bullet-})Cl]$ with O_2 resulted in the formation of $[Ni^{II}(L1^{ox})Cl]$, $[Ni^{II}(L2^{ox})Cl]$, $[Ni^{II}(L3^{ox})Cl]$, and $[Ni^{II}(L4^{ox})Cl]$ (**12-15**) respectively. Complexes **12-15** were characterized by mass spectrometry and infrared spectroscopy. Complexes **12** and **13** were further characterized by single crystal X-ray diffraction. In all of the isolated products, the bis(arylimino)pyridine ligand had undergone a C–C bond cleavage and formed a new C=O double bond. This was confirmed by a strong band in the IR spectra of the complexes consistent with a CO stretching vibration and also by mass spectral data consistent with loss of a methyl group and addition of an O atom for each complex. The crystal structures of **12** and **13** also revealed a C8–O1 distance consistent with a C=O double bond.

Extraction of the ligands of $[Ni^{II}(L1^{ox})Cl]$, $[Ni^{II}(L2^{ox})Cl]$, $[Ni^{II}(L3^{ox})Cl]$, and $[Ni^{II}(L4^{ox})Cl]$ was conducted, resulting in the formation of $HL1^{ox}$, $HL2^{ox}$, $HL3^{ox}$, and $HL4^{ox}$ (**16-19**) respectively. EIMS of **16-19** confirmed the loss of a CH_3 group and addition of an O atom on each ligand. ^1H NMR spectroscopy of $HL1^{ox}$, $HL2^{ox}$, and $HL3^{ox}$ confirmed loss of symmetry on the ligand as well as the loss of a CH_3 group.

The reaction of the deuterium-labeled $[Ni^{II}(L2^{\bullet-})Cl]$ with O_2 did not show any changes with respect to the half-life of the reaction, the course of the reaction, or the

isolated reaction product. The reactions of [$Ni^{II}(L3^{\bullet-})Cl$] and [$Ni^{II}(L4^{\bullet-})Cl$] with O_2 also did not show any changes with respect to the course of the reaction or the isolated product; however, the half-life of the reaction did increase. The increase in half-life follows the trend $R_1 = H < Br < Cl$, which is a trend of increasing electronegativity of the substituent at R_1 on the ligand. An analogous reaction with a bis(arylimino)pyridine ligand radical complex of Co^{II} (**21**) with O_2 resulted in a one-electron oxidation of the complex and not C–C bond cleavage, suggesting that the metal center plays a role in the reactivity. No Ni–O_x intermediates were observed in the reactions of the Ni complexes with O_2, and no short lived intermediates are likely based on the lack of substrate oxidation when the O_2 reactions with [$Ni^{II}(L1^{\bullet-})Cl$] were run in the presence of oxidizable substrates. This suggests that the initial steps of the mechanism are ligand-centered. The lack of a primary kinetic isotope effect observed in the O_2 reaction with the deuterium-labeled complex [$Ni^{II}(L2^{\bullet-})Cl$] suggests that the rate-determining step of the mechanism does not include hydrogen abstraction from the acetimino methyl group. This suggests that oxidation of the complexes could be initiated by direct attack of O_2 on an imino carbon atom.

CHAPTER 6

SUMMARY AND CONCLUSION

The activation of dioxygen with bis(arylimino)pyridine complexes of nickel was studied in this project. A series of 4-substituted 2,6-diisopropylanilines were prepared along with 2,6-diacetylpyridine-d_6 for the purposes of synthesizing a variety of Ni^{II} complexes with substituted bis(arylimino)pyridine ligands. The synthesis of previously unreported nickel complexes **2-7** was achieved, and characterization by X-ray crystallography of three complexes confirmed coordination of the Ni center by the three nitrogen donor atoms of the bis(arylimino)pyridine ligand and two chloro ligands with a distorted square pyramidal geometry about the Ni center. These results were described in Chapter 3.

Complexes **8-11** were synthesized by reaction with a sodium amalgam. These complexes are best characterized as ligand radical anion complexes of Ni^{II} on the basis of X-ray crystallography of **8** and **9** and electron paramagnetic resonance spectroscopy of complex **8**. On the basis of electronic absorption spectroscopy, complexes **10** and **11** can also be assigned as ligand radical complexes as they give the same signature in the Vis-NIR region as complexes **8** and **9**. These results were described in Chapter 4.

The reactivity of dioxygen with complexes **8-11** was studied in Chapter 5. These reactions were studied by UV-Vis spectroscopy, and the overall course of the reaction was similar for all four complexes. The half-life of the reaction was not affected by deuterium labeling of the acetimino methyl group but was affected by different substituents in the 4-position of the phenyl groups on the ligand. Products from each

reaction were isolated as the new complexes **12-15**, and in each case cleavage of a C–C bond was observed along with formation of a C=O double bond on the bis(arylimino)pyridine ligand. The structures of **12** and **13** were determined by X-ray crystallography. For all four complexes, the amidato group was identified by a strong band in the infrared spectra assignable to a CO stretching vibration. Furthermore, the new carboxamidato ligands **16-19** were removed from the metal center and isolated in their neutral form. Taken together, these results indicate that the activation of dioxygen occurs at the ligand and without an overall oxidation state change at the Ni center. The observed ligand-centered oxygenation in these reactions contrasts with the prevailing metal-centered chemistry of redox-active bis(arylimino)pyridine complexes and demonstrates that they can be directly involved in the activation and conversion of a small molecule.

The reactivity with dioxygen described in this thesis led to ligand-centerd oxygenation products. A more useful form of dioxygen activation entails reactivity that could be used for the transformation of organic substrates. Pushing the reactivity of these complexes toward metal-centered activation as opposed to ligand-centered activation may help to achieve the goal of substrate oxidation. Will decreasing the steric protection of the metal center cause the reactivity with dioxygen to shift to the metal-center? To this end, reducing the steric bulk of the aniline groups would open up access to the metal center. Currently, the 2- and 6-positions on the aniline rings are occupied by isopropyl groups, substitution with less sterically bulky groups will lessen the protection of the metal center. Another method to potentially push the reactivity towards the metal-center entails substituting the strong chloro ligand of the complexes with a more substitutionally labile ligand. The electronic properties of the bis(arylimino)pyridine ligand could also be

altered further, although this approach is less likely to push the reactivity toward the metal-center as altering the electronic properties of the ligand by substitution in the 4-position of the aniline rings did not alter the reaction product. However, there are other positions on the ligand that can be readily substituted, for example, substitution of the 4-position on the pyridine ring would also have an effect on the electronic properties of the ligand.

REFERENCES

1. Hill, C. L.; Weinstock, I. A. *Nature* **1997**, *388*, 332.

2. Blackmore, L. J.; Sly, M. B.; Haneline, M. R.; Ziller, J. W.; Heyduk, A. F. *Inorg. Chem.* **2008**, *47*, 10522.

3. Nguyen, A. I.; Blackmore, K. J.; Carter, S. M.; Zarkesh, R. A.; Heyduk, A. F. *J. Am. Chem. Soc.* **2009**, *131*, 3307.

4. Ringenberg, M. R.; Kokatam, S. L.; Heiden, Z. M.; Rauchfuss, T. B. *J. Am. Chem. Soc.* **2008**, *130*, 788.

5. Gibson, V. C.; Redshaw, C.; Solan, G. A. *Chem. Rev.* **2007**, *107*, 1745.

6. Enright, D.; Gambarotta, S.; Yap, G. P. A.; Budzelaar, P. H. M. *Angew. Chem. Int. Ed.* **2002**, *41*, 3873.

7. Seih, D.; Schlimm, M.; Andernach, L.; Angersbach, F.; Nückel, S.; Schöffel, J.; Šušnjar, N.; Burger, P. *Eur. J. Inorg. Chem.* **2012**, 444.

8. Smit, T. M.; Tomov, A. K.; Britovsek, G. J. P.; Gibson, V. C.; White, A. J. P.; Williams, D. J. *Catal. Sci. Technol.* **2012**, *2*, 643.

9. Milsmann, C.; Turner, Z.; Semproni, S. P.; Chirik, P. J. *Angew. Chem. Int. Ed.* **2012**, *51*, 5386.

10. Annibale, V. T.; Song, D. *RSC Adv.* **2013**, *3*, 11432.

11. Ketterer, N. A.; Fan, H.; Blackmore, K. J.; Yang, X.; Ziller, J. W.; Baik, M.–H.; Heyduk, A. F. *J. Am. Chem. Soc.* **2008**, *130*, 4364.

12. Caulton, K. G. *Eur. J. Inorg. Chem.* **2012**, 435.

13. Stanciu, C.; Jones, M. E.; Fanwick, P. E.; Abu-Omar, M. M. *J. Am. Chem. Soc.* **2007**, *129*, 12400.

14. Sugiyama, H.; Aharonian, G.; Gambarotta, S; Yap, G. P. A.; Budzelaar, P. H. M. *J. Am. Chem. Soc.* **2002**, *124*, 12268.

15. Bart, S. C.; Lobkovsky, E.; Chirik, P. J. *J. Am. Chem. Soc.* **2004**, *126*, 13794.

16. Alyea, E. C.; Ferguson, G.; Restivo, R. J. *Inorg. Chem.* **1975**, *14*, 2491.

17. Calderazzo, F.; Englert, U.; Pampaloni, G.; Santi, R.; Sommazzi, A.; Zinna, M. *Dalton Trans.* **2005**, 914.

18. Reardon, D.; Conan, F.; Gambarotta, S.; Yap, G.; Wang, Q. *J. Am. Chem. Soc.* **1999**, *121*, 9318.

19. Knijnenburg, Q.; Gambarotta, S.; Budzelaar, P. H. M. *Dalton Trans.* **2006**, 5442.

20. Suzuki, H.; Matsumura, S.-I.; Satoh, Y.; Sogoh, K.; Yasuda, H. *Reactive & Functional Polymers* **2004**, *58*, 77.

21. Fan, R.-Q.; Zhu, D.-S.; Mu, Y.; Li, G.-H.; Su, Q.; Ni, J.-G.; Feng, S.-H. *Chem. Res. Chin. Univ.* **2005**, *21*, 496.

22. Alyea, E. C.; Merrell, P. H. *Inorg. Chim. Acta* **1978**, *28*, 91.

23. Marganian, C. A.; Vazir, H.; Baidya, N.; Olmstead, M. M.; Mascharak, P. K. *J. Am. Chem. Soc.* **1995**, *117*, 1584.

24. Antonov, A. A.; Semikolenova, N. V.; Zakharov, V. A.; Zhang, W.; Wang, Y.; Sun, W.-H.; Talsi, E. P.; Bryliakov, K. P. *Organometallics* **2012**, *31*, 1143

25. Fan, R.-Q.; Fan, R.-J.; Lv, Z.-W.; Yang, Y.-L.; An, F.; Gu, D.-M. *J. Coord. Chem.* **2007**, *60*, 919.

26. de Bruin, B.; Bill, E.; Bothe, E.; Weyhermüller, T.; Wieghardt, K. *Inorg. Chem.* **2000**, *39*, 2936.

27. Trivedi, M.; Pandey, D.S.; Xu, Q. *Inorg. Chim. Acta* **2007**, *360*, 2492.

28. Liu, J.-Y.; Zheng, Y.; Li, Y.-G.; Pan, L.; Li, Y. S.; Hu, N.-H. *J. Organomet. Chem.* **2005**, *690*, 1233.

29. Long, Z.; Wu, B.; Yang, P.; Li, G.; Liu, Y.; Yang, X.-J. *J. Organomet. Chem.* **2009**, *694*, 3793.

30. Brandstadt, K.; Cook, S.; Nguyen, B.-T.; Surgenor, Q.; Taylor, R.; Tzou, M.-S. *PCT Int. Appl.* **2013**, WO 2013043846 A1 20130328

31. Zhu, D.; Thapa, I.; Korobkov, I.; Gambarotta, S.; Budzelaar, P. H. M. *Inorg. Chem.* **2011**, *50*, 9879.

32. Gibson, V. C.; Humphries, M. J.; Tellmann, K. P.; Wass, D. F.; White, A. J. P.; Williams, D. J. *Chem. Commun.* **2001**, 2252.

33. Vidyaratne, I.; Scott, J.; Gambarotta, S.; Duchateau, R. *Organometallics* **2007**, *26*, 3201.

34. Bart, S. C.; Chlopek, K.; Bill, E.; Bouwkamp, M. W.; Lobkovsky, E.; Neese, F.; Wieghardt, K.; Chirik, P. J. *J. Am. Chem. Soc.* **2006**, *128*, 13901.

35. Russell, S. K.; Lobkovsky, E.; Chirik, P. J. *J. Am. Chem. Soc.* **2009**, *131*, 36.

36. Yin, C.-X.; Finke, R. G. *J. Am. Chem. Soc.* **2005**, *127*, 9003.

37. Yin, C.-X.; Finke, R. G. *J. Am. Chem. Soc.* **2005**, *127*, 13988.

38. Lippert, C. A.; Arnstein, S. A.; Sherrill, C. D.; Soper, J. D. *J. Am. Chem. Soc.* **2010**, *132*, 3879.

39. Connelly, N. G.; Geiger, W. E. *Chem. Rev.* **1996**, *96*, 877.

40. Chang, D.; Malinski, T.; Ulman, A.; Kadish, K. M. *Inorg. Chem.* **1984**, *23*, 817.

41. *CRC Handbook of Chemistry and Physics*, 89th ed.; Lide, D. R., Ed.; CRC Press/Taylor & Francis: Boca Raton, FL, 2008.

42. Lucas, H. J.; Kennedy, E. R. *Org. Synth.* **1942**, *22*, 69.

43. Popeney, C.; Guan, Z. *Organometallics* **2005**, *24*, 1145.

44. Oskam, J. H.; Fox, H. H.; Yap, K. B.; McConville, D. H.; O'Dell, R.; Lichtenstein, B. J.; Schrock, R. R. *J. Organomet. Chem.* **1993**, 185.

45. Carver, F. J.; Hunter, C. A.; Livingstone, D. J.; McCabe, J. F.; Seward, E. M. *Chem. Eur. J.* **2002**, *8*, 2847.

46. Clentsmith, G. K. B.; Gibson, V. C.; Hitchcock, P. B.; Kimberley, B. S.; Rees, C. W. *Chem. Comm.* **2002**, 1498.

47. Esteruelas, M. A.; Lopez, A. M.; Mendez, L.; Olivan, M.; Onate, E. *Organometallics* **2003**, *22*, 395.

48. Bruker (2007). *Apex2*. Bruker AXS Inc., Madison, Wisconsin, USA.

49. Hooft, R. W. W. *Collect*; Nonius BV: Delft, The Netherlands, 1998.

50. Otwinowski, Z.; Minor, W. *Methods Enzymol.* **1997**, *276*, 307.

51. *SHELXTL: Program Library for Structure Solution and Molecular Graphics*, version 6.12; Bruker Analytical X-Ray Systems, Inc.: Madison, WI, 2001.

52. Sheldrick, G. M. *Acta Crystallogr., Sect. A: Found. Crystallogr.* **2008**, *A64*, 112.

53. Huang, Y.; Chen, J.; Chi, L.; Wei, C.; Zhang, Z.; Li, Z.; Li, A.; Zhang, L. *J. Appl. Polym. Sci.* **2009**, *112*, 1486.

54. Addison, A. W.; Rao, T. N. *J. Chem. Soc., Dalton Trans.* **1984,** *7*, 1349.

55. Manuel, T. D.; Rohde, J.-U. *J. Am. Chem. Soc.* **2009**, *131*, 15582.

56. Armarego, W. L. F.; Chai, C. *Purification of Laboratory Chemicals*, 5th ed.; Butterworth-Heinemann: Oxford, U.K., 2003.

57. Britovsek, G. J. P.; Gibson, V. C.; Kimberley, B. S.; Maddox, P. J.; McTavish, S. J.; Solan, G. A.; White, A. J. P.; Williams, D. J. *Chem. Commun.* **1998**, 849.

58. Kleigrewe, N.; Steffen, W.; Blömker, T.; Kehr, G.; Fröhlich, R.; Wibbeling, B.; Erker, G.; Wasilke, J.-C.; Wu, G.; Bazan, G. C. *J. Am. Chem. Soc.* **2005**, *127*, 13955.

59. Humphries, M. J.; Tellmann, K. P.; Gibson, V. C.; White, A. J. P.; Williams, D. J. *Organometallics* **2005**, *24*, 2039.

60. Knijnenburg, Q.; Hetterscheid, D.; Kooistra, T. M.; Budzelaar, P. H. M. *Eur. J. Inorg. Chem.* **2004**, 1204.

61. Donoghue, P. J.; Tehranchi, J.; Cramer, C. J.; Sarangi, R.; Solomon, E. I.; Tolman, W. B. *J. Am. Chem. Soc.* **2011**, *133*, 17602.

62. Kieber-Emmons, M. T.; Riordan, C. G. *Acc. Chem. Res.* **2007**, *40*, 618.

63. Yao, S.; Bill, E.; Milsmann, C.; Wieghardt, K.; Driess, M. *Angew. Chem. Int. Ed.* **2008**, *47*, 7110.

64. Chen, D.; Motekaitis, R. J.; Martell, A. E. *Inorg. Chem.* **1991**, *30*, 1396.

65. Hikichi, S.; Yoshizawa, M.; Sasakura, Y.; Komatsuzaki, H.; Moro-oka, Y.; Akita, M. *Chem.–Eur. J.* **2001**, *7*, 5011.

66. Suzuki, M. *Acc. Chem. Res.* **2007**, *40*, 609.